UNIVERSITY OF CALIFORNIA

Santa Barbara

# Molecular Engineering of Noninvasive Reporters for Background-Free MRI

A dissertation submitted in partial satisfaction of the

requirements for the degree Doctor of Philosophy

in Chemistry

by

Jason Hyunsoo Yun

Committee in charge:

Professor Arnab Mukherjee, Chair

Professor Kevin Plaxco

Professor Tod Kippin

Professor Gabriel Ménard

December 2021

The dissertation of Jason Hyunsoo Yun is approved.

_____
Gabriel Ménard

_____
Tod Kippin

_____
Kevin Plaxco

_____
Arnab Mukherjee, Committee Chair

December 2021

Molecular Engineering of Noninvasive Reporters for Background-Free MRI



by

Jason Hyunsoo Yun

ACKNOWLEDGEMENTS

First, I like to thank my advisor Arnab Mukherjee for taking a chance on me back when I was having a graduate career crisis. I had the privilege to help jumpstart his lab and further his post-doctoral work on aquaporins. Arnab has truly mentored me starting with a PCR all the way to finishing my project. I couldn't have been more fortunate to have an advisor that allowed me to problem solve my experiments and more importantly, trusting and believing in me to do so. Arnab, I am absolutely mind-blown how knowledgeable, hard-working, and creative you are as an academic in addition to how kind and willing you are to help those in need. You have pushed me to be a better scientist, thinker, and person, and I am forever grateful for that.

I'd like to thank my committee members first starting with Dr. Kevin Plaxco for providing useful input regarding my project and graduate path, Dr. Tod Kippin and Gabriel Ménard for allowing me to share my work with you. Without you all, I wouldn't have been able to graduate, literally.

I'd like to thank Harun Ozbakir, Nolan Anderson, Ray Borg, and Kang-Ching Fan in helping build the lab and working protocols from the beginning. Thank you to the Mukherjee lab, I wish you guys the best of luck in finishing graduate school. I have had the pleasure to mentor 4 outstanding undergraduates for my project: Eugene Li, Charles Yue, Audrey Chow, and Michelle Leong. Thank you for your hard work and handling my extremely high standards on how experiments should be conducted.

I would like to thank my family in supporting me during my graduate studies and specifically my mom for reminding me to take one day at a time. To my friends I've met during my undergraduate and graduate studies, thank you for walking through each step of graduate school with me and eating really good food anytime there was a reason to celebrate.

To my wonderful girlfriend Alice Yeh, you have been there for me celebrating my smallest victories and being there during my hardest moments in graduate school. I love you and thank you for your unwavering support and patience.

VITA OF JASON HYUNSOO YUN
December 2021

EDUCATION

Ph.D. Chemistry, University of California, Santa Barbara, December 2021
B.S. Pharmaceutical Chemistry University of California, Davis, June 2016

PROFESSIONAL EMPLOYMENT

Graduate Student Researcher 09/2016 – Present
University of California, Santa Barbara

Project Goal: To enhance MRI reporter sensitivity and longitudinal imaging capabilities for unambiguous detection of gene expression using MRI subtraction imaging techniques.
Advisor: Dr. Arnab Mukherjee, Ph.D.

- Engineered 27 stable cell lines comprised of CHO, RAW 264.7, U87, and Jurkat cell types to express the ligand-modulated MRI reporter gene.
- Optimized lentiviral transduction protocol for both suspension and adherent cell lines.
- Xenografted engineered cells subcutaneously in 25 immunocompromised NOD SCID Gamma (NSG) mice for tumor model imaging.
- Imaged and quantified MRI signal fold change in stable cell lines/mice using a 300 MHz NMR achieving up to 181% signal fold change in vitro and up to 60% signal fold change in vivo.
- Trained and assisted 10 lab members in lab and equipment protocols maintaining consistent results across different users.

Project Goal: To design a light-activated hollow-gold nanoshells to deliver biologically relevant proteins into cancer cells with spatiotemporal control.

- Appended proteins and cell targeting moieties to hollow-gold nanoshells through NHS-ester, biotin-streptavidin conjugation chemistry.
- Optimized the surface chemistry and synthetic methods of nanoshells using PEG linkers increasing nanoparticle stability in buffer solution.
- Developed two orthogonal assays using chemical etch & laser release to quantify the efficiency of protein load onto the final product achieving a maximal ~3000 dye-labeled proteins per nanoshell.
- Tracked the release of dye-labeled proteins inside HeLa cells using a 2-photon confocal microscope.

Teaching Assistant 09/2016 – 08/2020
To lead lab courses and grade lab reports, quizzes, and exams.

- General Chem Lab/1AL (Fall 16)
- General Chem Lab/1BL (Winter 17)
- General Chem Lab/1CL (Spring 17)

- Organic Chem Lab/6AL (Winter 18)
- Organic Chem Lab/6BL (Summer 18)
- Biochem Lecture/142A (Fall 17)
- Created in-class lecture & online quiz questions for 142A (Summer 17)
- Biochem Lab/110L (Fall 18)
- Biochem Lab/125L (Winter 19)
- Biochem Lab/112L (Spring 18)
- Organic Chem Lecture/109C (Summer 20)

Undergraduate Researcher 08/2014 – 07/2016
University of California, Davis

Project Goal: To develop an MRI biosensor using iron-oxide nanoparticles functionalized with an antioxidant responsive molecule.
Advisor: Dr. Angelique Louie, Ph.D.

- Investigated the use of functionalized spiropyrans attached to iron-oxide nanoparticles for biosensing glutathione levels relevant for disease prognosis.
- Ran 10 g scale reactions and performed multi-step synthesis of various spiropyrans.
- Characterized biosensors using a variety of analytical instruments to measure the particle size, stability, spectroscopic properties, and changes in relaxivity.

Downstream Process Development Intern 06/2015 – 09/2015
Sutro Biopharma, Inc.

- Successfully screened 18 in-house designed cationic tags achieving >95% purity of all 3 reagents using the most optimal cationic tag.
- Purified and upscaled all reagents using an FPLC mainly using ion-exchangers and hydrophobic columns.
- Detected protein purity and yield by SDS-PAGE and nanodrop. This culminated in purifying up to 230 mg of protein reagent from 1 L of cell culture.

## AWARDS

- Department of Chemistry & Biochemistry Summer Chair's Fellowship (06/2021)
- UCSB Center of BioEng Sponsored BMES Conference Travel Fellowship (09/2020)
- Outstanding Service to the UCSB Chemistry Department Award (06/2018)
- Departmental's Highest Honors UC Davis (06/2016)
- Dean's List for College of Letters and Science UC Davis (06/2013, 03/2014)

## PUBLICATIONS

- Garcia, J.; Addison, J. B.; Liu, S. Z.; Lu, S.; Faulkner, A. L.; Hodur, B. M.; Balmond, E. I.; Or, V. W.; **Yun, J. H.**; Trevino, K.M.; Shen, B.; Shaw, J. T.; Frank, N. L.; Louie, A.Y., Antioxidant Sensing by Spiropyrans: Substituent Effects and NMR Spectroscopic Studies. The Journal of Physical Chemistry B 2019.

PRESENTATIONS

- BMES 2020 Virtual Meeting October 7th, 2021; Oral: Engineering Chemogenetically Erasable Reporter Genes for Background-Free MRI
- BMES 2020 Virtual Meeting October 17th, 2020; Oral: Engineering Chemically Erasable Genetic Reporters for Background-Free MRI.
- UC Davis 27th Undergraduate Research Conference Davis, CA, April 9th, 2016; Poster: Design of Functionalized Spiropyrans for Glutathione Sensing and MRI Capabilities.
- UC Davis 26th Undergraduate Research Conference Davis, CA, May 2nd, 2015; Oral: Spiropyran Bound to an MRI Contrast Agent and its Glutathione Response.

## COVID-19 Impact Statement

Since the start of the infamous COVID-19 pandemic emerging in March 2020, lockdowns and its effects downstream have dramatically inhibited everyone's lives even to this day. We all feel the lingering effects of the pandemic on our mental psyche and our ability to work in our current jobs. UCSB, along with many other establishments, had made the executive decision to go on a 3-month lockdown, which was understandable as the world tried to fully grasp the seriousness of this viral outbreak. During that time, graduate student researchers were forced to stop all research.

Thankfully, as more research on COVID-19 were unfolding in various aspects such as the length of time SARS-CoV-2 is still viable on different surfaces, the vital 6 ft rule when encountering another human being, and the widely debated effectiveness of face masks, all the efforts that answered questions surrounding these results assisted in the revamping of campus research to continue. Unfortunately, as the months trailed on, campus researchers quickly realized the severity of the pandemic on several fronts that will forever change how academic research is conducted.

On a personal note, ordering basic supplies such as gloves, falcon tubes, pipette tips, things you never would have imagined to be a supply issue in a biology-based lab were the hardest items to get in a reasonable timeframe. Rooms necessary to perform animal surgeries here at the ARC facilities were being prepared at an astonishingly slow rate due to limits on the number of facilities personnel allowed to work at a given time in addition to the shortage of necessary supplies. On a global scale, the supply chain issue has made it extremely difficult for anything to be done in a timely manner. All this to say, the impact of this pandemic has definitely prolonged my graduate work by half a year and redefined normalcy in all areas of our lives and will continue to do so in ways we are still yet to experience.

ABSTRACT

Molecular Engineering of Noninvasive Reporters for Background-Free MRI

by

Jason Hyunsoo Yun

Molecular phenomena such as gene expression, protein-protein interactions, and the influence of pH, ion movement, and endogenous small molecules for cellular function have grown with increasing interest since the discovery of fluorescent proteins (FPs) in the 1960s and further development as a genetic reporter shortly after. The ability to precisely image "invisible" proteins by tagging them with FPs has revolutionized the field of molecular biology. Although FPs have immensely increased our understanding of biomolecular events, visualizing these same biological processes beyond cell cultures and into higher order mammals is greatly hindered due to photon absorption and scattering from tissue, severely limiting light penetration to a mere millimeter.

Due to these limitations, engineering a genetic reporter to monitor gene expression in deeper-seated tissue would greatly benefit the scientific community to study biomolecular phenomena in this context. Magnetic resonance imaging (MRI) based genetic reporters can help complement their fluorescent counterparts in deep tissue imaging with relatively high spatial resolution (~250 μm) and temporal resolution (<1s). However, current MRI reporters developed in the past 20 years are prone to lower sensitivity in the presence of physiological pathologies and abnormalities, thereby convoluting signal contrast.

Herein, we establish human aquaporin-1 (AQP1) as a viable MRI reporter that can functionally produce a switch-like signal upon chemical administration at the post-translational level. Post processing of the images obtained before and after ligand addition subtracted out endogenous background noise contributions enhancing reporter signal. We measured the response of 7 ligand-responsive degradation tags fused to either the N or C terminus of AQP1 conferring AQP1-dependent contrast in chinese hamster ovary tetracycline on (CHO tet ON) cells. Thereafter, we translated the best 2-3 tags to measure their performance in human glioblastoma U87 cells, human acute T-cell leukemia Jurkat cells, and murine macrophage RAW 264.7 cells demonstrating this reporter system in diverse cell types. Furthermore, we applied this reporter system in immunocompromised NOD scid gamma (NSG) mice using xenografted flank tumors demonstrating on-demand MRI signal in deeper-seated tissue. These results provide a novel proof of concept for obtaining higher MRI sensitivity in combination with gene reporting in physiological environments that have previously been difficult to detect.

TABLE OF CONTENTS

LIST OF FIGURES

# I. Introduction

## A. Magnetic Resonance Imaging and Diffusion-Weighted Imaging

Magnetic resonance imaging (MRI) is widely used in basic science and in the clinic to produce images noninvasively with high spatial and temporal resolution. The most familiar MRI pulse sequence to aid in understanding MRI is the spin-echo. A helpful basic overview of MRI can be found in the journal of RadioGraphics.[1] To initiate the imaging process, the patient or sample is placed in the scanner in which their hydrogen nuclear spins align in the presence of the main magnetic field along the longitudinal direction. A radiofrequency pulse is then applied such that the nuclear spins rotate 90º into the transverse plane. At this point, the spins dephase along the transverse plane known as T2 relaxation due to local field inhomogeneities. At the same time, the spins are relaxing back to the longitudinal plane albeit at a slower rate in comparison to T2 relaxation by dissipating their excitation energy to the surrounding tissue known as T1 relaxation. It is important to note T2 relaxation happens much faster than T1 relaxation in physiological contexts, which is helpful for the downstream spin-echo process in forming a readout signal known as an echo. After some time, another 180º radiofrequency pulse is applied causing the spins that were dephasing along the transverse plane to align in phase. The echo is formed in phase after applying the 180˚ second radiofrequency pulse, because the spins that were dephasing more quickly will have a much longer path to realign spins as opposed to the initially slower spins. This process produces an echo signal picked up by the receiver coil and ultimately contributes to a processed anatomical MR image. Various tissue in the body have intrinsically different T1, T2, and proton density values that provides the difference in contrast on images.

In diffusion weighted imaging (DWI), the spin echo can be used with applied diffusion gradients to distinguish between fast diffusing protons (unrestricted diffusion) and slower diffusing protons (restricted diffusion). Diffusion gradients are applied in an equal-yet-opposite direction with mixing time allowing for free proton diffusion in between the dephasing and rephasing diffusion gradients. If there is little to no net movement of protons during the mixing time, the dephased spins will rephase properly, providing a higher signal intensity equating to a brighter contrast. Conversely, signal decrease occurs when proton diffusion is significant enough such that the rephasing diffusion gradient doesn't properly realign the spins equating to a darker contrast. This modality of MRI is essentially helpful for imaging water diffusion within a given 3-dimensional pixel known as a voxel. The following chapters explain the use of a protein-based metal free water channel used as an MRI reporter.

**B. Synthetic-Based MRI Contrast Agents**

MRI can image physiological pathologies in the human body. However, these same abnormalities can produce similar contrast as the surrounding tissue disguising themselves from being clinically treated. To aid in this front, the development of synthetic MRI contrast agents has greatly improved diagnostic accuracy typically by altering the T1 and T2 relaxation rates of surrounding protons on water.[2]

Gd-DTPA was the first clinically approved gadolinium-based MRI contrast agent and has been helpful in enhancing tumor contrast within the brain.[3] Contrast enhancement occurs by the proton interactions on water with the $Gd^{3+}$ contrast agent. $Gd^{3+}$ chelated by DTPA acts as a powerful microscopic magnet due to its seven unpaired f-orbital electrons, thereby allowing water molecules that chelate to the complex to undergo T1 relaxation almost instantaneously. As a result, signal intensity increases within the region $Gd^{3+}$ has

accumulated, thus producing a bright contrast in T1-weighted images. Researchers have also synthesized $Gd^{3+}$-based MRI sensors for pH, metals, and enzymes.[4,5,6]

Another class of MRI contrast agents comprised of superparamagnetic iron-oxide nanoparticles (SPIO) are typically less than 50 nm in size with biocompatible coating. Within the tissues that have accumulated SPIOs, they induce additional magnetic susceptibilities that produce a darkening effect observed in T2-weighted images due to prominent T2 relaxation at sub-micromolar concentrations. In the clinic, SPIOs have been used to image lesions within the body.[7] Furthermore, this class of contrast agents have been engineered to detect oligonucleotides, proteins, and $Ca^{2+}$.[8,9,10]

**C. Metallic Genetically Encodable MRI Reporters**

Synthetic contrast agents have greatly improved diagnostics and use in the clinic to image biomolecular phenomena and pathologies. However, they fail to provide any genetic information within the same context. Given the impact by fluorescent reporters in the field of molecular biology, genetically encodable MRI reporters have emerged to circumvent the limitations of their fluorescent partners to image these same molecular events in deeper embedded tissue.

| Genetically Encodable Reporter | Mechanism | Modality | Observed MRI Response | Reference |
|---|---|---|---|---|
| β-galactosidase | β-galactosidase cleaves off the sugar residue exposing a water coordination site on $Gd^{3+}$ for enhanced T1 relaxation of bulk water protons | T1 | 57% increase in *X. laevis* embryo after 24 h incubation with 1.6 µmol EGadMe and 2 ng β -gal mRNA | 11 |
| Tyrosinase (TYR) | Produces melanin, which chelates $Fe2^{+}$ | T1 | 37.2 ± 1.0 % increase in HEK 293 cells | 12 |
| Calprotectin | Binds 2 $Mn^{2+}$ ions upon binding to 4 $Ca^{2+}$ ions | T1 | 22 ± 4% increase in CHO cells upon 5 mM calcium and 10 µM calcimycin addition | 13 |
| Divalent Metal Transporter 1 (DMT1) | Transports divalent metal ions in and out of cells | T1 | 75 ± 30% increase in GL261 brain xenografts after 8 h IP injection of 80 mg/kg $MnCl_2$ | 14 |
| Rat Organic Anion Transporting Protein 1a1 (OATp1a1) | Transports synthetic contrast agents in and out of cells | T1 | 6.8 fold increase in HEK 293T flank xenografts after 1 h of 0.664 mmol/kg Gd-EOB-DTPA administration | 15 |
| Biotin Acceptor Peptide-Transmembrane Domain (BAP-TM) | Platelet-derived growth factor receptor (PDGFR) containing biotin acceptor peptide (BAP) conjugates to streptavidin-horseradish peroxidase which induces T1 relaxation from $Gd^{3+}$-CAor streptavidin-magnetic nanoparticles causing T2 relaxation | T1/T2 | 3.3 fold enhancement of T1 signal and 2 fold enhancement of T2 signal | 17 |
| T-cell Immunoglobulin and mucin domain containing protein 2 (Timd2) | Mediates ferritin endocytosis | T1/T2 | ~9% increase in HEK 293T flank xenografts after 24 h of 11.2 mg ferritin injection | 18 |
| Transferrin Receptor (TfR) | Facilitates $Fe^{3+}$ binding transferrin transport in and out of cells | T2 | 81 ± 16 % decrease in rat 9L gliosarcoma flank xenografts 24 h after 3 mg Fe transferrin conjugated SPIO injection | 19 |
| Ferritin (Ft) | Encapsulated iron forming an iron oxide nanoparticle core | T2 | 6.6 ± 1.7 increase in $T_2$-weighted CNR and 16.2 ± 1.6 increase $T_2^*$-weighted CNR in AdV transduced mice brain | 20 |
| MagA | Induce mineralization of iron oxide nanoparticles within cells | T2 | 300% increase in 293FT cells with 1 µg/mL doxycycline and 200 µM $Fe^{3+}$ incubation for 2 days | 21 |

**Figure I.B.1.** List of all first-in-class metallic-based genetically encodable MRI reporters.

| Genetically Encodable Reporter | Mechanism | Modality | Observed MRI Response | Reference |
|---|---|---|---|---|
| Gas Vesicles (GVs) | Collapsible protein nanostructures that contain magnetically susceptible air | T2/HyperCEST | ~20% saturation contrast after overnight exposure to ~32 µM IPTG in *E. coli*. | 24 |
| Lysine Rich Protein (LRP) | Embedded with lysine rich exchangeable protons that get saturated by radiofrequencies reducing background signal | CEST | 134.3 ± 137% increase in 9L rat glioma brain xenografts | 27 |
| Human Protamine-1 (hPRM1) | Embedded with arginine rich exchangeable protons that get saturated by radiofrequencies reducing background signal | CEST | ~6% increase in HEK 293 cells | 29 |
| Calcitonin Gene-Regulated Peptide (CGRP) | Induce dilation of intracerebral arterioles detected by BOLD imaging | BOLD | 228.6 ± 71.8% increase after 24 h in HEK293FT xenografts in rat brain | 33 |
| Creatine Kinase (CK) | ATP hydrolysis produces phosphocreatine (PCr) detected by $^{31}P$ MRS | $^{31}P$ MRS | — | 34 |
| Cytosine Deaminase (CD) | Catalyzes prodrug 5-fluorocytosine (5-FC) to 5-fluorouracil (5-FU) monitored by $^{19}F$ MRS | $^{19}F$ MRS | — | 35 |
| Urea-Transporter B (UT-B) | Urea transport detected by $^{13}C$ MRS and water diffusion in and out of cells | $^{13}C$ MRS/DWI | 121.7 ± 59.3% increase in lentiviral transduced rat brain tissue | 41 |
| Human aquaporin-1 (hAQP1) | Water diffusion in and out of cells | DWI | 39.4 ± 6.5% decrease in mice brain xenografts after 48 h incubation with 75 µg injection of doxycycline | 42 |

**Figure I.B.2.** List of all first-in-class genetically encodable non-metallic MRI reporters.

In the past 30 years, researchers have dabbled at the thought of using MR responsive genetically encodable proteins that could provide enough contrast beyond the physiological background to probe molecular biology. The quest for an MRI analog of fluorescent proteins has been taken more seriously in the past 20 years by discovering and engineering proteins that leverage the physical mechanisms among the different MRI modalities: T1, T2, diffusion-weighted MRI, chemical exchange saturation transfer (CEST), hyperCEST, and functional MRI (fMRI). Starting with T1-based reporters, Louie et al. injected *X. laevis* embryos with mRNA encoding β-galactosidase that catalyzed the sugar residue off the gadolinium contrast agent EGadMe. In doing so, this exposed a water coordination site on $Gd^{3+}$ leading to inner-sphere T1 relaxation. At a later stage in the embryonic development post injection, a 57% increase in MRI signal was detected.[11] Another enzyme-activating transgene known as tyrosinase was shown to induce melanin production though the catalysis of tyrosine. Cleverly using the catalytic reaction, Weissleder et al. were able to achieve 37 ± 2% increase in T1-weighted signal in transfected HEK 293 cells expressing tyrosinase due to the iron binding properties of melanin.[12] Non-enzymatic metal-based reporters have also been developed to directly produce MRI signals by binding paramagnetic metals. Recently, the Mukherjee lab has published work on a $Mn^{2+}$ binding protein upon calcium binding known as calprotectin. Ozbakir et al. achieved 22 ± 4% increase in CHO cells upon the addition of calcium and calcimycin, an intracellular calcium inducing compound. This work showcases the first calcium sensing MRI genetic sensor that could be vital to understanding neuronal studies in deeper regions of the brain.[13]

Membrane proteins have also been used to facilitate transport of paramagnetic ions and paramagnetic ion binding proteins into cells to alter T1 and T2 MR signal contrast. Divalent metal transporter 1 (DMT1) has been shown to transport $Mn^{2+}$ ions into GL261

brain xenografts thereby increasing T1-weighted contrast by 75 ± 30%.[14] Clinically approved gadolinium contrast agent Gadoxetic acid (Gd-EOB-DTPA) has been used in conjunction with rat organic anion transporting protein 1a1 (OATp1a1) transgene to increase T1-weighted signal intensity by 6.8 fold in HEK 293T flank xenografts.[15]An elaborate biosynthetic reporter system was engineered to enable either T1 or T2 relaxation by incorporating a membrane protein as an anchor for MR signal production. Tannous et al. inserted a biotin-acceptor peptide (BAP) domain into the membrane bound platelet-derived growth factor receptor (PDGFPR). Using the endogenous biotin ligase machinery in cells, a biotin molecule was conjugated to the BAP domain on PDGFPR as it was getting membrane trafficked. Knowing homotetramer streptavidin (SA) proteins bind biotin with extremely high affinity ($K_d \leq 10^{-15}$ M)[16] Tannous et al. conjugated IONPs to SA and administered the contrast agent to the biotinylated surface on cells where the biotin-SA complex formed resulting in a 2 fold T2 enhancement. For T1 relaxation, SA conjugated to horseradish peroxidase (HRP) was added to the biotinylated surface of cells and subsequently a peroxidase activatable gadolinium contrast agent was then administered to the HRP-SA-BAP-PDGFPR complex to induce 3.3 fold T1 enhancement. [17] Although this system is a bit complex requiring multiple add ons to produce MRI signal, it shows how creative researchers can be using known biochemical interactions to their advantage.

T-cell immunoglobulin and mucin domain containing protein 2 (Timd2) was induced to increase expression of Timd2 on the membrane thus leading to higher influx of iron binding ferritin biomolecules. Engineered HEK 293T flank xenografts showed a moderate 9% signal increase after 24 h post ferritin injection.[18] A similar concept using a transferrin receptor (TfR) mediates iron binding transferrin transport. In order to attain high enough signal, transferrin was conjugated to dextran-coated iron oxide nanoparticles (Tf-IONPs)

and was able to achieve an 81 ± 16% decrease in rat 9L glioscarcoma flank xenografts 24 h post Tf-IONP injection.[19]

As mentioned earlier, iron sequestering proteins such as ferritin and MagA transgene have also been explored to provide MRI contrast. Both reporters encapsulate free iron ions thus, preventing fenton's reaction occurring within the cell maintaining iron homeostasis. Work done by Genove et al. used ferritin for the first time as an MRI reporter in the mouse brain through adenovirus transduction. However, only a 6.6 ± 1.7 increase in $T_2$-weighted CNR and 16.2 ± 1.6% in $T_2^*$-weighted CNR were measured in this study, which suggests further supplementation with iron or elaborate engineering to increase reporter sensitivity is needed.[20] Inspiration for MRI contrast has also come from bacterial origins. The transgene MagA is responsible for forming magnetosomes found in magnetotactic bacteria. These magnetosomes contain iron oxide nanoparticles and have been used in a mammalian context similar to ferritin. A 300% increase in T2-weighted contrast was measured in HEK 293FT cells with 1 µg/mL doxycycline induction and 200 µM $Fe^{3+}$ incubation over 48 h.[21]

**D. Non-Metallic Genetically Encodable MRI Reporters**

The previously mentioned reporters have contributed significantly to the field of MRI genetic reporters looking to nature as a starting ground. However, they all require potentially toxic amounts of supplemented paramagnetic ions such as $Gd^{3+}$, $Fe^{2+}$, $Fe^{3+}$, or $Mn^{2+}$ in vivo in order to obtain a high enough sensitivity. Futhermore, these reporters are dependent on the biodistribution of the supplemented ions, which has its own barriers in a living animal context. Other modalities besides T1- and T2-weighted imaging used in the clinic are not dependent on parmagnetic metal supplementation such as CEST imaging, blood-oxygen-level-dependent (BOLD) imaging used in fMRI studies, magnetic resonance spectroscopy (MRS), and diffusion-weighted imaging (DWI) to name a few. This begs the

question whether there are proteins found in nature that operate under these physical parameters, which the answer is a clear yes.

A technique known as HyperCEST has involved the use of hyperpolarized $^{129}Xe$ gas to enhance MRI signal by $>10^4$.[22] Xenon gas, when entrapped in a closed environment, has a different chemical shift from free aqueous xenon allowing for a saturating radiofrequency to be applied to the bound xenon.[23] After xenon interacts with a reporter, saturation pulses at its chemical shift are applied leading to signal attentuation. This process of exhanging saturated xenon with the bulk solution of xenon leads to overall bulk background signal loss thereby enhancing reporter MRI signal. Shaprio et al. engineered the use of protein nanostructures called gas vesicles (GVs) found in buoyant microbes to embed hyperpolarized $^{129}Xe$ gas inside. After performing HyperCEST MRI scan, ~20% saturation contrast was measured in *E. coli*.[24]

A follow up paper conducted by Lu et al. induced the collapse of GVs using ultrasound enabling MRI subtraction imaging where the signal produced is maintained yet the endogenous background contrast is digitally subtracted out forming a hyperintense MRI signal.[25] This was made possible without the use of hyperpolarzied xenon, since the air pockets in GVs are magnetically susceptible to produce $T_2$ and $T_2^*$ contrast. However, in both of the GV papers, they were only able to encode GVs in *E. coli* and not in a mammalian context due their complex genetic demands requiring expression of anywhere from 8 to 11 genes. Since then, the Shapiro group has managed to encode GVs in mammalian cells but for ultrasound imaging.[26] With further fine-tuning, these GVs can be genetically encoded for MRI imaging in mammalian cells.

Biosynthetic CEST reporters such as lysine rich protein (LRP) and human protamine-1 (hPRM1) work similarly to HyperCEST mentioned above but without the use

of a hyperpolarized atom. CEST images are produced when saturation pulses are applied to the exchangeable protons embedded on protonated lysine in LRP and protonated arginines in hPRM1. Continual rounds of saturated protons exchange with bulk water protons leading to a decrease in background water signal and increase in reporter signal. Gilad et al. designed a lysine repeating protein to generate enough exchangeable protons to provide a 134 ± 137% increase in CEST signal in 9L rat glioma brain xenografts. This reporter generated high signal variablity even with millimolar concentrations typical for CEST reporters due to nonspecific RF saturation frequencies and counteracting T1 relaxation of the saturated protons exchanged on water.[23,27] In addition, LRP contained multiple gene repeats leading to recombination issues, which hindered optimal expression of LRP. Further optimizations have been done to LRP to minimize recombination events ensuring protein stability and truncating its size as a reporter. In doing so, this second generation of LRP achieved a 35.2 ± 13.5% increase in signal fold change in murine glioma xenografts in mice brains.[28] Another CEST reporter known as human protamine-1 (hPRM1) was chosen by some of the researchers from the same group for having the highest abundance of arginines among the other human protamine group. Using the naturally encoded protein reporter, it produced a minimal 6% increase in CEST signal engineered in HEK 293 cells.[29]

BOLD imaging is similar to CEST in the sense that you can use endogenous proteins to provide an MRI signal output. Functional MRI (fMRI) studies use the BOLD mechanism to obtain information of blood flow within the brain. This is possible to detect thanks to the contributions of naturally expressed deoxygenated hemoglobin (DeoxyHb) and oxygenated hemoglobin (oxyHb). The former contains paramagnetic properties from the bound iron (II) ion chelated in the porphyrin stucture that help induce T2 relaxation in the surrounding water protons. Blood flow facilitates the movement of deoxy and oxyhemoglobin, which can

be detected by MRI within 1-5% change in signal in human patients.[30-32] Desai et al. capitalized on this imaging mechanism by engineering calcitonin gene-regulated protein (CGRP), a known human vasodilatory peptide that binds to the receptor activity-modifying protein 1 (RAMP1) and calcitonin receptor-like receptor (CLR) heterodimers, to induce dilation of the intracebral arterioles.[33] In HEK 293FT rat brain xenografts, they were able to achieve 228.6 ± 71.8% increase in signal relative to control cells after 24 h post cell injection.

Mgnetic resonance spectroscopy (MRS) reporters have been used to quantify relative levels of important drug and biomarker metabolites. MRS detects the varying resonant frequencies a nuclei of interest experiences due to the influence of surrounding electrons. Although not mentioned first in this introduction, creatine kinase (CK) was the first reported genetically encodable MRI reporter responsible for the conversion of creatine to phosphocreatine through ATP hydrolysis. Koretsky et al, measured the production of phosphocreatine and ADP levels in living mice using $^{31}$P MRS. Using this technique, they calculated 0.059 ± 0.004 μmol/g (wet weight of tissue) of ADP, a molecule of particular interest in understanding its role in regulating liver metabolism.[34] The beauty of MR techniques is in their versatility to detect any paramagnetic nuclei given the respective coil has been machined. $^{19}$F MRS has been used to monitor prodrug 5-fluorocytosine (5-FC) metabolism into chemotherapeutic 5-fluorouracil (5-FU) by the expression of the cytosine deaminase (CD) transgene. Stegman et al. were able to measure the rate constants for 5-FC to 5-FU conversion in addition to the metabolism and efflux of 5-FU in subcutaneous tumor models.[35]

These first-in-class MRI reporters, including the reporters in the next section, pioneered the creativity and careful engineering in capturing biomolecular events

noninvasively. The literature mentioned here have laid the foundations for current use of these same reporters. Since their initial showcase, researchers have extended the work on of these MRI reporters with increased sensitivity, dynamic range in biosensor developments, and in vivo applications.[36-40]

**E. Establishing Aquaporins as a new MRI Reporter**

Currently, the MRI community is in need for an MRI reporter that mimics the ease-of-use as green fluorescent protein (GFP) to push forth the benefits MRI has to offer as a viable imaging methodology. GFP has many qualities that an MRI analog would greatly benefit from: 1) no administration of an exogenous molecule to produce a signal 2) expression from a single gene 3) non-toxic to cells (4) metal-free and (5) sub-µM sensitivity. So far, some of the previously mentioned reporters require addition of paramagnetic contrast agents or ions to produce enough signal, which as a side effect increases cellular toxicity. For some of the non-metallic reporters, although they don't need exogenous agents to produce an MR signal, as a result, they suffer from MR sensitivity. A new class of MRI reporters using human water channels known as aquaporins have emerged as a step in right direction to become the MRI analog of GFP.

Mentioned earlier in the introduction, MRI can be used to detect the diffusion of water protons. It would be reasonable then to hypothesize the overexpression of water transporters to influence the contrast produced in within a voxel of engineered cells in contrast to nonengineered cells. Schilling et al. used a unique diffusion imaging technique known as filter-exchange imaging (FEXI) used to measure the apparent exchange rate (AXR) between extracellular and intracellular water diffusion. A diffusion filter is used to remove the magnetization of fast diffusing extracellular water and subsequently measures the return of the magnetization to equilibrium after the exchange of water from the

extracellular to intracellular space. They measured a 121.7 ± 59.3% increase in lentiviral transduced rat brain tissue expressing a urea transporter-B (UT-B) aquaporin.[41] Similarly, human aquaporin-1 (hAQP1) developed by Mukherjee et al. used DWI to measure water exchange improving signal contrast. They used a doxycycline inducible cytomegalovirus promoter to induce hAQP1 expression achieving 39 ± 6.5% signal decrease after 48 h incubation with 75 µg doxycycline injection in CHO mouse brain xenografts.[42] This signal contrast was achieved with an impressive 3 µM AQP1 on the cellular membrane contrast to the non-metallic CEST reporters achieving about 5-10% signal with millimolar concentrations of reporter expression. Additionally, concentrations as low as 0.5 µM of hAQP1 were able to be detected using DWI in cell pellets. hAQP1 has also been shown to be non-toxic to cells verified by resazurin assay, ATP content, LDH release, and ethidium staining.

With growing interest in understanding molecular events in deeper-seated tissue such as the gut microbiome and neurobiology, it is paramount that the development of MRI reporters is supported in its efforts to provide viable and sensitive molecular imaging capabilities. Aquaporins have promising attributes to provide sensitive MR signal endogenously without the use of toxic metals and can potentially offer the same ease-of-use GFP. This thesis attempts to establish hAQP1 as the MRI analog reporter to GFP by engineering its applications towards dynamic and sensitive imaging capabilities.

**F. References**


1. Bitar, R.; Leung, G.; Perng, R.; Tadros, S.; Moody, A. R.; Sarrazin, J.; McGregor, C.; Christakis, M.; Symons, S.; Nelson, A.; et al. MR Pulse Sequences: What Every Radiologist Wants to Know but Is Afraid to Ask. *RadioGraphics* **2006**, *26* (2), 513-537. DOI: 10.1148/rg.262055063 (acccessed 2021/09/21).
2. Bellin, M.-F. MR contrast agents, the old and the new. *European Journal of Radiology* **2006**, *60* (3), 314-323. DOI: https://doi.org/10.1016/j.ejrad.2006.06.021.
3. Haughton, V. M.; Rimm, A. A.; Czervionke, L. F.; Breger, R. K.; Fisher, M. E.; Papke, R. A.; Hendrix, L. E.; Strother, C. M.; Turski, P. A.; Williams, A. L. Sensitivity of Gd-DTPA-enhanced MR imaging of benign extraaxial tumors. *Radiology* **1988**, *166* (3), 829-833. DOI: 10.1148/radiology.166.3.3340779 (acccessed 2021/09/21).
4. Woods, M.; Kiefer, G. E.; Bott, S.; Castillo-Muzquiz, A.; Eshelbrenner, C.; Michaudet, L.; McMillan, K.; Mudigunda, S. D. K.; Ogrin, D.; Tircsó, G.; et al. Synthesis, Relaxometric and Photophysical Properties of a New pH-Responsive MRI Contrast Agent: The Effect of Other Ligating Groups on Dissociation of a p-Nitrophenolic Pendant Arm. *Journal of the American Chemical Society* **2004**, *126* (30), 9248-9256. DOI: 10.1021/ja048299z.
5. Hanaoka, K.; Kikuchi, K.; Urano, Y.; Nagano, T. Selective sensing of zinc ions with a novel magnetic resonance imaging contrast agent. *Journal of the Chemical Society, Perkin Transactions 2* **2001**, (9), 1840-1843, 10.1039/B100994J. DOI: 10.1039/B100994J.
6. Moats, R. A.; Fraser, S. E.; Meade, T. J. A "Smart" Magnetic Resonance Imaging Agent That Reports on Specific Enzymatic Activity. *Angewandte Chemie International Edition*

*in English* **1997**, *36* (7), 726-728, https://doi.org/10.1002/anie.199707261. DOI: https://doi.org/10.1002/anie.199707261 (acccessed 2021/11/22).

7. Namkung, S.; Zech, C. J.; Helmberger, T.; Reiser, M. F.; Schoenberg, S. O. Superparamagnetic iron oxide (SPIO)-enhanced liver MRI with ferucarbotran: Efficacy for characterization of focal liver lesions. *Journal of Magnetic Resonance Imaging* **2007**, *25* (4), 755-765, https://doi.org/10.1002/jmri.20873. DOI: https://doi.org/10.1002/jmri.20873 (acccessed 2021/09/23).
8. Josephson, L.; Perez, J. M.; Weissleder, R. Magnetic Nanosensors for the Detection of Oligonucleotide Sequences. *Angewandte Chemie International Edition* **2001**, *40* (17), 3204-3206, https://doi.org/10.1002/1521-3773(20010903)40:17<3204::AID-ANIE3204>3.0.CO;2-H. DOI: https://doi.org/10.1002/1521-3773(20010903)40:17<3204::AID-ANIE3204>3.0.CO;2-H (acccessed 2021/09/23).
9. Perez, J. M.; Josephson, L.; O'Loughlin, T.; Högemann, D.; Weissleder, R. Magnetic relaxation switches capable of sensing molecular interactions. *Nature Biotechnology* **2002**, *20* (8), 816-820. DOI: 10.1038/nbt720.
10. Atanasijevic, T.; Shusteff, M.; Fam, P.; Jasanoff, A. Calcium-sensitive MRI contrast agents based on superparamagnetic iron oxide nanoparticles and calmodulin. *Proceedings of the National Academy of Sciences* **2006**, *103* (40), 14707. DOI: 10.1073/pnas.0606749103.
11. Louie, A. Y.; Hüber, M. M.; Ahrens, E. T.; Rothbächer, U.; Moats, R.; Jacobs, R. E.; Fraser, S. E.; Meade, T. J. In vivo visualization of gene expression using magnetic resonance imaging. *Nature Biotechnology* **2000**, *18* (3), 321-325. DOI: 10.1038/73780.
12. Weissleder, R.; Simonova, M.; Bogdanova, A.; Bredow, S.; Enochs, W. S.; Bogdanov, A. MR imaging and scintigraphy of gene expression through melanin induction.

*Radiology* **1997**, *204* (2), 425-429. DOI: 10.1148/radiology.204.2.9240530 (acccessed 2021/09/28).

13. Ozbakir, H. F.; Miller, A. D. C.; Fishman, K. B.; Martins, A. F.; Kippin, T. E.; Mukherjee, A. A Protein-Based Biosensor for Detecting Calcium by Magnetic Resonance Imaging. *ACS Sensors* **2021**, *6* (9), 3163-3169. DOI: 10.1021/acssensors.1c01085.
14. Bartelle, B. B.; Szulc, K. U.; Suero-Abreu, G. A.; Rodriguez, J. J.; Turnbull, D. H. Divalent metal transporter, DMT1: A novel MRI reporter protein. *Magnetic Resonance in Medicine* **2013**, *70* (3), 842-850, https://doi.org/10.1002/mrm.24509. DOI: https://doi.org/10.1002/mrm.24509 (acccessed 2021/09/28).
15. Patrick, P. S.; Hammersley, J.; Loizou, L.; Kettunen, M. I.; Rodrigues, T. B.; Hu, D.-E.; Tee, S.-S.; Hesketh, R.; Lyons, S. K.; Soloviev, D.; et al. Dual-modality gene reporter for in vivo imaging. *Proceedings of the National Academy of Sciences* **2014**, *111* (1), 415. DOI: 10.1073/pnas.1319000111.
16. Green, N. M. AVIDIN. 3. THE NATURE OF THE BIOTIN-BINDING SITE. *Biochemical Journal* **1963**, *89* (3), 599-609. DOI: 10.1042/bj0890599 (acccessed 10/3/2021).
17. Tannous, B. A.; Grimm, J.; Perry, K. F.; Chen, J. W.; Weissleder, R.; Breakefield, X. O. Metabolic biotinylation of cell surface receptors for in vivo imaging. *Nature Methods* **2006**, *3* (5), 391-396. DOI: 10.1038/nmeth875.
18. Patrick, P. S.; Rodrigues, T. B.; Kettunen, M. I.; Lyons, S. K.; Neves, A. A.; Brindle, K. M. Development of Timd2 as a reporter gene for MRI. *Magnetic Resonance in Medicine* **2016**, *75* (4), 1697-1707, https://doi.org/10.1002/mrm.25750. DOI: https://doi.org/10.1002/mrm.25750 (acccessed 2021/09/29).

19. Weissleder, R.; Moore, A.; Mahmood, U.; Bhorade, R.; Benveniste, H.; Chiocca, E. A.; Basilion, J. P. In vivo magnetic resonance imaging of transgene expression. *Nature Medicine* **2000**, *6* (3), 351-354. DOI: 10.1038/73219.

20. Genove, G.; DeMarco, U.; Xu, H.; Goins, W. F.; Ahrens, E. T. A new transgene reporter for in vivo magnetic resonance imaging. *Nature Medicine* **2005**, *11* (4), 450-454. DOI: 10.1038/nm1208.

21. Zurkiya, O.; Chan, A. W. S.; Hu, X. MagA is sufficient for producing magnetic nanoparticles in mammalian cells, making it an MRI reporter. *Magnetic resonance in medicine* **2008**, *59* (6), 1225-1231. DOI: 10.1002/mrm.21606 PubMed.

22. Walker, T. G.; Happer, W. Spin-exchange optical pumping of noble-gas nuclei. *Reviews of Modern Physics* **1997**, *69* (2), 629-642. DOI: 10.1103/RevModPhys.69.629.

23. Jayapaul, J.; Schröder, L. Nanoparticle-Based Contrast Agents for (129)Xe HyperCEST NMR and MRI Applications. *Contrast media & molecular imaging* **2019**, *2019*, 9498173-9498173. DOI: 10.1155/2019/9498173 PubMed.

24. Shapiro, M. G.; Ramirez, R. M.; Sperling, L. J.; Sun, G.; Sun, J.; Pines, A.; Schaffer, D. V.; Bajaj, V. S. Genetically encoded reporters for hyperpolarized xenon magnetic resonance imaging. *Nature Chemistry* **2014**, *6* (7), 629-634. DOI: 10.1038/nchem.1934.

25. Lu, G. J.; Farhadi, A.; Szablowski, J. O.; Lee-Gosselin, A.; Barnes, S. R.; Lakshmanan, A.; Bourdeau, R. W.; Shapiro, M. G. Acoustically modulated magnetic resonance imaging of gas-filled protein nanostructures. *Nature Materials* **2018**, *17* (5), 456-463. DOI: 10.1038/s41563-018-0023-7.

26. Farhadi, A.; Ho Gabrielle, H.; Sawyer Daniel, P.; Bourdeau Raymond, W.; Shapiro Mikhail, G. Ultrasound imaging of gene expression in mammalian cells. *Science* **2019**, *365* (6460), 1469-1475. DOI: 10.1126/science.aax4804 (acccessed 2021/09/30).

27. Gilad, A. A.; McMahon, M. T.; Walczak, P.; Winnard, P. T.; Raman, V.; van Laarhoven, H. W. M.; Skoglund, C. M.; Bulte, J. W. M.; van Zijl, P. C. M. Artificial reporter gene providing MRI contrast based on proton exchange. *Nature Biotechnology* **2007**, *25* (2), 217-219. DOI: 10.1038/nbt1277.

28. Perlman, O.; Ito, H.; Gilad, A. A.; McMahon, M. T.; Chiocca, E. A.; Nakashima, H.; Farrar, C. T. Redesigned reporter gene for improved proton exchange-based molecular MRI contrast. *Scientific Reports* **2020**, *10* (1), 20664. DOI: 10.1038/s41598-020-77576-z.

29. Bar-Shir, A.; Liu, G.; Chan, K. W. Y.; Oskolkov, N.; Song, X.; Yadav, N. N.; Walczak, P.; McMahon, M. T.; van Zijl, P. C. M.; Bulte, J. W. M.; et al. Human Protamine-1 as an MRI Reporter Gene Based on Chemical Exchange. *ACS Chemical Biology* **2014**, *9* (1), 134-138. DOI: 10.1021/cb400617q.

30. Jia, X.-Z.; Sun, J.-W.; Ji, G.-J.; Liao, W.; Lv, Y.-T.; Wang, J.; Wang, Z.; Zhang, H.; Liu, D.-Q.; Zang, Y.-F. Percent amplitude of fluctuation: A simple measure for resting-state fMRI signal at single voxel level. *PLOS ONE* **2020**, *15* (1), e0227021. DOI: 10.1371/journal.pone.0227021.

31. Grill-Spector, K.; Knouf, N.; Kanwisher, N. The fusiform face area subserves face perception, not generic within-category identification. *Nature Neuroscience* **2004**, *7* (5), 555-562. DOI: 10.1038/nn1224.

32. Tambini, A.; Ketz, N.; Davachi, L. Enhanced Brain Correlations during Rest Are Related to Memory for Recent Experiences. *Neuron* **2010**, *65* (2), 280-290. DOI: https://doi.org/10.1016/j.neuron.2010.01.001.

33. Desai, M.; Slusarczyk, A. L.; Chapin, A.; Barch, M.; Jasanoff, A. Molecular imaging with engineered physiology. *Nature Communications* **2016**, *7* (1), 13607. DOI: 10.1038/ncomms13607.

34. Koretsky, A. P.; Brosnan, M. J.; Chen, L. H.; Chen, J. D.; Van Dyke, T. NMR detection of creatine kinase expressed in liver of transgenic mice: determination of free ADP levels. *Proceedings of the National Academy of Sciences of the United States of America* **1990**, *87* (8), 3112-3116. DOI: 10.1073/pnas.87.8.3112 PubMed.

35. Stegman, L. D.; Rehemtulla, A.; Beattie, B.; Kievit, E.; Lawrence, T. S.; Blasberg, R. G.; Tjuvajev, J. G.; Ross, B. D. Noninvasive quantitation of cytosine deaminase transgene expression in human tumor xenografts with in vivo magnetic resonance spectroscopy. *Proceedings of the National Academy of Sciences* **1999**, *96* (17), 9821. DOI: 10.1073/pnas.96.17.9821.

36. Szulc, D. A.; Lee, X. A.; Cheng, H.-Y. M.; Cheng, H.-L. M. Bright Ferritin—a Reporter Gene Platform for On-Demand, Longitudinal Cell Tracking on MRI. *iScience* **2020**, *23* (8), 101350. DOI: https://doi.org/10.1016/j.isci.2020.101350.

37. Shapiro, M. G.; Westmeyer, G. G.; Romero, P. A.; Szablowski, J. O.; Küster, B.; Shah, A.; Otey, C. R.; Langer, R.; Arnold, F. H.; Jasanoff, A. Directed evolution of a magnetic resonance imaging contrast agent for noninvasive imaging of dopamine. *Nature Biotechnology* **2010**, *28* (3), 264-270. DOI: 10.1038/nbt.1609.

38. Shapiro, M. G.; Szablowski, J. O.; Langer, R.; Jasanoff, A. Protein Nanoparticles Engineered to Sense Kinase Activity in MRI. *Journal of the American Chemical Society* **2009**, *131* (7), 2484-2486. DOI: 10.1021/ja8086938.

39. Oskolkov, N.; Bar-Shir, A.; Chan, K. W. Y.; Song, X.; van Zijl, P. C. M.; Bulte, J. W. M.; Gilad, A. A.; McMahon, M. T. Biophysical Characterization of Human Protamine-1

as a Responsive CEST MR Contrast Agent. *ACS Macro Letters* **2015**, *4* (1), 34-38. DOI: 10.1021/mz500681y.

40. Ohlendorf, R.; Wiśniowska, A.; Desai, M.; Barandov, A.; Slusarczyk, A. L.; Li, N.; Jasanoff, A. Target-responsive vasoactive probes for ultrasensitive molecular imaging. *Nature Communications* **2020**, *11* (1), 2399. DOI: 10.1038/s41467-020-16118-7.
41. Schilling, F.; Ros, S.; Hu, D.-E.; D'Santos, P.; McGuire, S.; Mair, R.; Wright, A. J.; Mannion, E.; Franklin, R. J. M.; Neves, A. A.; et al. MRI measurements of reporter-mediated increases in transmembrane water exchange enable detection of a gene reporter. *Nature Biotechnology* **2017**, *35* (1), 75-80. DOI: 10.1038/nbt.3714.
42. Mukherjee, A.; Wu, D.; Davis, H. C.; Shapiro, M. G. Non-invasive imaging using reporter genes altering cellular water permeability. *Nature Communications* **2016**, *7* (1), 13891. DOI: 10.1038/ncomms13891.

# II. Genetically Encodable Aquaporins for Noninvasive Background-Free MRI

## A. Abstract

A key challenge with improving safety and efficacy of gene and cell-based therapies is the inability to precisely locate and track these therapeutics in the context of living subjects. Optical genetic reporters provide the specificity needed for these technologies but cannot visualize deep-seated tissues in live animals. Reporter genes compatible with magnetic resonance imaging (MRI) achieve excellent depth penetration with a spatial resolution approaching 250 μm. However, detection of cells and gene expression using MRI reporters can be confounded by endogenous background contrast. To this end, we have developed an approach for MRI subtraction-imaging based on chemogenetically degradable water channels known as aquaporins (AQP1). AQP1 was recently introduced as a metal-free MRI reporter that generates contrast by altering transmembrane water exchange. Here, we use small molecule-controlled ligand-induced stabilization (LIS) and ligand-induced degradation (LID) tags to conditionally degrade AQP1 using the proteasomal degradation machinery found in cells, thereby enabling on-demand control over AQP1 contrast. To implement this technique, we acquire two sets of images: (1) an "off" image of the degraded reporter (2) an "on" image stabilizing the reporter. By digitally subtracting the "off" and "on" images, we can remove background contrast, enabling specific detection of AQP1 signal. We screened 7 degradation tagged AQP1 constructs in 4 cell types and identified the most optimal degron FKBP12LIS for *in vitro* and *in vivo* MRI subtraction imaging.

## B. Introduction

The ability to localize and track gene and cell-based therapeutics in a living context using genetically encodable MRI reporters has aided in understanding cellular phenomena and prognosis of disease states. Unlike their synthetic counterparts, genetically encodable MRI reporters do not get diluted with cell division and allow for long term tracking of cell proliferation, migration, and differentiation.[1] A few of the early developed MRI reporters such as β-Gal, an enzyme that activates a gadolinium-based contrast agent termed EGadMe, engineered transferrin receptor (ETR) a membrane transporter of superparamagnetic nanoparticles, and iron mineralizing heavy chain ferritin were used to evaluate cell proliferation.[2-4] Additionally, heavy chain ferritin has been used to track cell migration and differentiation.[5-7] Since then, some of these earlier and nascent reporters have been further engineered using clever synthetic and biosynthetic tools to improve overall sensitivity and safety profile for these same applications.[8-10]

Complementary to increasing reporter sensitivity through thoughtful engineering, signal enhancement of MRI reporters has been achieved using a technique known as subtraction imaging. This process involves acquiring a pre-enhanced image and a post-enhanced image after injection of the gadolinium contrast agent. Subsequently, the two sets of images are digitally subtracted, thereby removing signal contributions from the background and enhancing the localized reporter signal. This technique has improved diagnostics of detecting tumor lesions and hemorrhagic cysts.[11] However, synthetic-based reporters fail to provide any genetic information and some genetically encodable reporters suffer from low sensitivity in the presence of human pathologies and abnormalities.[12]

To address the sensitivity issue, we looked towards a recently established MRI reporter known as aquaporin-1 (AQP1). AQP1 expressing xenografts have shown viable

MRI signal relative to wild-type xenografts in mice brains expressed from a single gene without the need for paramagnetic metal supplementation.[13] Due to its simplistic properties analogous to fluorescent proteins requiring only the expression of the reporter, we have sought to use subtraction imaging as a proof of concept to enhance the MRI sensitivity of AQP1. Subtraction imaging can easily be done obtaining a pre-image where the reporter has not been induced for expression and subsequently obtaining a post-image after inducing reporter expression. However, this restricts subtraction imaging of genetically encodable reporters to using only inducible promoters and limits the longitudinal and repetitive imaging capabilities MRI provides within the same patient. Thus, to overcome these restrictions, we have fused ligand responsive degradation tags known as degrons to AQP1 to confer switch-like readout.

There are two classes of degrons that induce protein stabilization or protein degradation in the presence of cognate ligand.[14] To highlight a couple, FK506- and rapamycin-binding protein (FKBP12) was engineered to have an F36V mutation that created a "hole" in the destabilizing domain allowing tighter ligand binding into this pocket as opposed to wild-type FKBP enabling orthogonal protein stabilization.[15] Laura Banaszynski et al. took this variant through several rounds of selection and created an additional L106P mutation that bound a more intracellular penetrating and potent stabilizing ligand known as Shield-1.[16] In contrast, a plant-based degron known as auxin-inducible degron (AID) has been used in mammalian cells to confer protein degradation in the presence of plant hormone ligand indole-3-acetic acid.[17] Ectopic expression of an F-box transport inhibitor response 1 (TIR1) protein found only in plant species is required to hijack the preexisting proteasomal degradation machinery found endogenously in mammalian cells for ligand induced protein degradation to occur. In both cases, degrons allow for modulating reporter signals at the

protein level rather than at the transcriptional level permitting faster contrast change in repetition. This work enables sensitive gene expression in deeper-seated tissue with a tunable nonmetallic reporter.

## C. Results

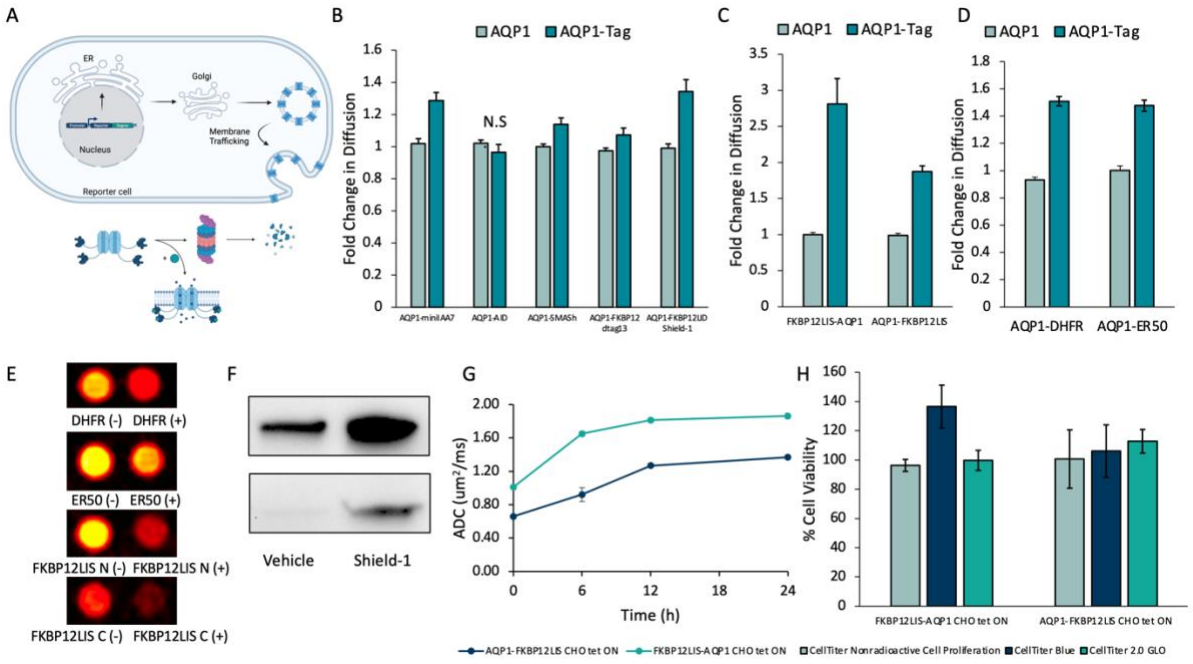


**Figure II.1. Degradation of AQP1 in CHO tet ON cells.** (A) Proposed mechanism of tagged-AQP1 degradation and ligand stabilization. (B) Diffusion fold change with and without ligand for LID tags. $P < 0.05$, n ≥ 4 biological replicates, t-test. (C) Diffusion fold change in N/C of FKBP12LIS tagged-AQP1. $P < 0.05$, n ≥ 4 biological replicates, t-test. (D) Diffusion fold change with and without ligand for LIS tags. $P < 0.05$, n ≥ 4 biological replicates, t-test. (E) Representative diffusion-weighted images of cell pellets with and without ligand. (F) Membrane fractioned western blot of N/C FKBP12LIS tagged-AQP1. (G) Kinetic profile of Shield-1 stabilization in N/C FKBP12LIS tagged-AQP1. n = 3 biological replicates. (H) Cell toxicity profile of Shield-1 in N/C

FKBP12LIS tagged-AQP1. n = 3 biological replicates. Error bars are represented as standard error mean (s.e.m.).

**1. Degradable aquaporins function as switchable contrast agent under ligand control**

To determine if degrons fused to AQP1 would alter water diffusion under ligand control at the protein level, we inserted both LID and LIS degrons to the C-terminus of AQP1 to actuate protein degradation with chemogenetic control downstream of a doxycycline-inducible cytomegalovirus (CMV) promoter in CHO tet ON cells that express a reverse tetracycline transactivator (rtTA) (Figure 1A).[16,18-23] We chose to initially place degrons on the C-terminus, because the number of amino acid residues of AQP1 protruding from the inner leaflet of the cell membrane to the C-terminus is longer than the N-terminus end, thus potentially allowing easier recognition for protein degradation. Lentiviruses were used to engineer CHO tet ON cells for stably expressing tagged-AQP1 along with enhanced green fluorescent protein (EGFP) necessary for subsequent fluorescence-activated cell sorting. After sorting, stable cells were grown with either 0.1% DMSO vehicle control or cognate ligand for 24 h and pelleted for diffusion weighted imaging (DWI). Diffusion-weighted images were analyzed to determine the apparent diffusion coefficient which is a direct measurement of the relative levels of tagged-AQP1 with or without ligand based off the signal intensities from DWI.

Among the LID degrons, miniIAA7 and FKBP12LID had the highest increase the fold change in diffusion of 26.4 ± 1.1% and 35.6 ± 1.2% relative to AQP1 control with and without ligand, respectively (Figure 1B). Given that the FKBP12LID construct provided the highest fold change out of the LID constructs, we pursued an LIS version of the degron placed on both termini of AQP1 achieving much greater increase in fold

changes of 181.1 ± 5.8% and 89.2 ± 2.7% for the N-terminus and C-terminus placements, respectively, which demonstrates the utility in this platform (Figure 1C). Inspired by the efficiency of AQP1 modulation with LIS degrons, we screened two other degrons DHFR and ER50 achieving a modest 67.1 ± 1.6% and 47.5 ± 1.9% increase in diffusion fold change, respectively (Figure 1D).

Moving forward, we focused on using LIS constructs for subsequent experiments given their higher degradation efficiencies relative to LID constructs. Representative images of tagged-AQP1 constructs showed a dark contrast after addition of cognate ligand signifying stabilization of AQP1 on the membrane (Figure 1E). To probe tagged-AQP1 levels on the cell membrane based off western blot, we membrane fractioned FKBP12LIS tagged AQP1 from CHO tet ON cells that were either treated with 0.1% DMSO vehicle or 1 μM Shield-1 and found the relative intensity of cells treated with vehicle had less expression and membrane trafficked FKBP12LIS tagged-AQP1 compared to the Shield-1 treated cells (Figure 1F). We were interested in how quickly ligand stabilization of FKBP12LIS tagged-AQP1s occurred and found saturation in diffusion signal within 6-12 h after Shield-1 administration, which is useful for capturing gene expression within a reasonable timeframe (Figure 1G). This signified protection of ligand stabilized tagged-AQP1 from the protein degradation machinery. As with any reporter system, cell toxicity tests were conducted on engineered CHO tet ON cells expressing FKBP12LIS tagged-AQP1 with or without Shield-1 displaying minor cell toxicity important for imaging healthy, native cellular activity important for downstream applications (Figure 1H).

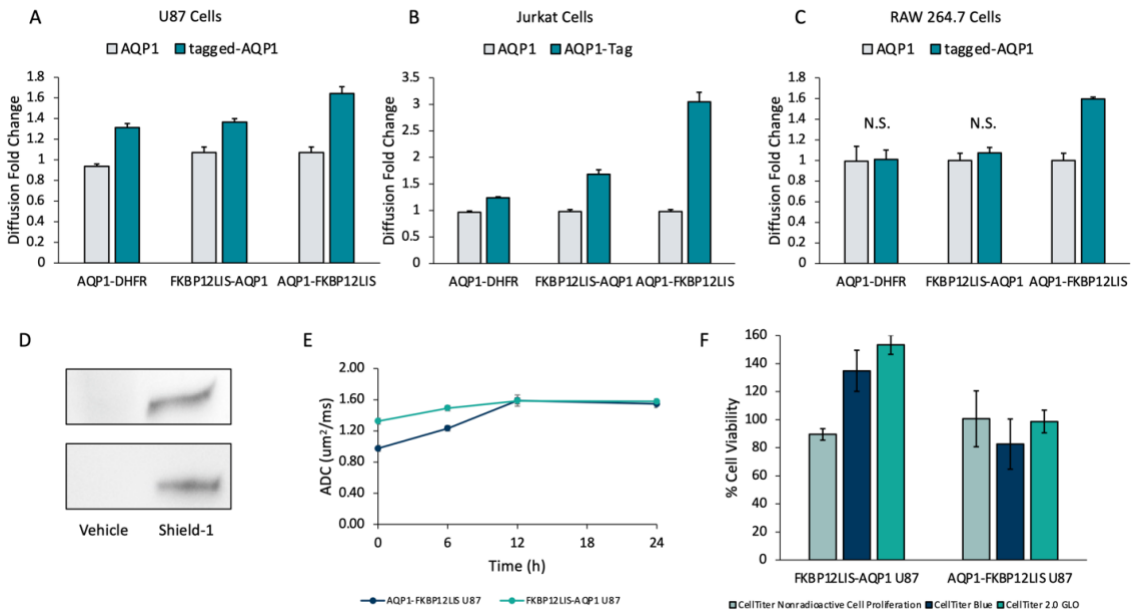


**Figure II.2. Erasable AQP1 in diverse cell types.** Diffusion fold changes of LIS tagged-AQP1 in (A) U87 cells $P < 0.05$, n = 4 biological replicates, t-test. (B) Jurkat cells $P < 0.05$, n = 4 biological replicates, t-test. (C) RAW 264.7 cells $P < 0.05$, n = 4 biological replicates, t-test. (D) Western blot of N/C FKBP12LIS tagged-AQP1 U87 cells. (E) Kinetic profile of Shield-1 stabilization in N/C FKBP12LIS tagged-AQP1 U87 cells. n = 3 biological replicates. (F) Cell toxicity profile of Shield-1 in N/C FKBP12LIS tagged-AQP1 in U87 cells. n = 3 biological replicates. Error bars are represented as standard error mean (s.e.m.).

## 2. Versatility of degradable aquaporins in several cell types

DHFR and FKBP12LIS showed the most efficient fold changes in diffusion in CHO cells and their cognate ligands have been proven to cross the blood-brain barrier.[20,24] We therefore engineered DHFR and both N and C terminus FKBP12LIS tagged AQP1 in human U87 glioblastoma, human Jurkat acute T cell leukemia, and murine RAW 264.7 cells to test the versatility of this platform in diverse cell types. We found the same

increasing diffusion fold change trend across all cells (Figure 2A,B,C). Interestingly, C-terminal FKBP12LIS tagged-AQP1 had the highest diffusion fold changes across these cells and DHFR and N-terminal FKBP12LIS tagged-AQP1 show non-significant diffusion contrast with and without Shield-1 in RAW 264.7 cells (Figure 2C). This observation is expected given the differences in degron placement affect reporter degradation fate.[16,19,20,22,26] Given the wide use of U87 glioblastoma cells as a model for aggressive tumor characteristics, we focused further characterization of the platform using this cell line.[27,28] In addition, U87 is known to have relatively higher expression of endogenous aquaporin background, which is an ideal cell line to demonstrate the removal of high background signal contributions.[29] FKBP12LIS placed on either terminus of AQP1 exhibited higher expression and membrane trafficking in the presence of Shield-1 than with vehicle (Figure 2D) and reached saturating levels of stabilization within 6-12 h post Shield-1 addition (Figure 2E). In addition, expression of FKBP12LIS-tagged AQP1 with the addition of 1 µM Shield-1 in U87 cells showed little to no toxicity (Figure 2F).

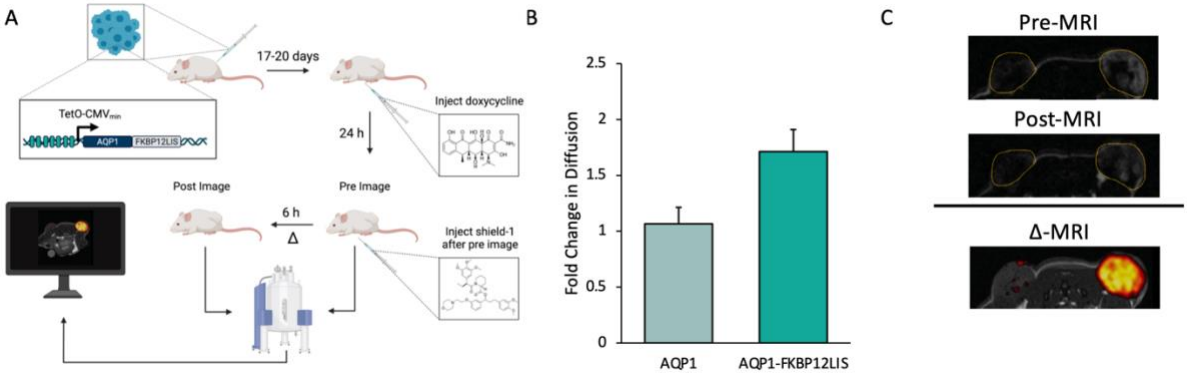


**Figure II.3. Erasable AQP1-FKBP12LIS CHO tet ON xenografts in vivo.** (A) Workflow for obtaining diffusion-weighted in vivo subtraction images of xenografts. (B) Diffusion fold change of AQP1 control CHO tet on and AQP1-FKBP12LIS CHO tet ON

xenografts. $P < 0.05$, n = 4 biological replicates, t-test. (C) Representative subtraction image of bilateral flank tumors. Error bars are represented as standard error mean (s.e.m.).

### 3. Erasable AQP1 xenografts enable subtraction imaging in vivo

Based off the in vitro work, we used the C-terminal FKBP12LIS tagged AQP1 construct for small animal model imaging as it had shown the most promising fold changes in diffusion in all cell types. We first injected AQP1-FKBP12LIS CHO tet ON cells subcutaneously in the flanks of immunocompromised NOD scid gamma (NSG) mice. At sufficient tumor growth, mice were intraperitoneally (i.p.) injected with 50 mg/kg body weight of doxycycline 24 h prior to imaging. After obtaining a pre-ligand anatomical and DW image, mice were i.p. injected with 10 mg/kg body weight of Shield-1 and allowed 6 h of rest for Shield-1 biodistribution. Another image was taken after tagged-AQP1 stabilization where the fold changes in diffusion in FKBP12LIS tagged-AQP1 tumors increased by 60.9 ± 11.1% relative to AQP1 control after (Figure 3B). Further image post-processing was performed showing a representative subtraction image (Figure 3C). N-terminal FKBP12LIS tagged-AQP1 CHO tet ON showed nonsignificant fold change in diffusion after Shield-1 injection (Supplementary Figure S6).

## D. Discussion

Using the pre-established metal-free AQP1 reporter for diffusion-weighted MRI[13], we further engineered AQP1 to provide switch-like contrast using ligand-responsive degradation tags. Having on-demand contrast enhancement allows for feasible subtraction imaging to take place. AQP1 is best suited for this application given that it does not require metal supplementation unlike metal-dependent reporters that naturally have increased background

signal contributions due to the non-specific biodistribution of metals to adjacent native cells.[4,30] Several degrons have been screened to shown AQP1-dependent contrast in on and off states in four different cell types with relatively no cell toxicity in the presence of stabilizing ligand. Through the screening process, we found FKBP12LIS to be the most efficient degron enabling saturating levels AQP1 stabilization within 6-12 hours post Shield-1 administration. One limitation of this system is the time window for the biodistribution of modulating ligand to reach target cells. This would prevent faster imaging acquisitions, which would necessitate further molecular engineering of AQP1 to allow pore gating of water transport in the presence of stimulant. A plant-based aquaporin with remarkably similar homology to AQP1 known as SoPIP2;1 could be a reasonable starting point with further modifications to adapt this construct in mammalian cells.[31] Alternatively, LID constructs can be engineered to induce faster degradation in the presence of ligand and optimizing proteasomal degradation machinery to achieve the same purpose.[18,21,32]

We have demonstrated subtraction imaging capabilities as a proof of concept *in vivo* using flank xenograft tumors, minimizing the endogenous background noise. Additionally, we plan to incorporate the FKBP12LIS tagged-AQP1 xenografts in the brain where there is more interest as a model organ to image. This would allow for easier biodistribution of Shield-1 stabilizing ligand to the brain than subcutaneous tumors due to the leaky vasculature formed during tumor maturation exposing blood-brain-barrier permeability thus, potentially improving higher AQP1-dependent signal fold changes.[33]

Furthermore, the use of degrons fused to AQP1 allows for dynamic contrast enhancement (DCE), which can be thought of as subtraction imaging with multiple timepoints within the same test subject.[34] This would greatly maximize the advantages of MRI to image whole volumes of organs, unlike the current optical imaging tools that have

limited field-of-view especially when imaging neuronal stimulation in the brain, although with exceptionally high-resolution that MRI could only dream of obtaining.[35] Additionally, using this technology could potentially enable "time-locking" gene-expression by induction of behavioral stimuli.[36] This is achieved by AND-gate logic such that if a stimulus is applied and simultaneously the stabilizing ligand is administered, then AQP1 signal is thereby time-locked the moment when the stimulus was applied. In our case, we have shown doxycycline-induced expression to represent a behavioral stimulus introduced by the user and capturing the triggering event with Shield-1. This platform could ensure non-specific signals are not captured before the user-defined time point and permit longitudinal studies for tracking behavioral responses within the same patient with high sensitivity. All in all, our AQP1 degron technology enables high switch-like contrast with dynamic imaging capabilities that will unlock undiscovered knowledge in the field of biomedicine.

## E. Materials and Methods

### 1. Construction of erasable aquaporin expressing cell lines

DHFR (29326, Addgene), ER50 (37261, Addgene), FKBP12LIS (17416, Addgene), FKBP12LID (31767, Addgene), miniIAA7 (129721, Addgene), and SMASh (68853, Addgene) degradation tags were PCR amplified with Q5 High-Fidelity 2X Master Mix (M0492, NEB) and Gibson assembled (E2611, NEB) into a lentiviral vector either directly downstream or upstream AQP1. Tagged-AQP1 expression were controlled by a doxycycline-regulated CMV (26431, Addgene) or constitutive EF1a (60058, Addgene) promoters. Ectopic expression of AtFB2 (129718, Addgene) and OSTIR1 (Addgene, 72834) F-box proteins were cloned downstream of doxycycline-regulated CMV promoter with an mCherry marker necessary for AQP1-miniIAA7 and AQP1-AID degradation machinery, respectively. Depending on the placement of the degradation tag on AQP1, the FLAG tag was cloned on the opposite termini. Enhanced GFP or mCherry located downstream of the IRES assisted in fluorescence-activated cell sorting (SH800, Sony) for enriching lentiviral engineered cell lines after transduction.

Lentiviral packaging was achieved by adding 22 µg of packaging plasmid to express the capsid genes from a CMV promotor, 22 µg of constructed plasmid harboring gene of interest (AQP1-degron-IRES-EGFP, degron-AQP1-IRES-EGFP) flanked by long terminal repeat sequences, 4.5 µg of VSV-G plasmid that expresses vesicular stomatitis virus G proteins to provide wide tropism of lentiviruses created, and 150 mM sterile filtered NaCl up to 600 µL in a 1.5 mL tube. In a separate 1.5 mL tube, 485 µL of 2.58 mg/mL 25 kDa linear polyethyleneimine (23966-1, Polysciences Inc.) and 115 µL of 150 mM sterile filtered NaCl were added together. The two tubes were mixed for a maximum of 12 min to form polymeric particles containing lentiviral plasmids and was added to a

10 cm plate of 70% confluent HEK 293T cells (ATCC). Roughly, 17 to 24 h post transfection, 10 mM sodium butyrate was added to the cell media of transfected cells to further assist in the expression of packaging genes. Viral production occurred for approximately 72 h followed by centrifugation of HEK 293T cell debris at 500 g for 10 min. Viral supernatant was collected and mixed at one-tenth the volume of Lenti-X concentrator (631232, Takara) to sit at 4°C for roughly 24 h. Lentiviral particles were centrifuged at 1500 g for 45 min at 4°C and resuspended in 200 µL of DMEM medium. Immediately after, concentrated lentiviral particles were used to transduce CHO tet ON (Takara Bio), Jurkat, U87, and RAW 264.7 (ATCC) cells to generate stable cell lines. For adherent cell lines, cells were grown to 70-80% confluency in a six-well plate format. After 24 h, spent cell media was aspirated from the wells and replaced with 800 µL of viral solution containing the following: concentrated lentiviral particles, 8 µg/mL polybrene (sc-134220, Santa Cruz Biotechnology), and the remaining volume with DMEM media. The cells were then spinfected at 1048 g for 90 min at 30°C. After the spinfection, plates were returned to the 37°C incubator for 48 h before checking for green fluorescent cells. CHO tet ON transduced cells after spinfection were treated with 1 µg/mL doxycycline hyclate (D9891-1G, Sigma Aldrich) to induce EGFP expression over 48 h. For Jurkat suspension cells, cells were plated at 70-80% confluency in a six-well plate the same day as viral concentration. Jurkat cells were then centrifuged at 300 g for 10 min and resuspended the pellet with 800 µL of viral solution containing the following: 25 µL of concentrated lentiviral particles, 8 µg/mL polybrene, and the remaining volume with DMEM media. The cells were then spinfected at 1048 g for 90 min at 30°C and plates were returned to the 37°C incubator.

AQP1 control cell lines and lentiviral plasmids were acquired from the principal investigator's previous lab (Caltech). DMEM (D5648-50L, Sigma Aldrich) and RPMI (1187920, Thermo Fisher) cell media were supplemented with 10% FBS (10437-028, Gibco), 1 mM sodium pyruvate (S8636-100ML, Sigma-Aldrich), and 100 units/mL penicillin and 100 µg/mL streptomycin (P4333-100ML, Sigma-Aldrich). Periodically, cell lines were checked for Mycoplasma contamination using the MycoAlert Plus Mycoplasma Detection Kit (LT07-701, Lonza).

**2. Determination of cell viability**

Cell viability was measured using three different 96-well plate viability assays. CytoTox-ONE Homogeneous Membrane Integrity Assay (G7890, Promega) was used to measure lactate dehydrogenase release, CellTiter-GLO 2.0 Cell Viability Assay (G9241, Promega) was used to measure ATP presence, and CellTiter-Blue Cell Viability Assay (G8080, Promega) was used to measure resazurin reduction. For each assay, cells were grown until 80-90% confluency in 96-well plates per well and mixed with respective assay reagent amounts per manufacturer's protocol. Fluorescence (resazurin reduction and lactate dehydrogenase release) and luminescence (ATP content) were measured using a Tecan Spark fluorescence plate reader using an excitation wavelength of 560 nm and emission filter set to 590 nm for fluorescence. Integration time for luminescence measurements was set to 1 s.

**3. Membrane Fractioned Western blot for tagged-AQP1 expression in stabilized and destabilized states**

Relative FKBP12LIS tagged-AQP1 expression in destabilized and stabilized states were imaged via western blotting. Engineered CHO tet ON cell were treated with 1 µg/mL doxycycline for 24 h to induce protein expression. The following day, vehicle

control plates of FKBP12LIS tagged AQP1 CHO tet ON cells were exposed to 0.1% DMSO and FKBP12LIS tagged AQP1 CHO tet ON cells were exposed to 1 µM Shield-1 (AOB1848, Aobious) dissolved in DMSO for 24 h. The same procedure was performed for engineered U87 cells without the need for doxycycline induction. Membrane fractions were isolated using ProteoExtract native membrane protein extraction kit (444810, EMD Millipore) and concentrated using 10 kDa Amicon Ultra-15 Centrifugal Filters (R1CB10908, EMD Millipore). Total protein concentration was quantified using a BSA assay. Protein samples of 20 µL were denatured in equal volume of 2X Laemmli (1610737, Biorad) and 5% beta-mercaptoethanol (63689-25ML-F, Sigma) solution at 37°C for at least 1 h followed by boiling at 95°C for 8 min and resolved on a pre-casted denaturing SDS-PAGE gel (4568094, Biorad) at 120 V for 45 min at 4°C. The gel was then transferred to a polyvinylidene difluoride membrane (170-4274, Biorad) using a Biorad Transblot Turbo and blocked in 50 mL of TBST containing 5% (w/v) non-fat dried milk (1706404, Biorad) for 1 h. Afterwards, the blot was stained overnight in 50 mL of 1 µg/mL mouse anti-FLAG primary antibodies (F1804-200UG, Sigma) in 5% (w/v) non-fat dried milk TBST solution at 4°C and subsequently washed three times with 50 mL of TBST for 15 min each. The blot was then probed with 50 mL of 0.5 µg/mL horseradish peroxidase-conjugated goat anti-mouse IgG secondary antibodies (TL280988, Thermo Fisher) in 5% (w/v) non-fat dried milk TBST solution and further washed with 50 mL of TBST for 15 min repeated 3 times. Signal detection was achieved using the Clarity Western ECL Substrate (170-5060, Biorad). As a protein ladder, 5 µL of WesternSure Pre-stained chemiluminescent Protein Ladder (926-98000, LI-COR) was used. All protein samples with and without Shield-1 ligand were standardized to the same amount based off a BSA assay to ensure comparable relative band intensities.

**4. Biotinylation quantification assay of tagged-AQP1 expression in stabilized and destabilized states**

Engineered CHO tet ON cells were seeded with 1µg/mL doxycycline in a 6-well plate format such that they would be 80% confluent within 48 h. The next day, vehicle control plates were exposed to 0.1% DMSO or 1 µM Shield-1 for 24 h. The same procedure was performed for engineered U87 cells without the need for doxycycline induction. On the third day, the cells were washed with 1 mL of 1X PBS three times and 600 µL of 0.5 mg/mL EZ-link biotinylation reagent (PIA39258, Thermo Scientific) was added to the cells for 30 min at 4ºC. After the allotted time, the cells were washed with 1X PBS three times. The cells were lysed using RIPA/protease cocktail inhibitor cell lysis kit (sc-24948, SantaCruz Biotech). The lysate samples were concentrated and buffer exchanged with 20 mM HEPES pH 7.4 by centrifuging three times at 14,000 g for 10 min at 4˚C using 10 kDa amicon ultra centrifugal filter units (UFC501024, EMD Millipore). After concentrating and buffer exchanging, the total protein concentration was calculated using a BSA assay. At this point, the wells going to be used on the pre-blocked 96-well NeutrAvidin coated white plates (PI15216, Thermo Scientific) were washed three times with 200 µL of 1X TBST. Total lysate samples standardized to the same amount for each tagged-AQP1 and cell line pair were added to the wells and incubated for 2 h at ambient temperature. The wells were then washed three times with 200 µL of TBST solution. Afterwards, the wells were incubated with 100 µL of 1 µg/mL mouse anti-FLAG primary antibodies (F1804-200UG, Sigma) in 5% (w/v) non-fat dried milk TBST solution at ambient temperature for 30 min and subsequently washed three times with 200 µL of TBST. The samples were then probed with 100 µL of 0.5 µg/mL horseradish peroxidase-conjugated goat anti-mouse IgG secondary antibodies (TL280988, Thermo Fisher) in 5%

(w/v) non-fat dried milk TBST solution at ambient temperature for 30 min and further washed three times with 200 µL of TBST. Chemiluminescent signal detection was achieved using 100 µL of Clarity Western ECL Substrate solution (170-5060, Biorad).

**5. Diffusion-weighted MRI ADC fold change measurements of cell pellets**

Cells were seeded such that they were fully confluent within 48 h. Engineered CHO tet ON cells required 1 µg/mL doxycycline the same day of seeding. After 24 h, cells were treated with cognate ligand respective to the degron used for an additional 24 h: DHFR, 10 µM TMP (AC455120050, Fisher) in DMSO, ER50, 1 µM 4-OHT (34-1210, Fisher) in DMSO, FKBP12LIS/LID 1 µM Shield-1 (AOB1848, Aobious) in DMSO, miniIAA7, 500 µM Indole-3-Acetic Acid (SIAL-I2886-5G, Neta Scientific) in EtOH, and SMASh, 3 µM ASV (A11295-5, Adooq Biosciences) in DMSO. Post ligand incubation, the cells were harvested into 0.2 mL PCR tubes and spun down at 500 g for 5 min to form a cell pellet. Subsequently, the tubes were placed in 1% agarose molded wells in a phantom and imaged using a Bruker 7T vertical MRI scanner. Diffusion-weighted images were acquired with a 1 to 2 mm-thick horizontal slice through the cell pellets using a stimulated echo DWI pulse sequence with the following parameters: echo time, $T_E$ = 18 ms, repetition time, $T_R$ = 1000 ms, gradient duration, $\delta$ = 5 ms, matrix size = 128 x 128, field of view (FOV) = 5.08 x 5.08 $cm^2$, number of averages = 5, gradient interval, $\Delta$ = 300 ms, strength and time of single-axis diffusion gradients, *b*-values = 0, 400, 600, 800 s $mm^{-2}$. For each value of $\Delta$, ADC was calculated from the slope of logarithmic decay in MRI signal intensity versus b-value. Images were analyzed using custom plugins in Fiji. Least-squares regression fitting was performed using Matlab (2021).

**6. Diffusion-weighted MRI of wild-type and tagged AQP1 stabilization kinetics in cell pellets**

Cells were seeded such that they were fully confluent within 24 h. Engineered CHO tet ON cells required 1 µg/mL doxycycline the same day of seeding. After 24 h, cells were treated with 1 µM Shield-1 in DMSO adding to the 24 h time point cells first and ending with the 0 h time point cells. Starting with 0 h time point cells, the cells were harvested into 0.2 mL PCR tubes and spun down at 500 g for 5 min to form a cell pellet. Subsequently, the tubes were placed in 1% agarose molded wells in a phantom and imaged using a Bruker 7T vertical MRI scanner. This continued until the 6, 12, and 24 h time point cells were imaged. Diffusion-weighted images were acquired and analyzed identical to the section above regarding diffusion-weighted MRI of cell pellets.

**7. Mouse flank tumor xenografts injections**

All animal protocols were approved by the Institutional Animal Care and Use Committee of the University of California, Santa Barbara. For subcutaneous flank xenografts, cells were grown until 80-90% confluency, approximately $10^6$-$10^7$ cells. Cells were spun down at 300 g for 5 min and resuspended in 100 µL of 0.9% saline. Equal volume of Matrigel (80094-328, Corning) was mixed with the cells and loaded into 1 mL syringes with 25G needles stored on ice. AQP1 and tagged-AQP1 cells were injected underneath the left and right hind legs of 5-7 weeks old female NOD/SCID/γ-mice (NSG, Jackson Labs, 005557). Tumor size was measured every other day using calipers and tumor volume was calculated as 0.52 x (short axis)$^2$ x (long axis)$^2$ ensuring the combined mean diameter of both tumors did not exceed 1.5 cm.

## 8. In vivo diffusion-weighted MRI ADC fold change measurements of tumor xenografts

Diffusion-weighted MRI of mouse xenografts were performed using a Bruker 7T vertical bore MRI scanner. Mice were anesthetized using 2-3% isoflurane, respiration and temperature were monitored using a pressure pad (Biopac Systems) and thermal fiber optic rectal probe (OpSens). Heating was applied to the mouse using Bruker's TopSpin v3.2 software controlling the built-in heating filament inside the MiniWB57 coil connected with air tubing. The temperature was set to 316 K and air flow to 800 lph to maintain internal body temperature at 35°C. Gene expression was induced in CHO tet ON engineered cells by injecting 50 mg/kg of doxycycline (NDC 63323-130-02, Fresenius Kabi USA, LLC) intraperitoneally 24 h before imaging. Subcutaneous tumors were allowed to grow for 17-21 days before imaging whereas brain xenografts were imaged 5 days post intracranial injection to monitor tumor growth.

On the day of taking pre- and post-ligand diffusion weighted images, T1-weighted multislice images were taken to identify the tumor using RARE pulse sequence with the following parameters: echo time, $T_E$ = 14.22 ms, repetition time, $T_R$ = 660.2 ms, RARE factor = 4, matrix size = 256 x 256, field of view (FOV) = 3.5 x 3.5 $cm^2$, number of averages = 10, slice thickness 1 mm, number of slices = 10. After identifying a suitable tumor slice image, a diffusion-weighted image was taken at the same position with a 1 mm-thick horizontal slice through the tumor using a stimulated echo DWI pulse sequence with the following parameters: echo time, $T_E$ = 18 ms, repetition time, $T_R$ = 1000 ms, gradient duration, $\delta$ = 5 ms, matrix size = 96 x 96, field of view (FOV) = 3.5 x 3.5 $cm^2$, number of averages = 18, gradient interval, $\Delta$ = 300 ms, strength and time of single-axis diffusion gradients, *b*-values = 0 and 1000 s $mm^{-2}$. After obtaining an anatomical T1-

weighted and diffusion weighted image, the mouse was intraperitoneally injected with 10 mg/kg Shield-1 dissolved in 50% *N*,*N*-dimethylformamide (185884-500, Sigma Aldrich) and 50% 9:1 PEG-400 (PX1286B-2, Sigma Aldrich): Tween-80 (P1754-25ML, Sigma Aldrich) mixture. 6 h post ligand injection, the mouse was imaged again acquiring both anatomical and diffusion-weighted images ensuring mouse placement was exactly in the same position 6 h prior. For each value of Δ, ADC was calculated from the slope of logarithmic decay in MRI signal intensity versus b-value. Images were analyzed using custom plugins in Fiji. Least-squares regression fitting was performed using Matlab (2021).

## F. References


1. Vandsburger, M. H.; Radoul, M.; Cohen, B.; Neeman, M. MRI reporter genes: applications for imaging of cell survival, proliferation, migration and differentiation. *NMR in Biomedicine* **2013**, *26* (7), 872-884, https://doi.org/10.1002/nbm.2869. DOI: https://doi.org/10.1002/nbm.2869 (acccessed 2021/10/18).
2. Louie, A. Y.; Hüber, M. M.; Ahrens, E. T.; Rothbächer, U.; Moats, R.; Jacobs, R. E.; Fraser, S. E.; Meade, T. J. In vivo visualization of gene expression using magnetic resonance imaging. *Nature Biotechnology* **2000**, *18* (3), 321-325. DOI: 10.1038/73780.
3. Weissleder, R.; Moore, A.; Mahmood, U.; Bhorade, R.; Benveniste, H.; Chiocca, E. A.; Basilion, J. P. In vivo magnetic resonance imaging of transgene expression. *Nature Medicine* **2000**, *6* (3), 351-354. DOI: 10.1038/73219.
4. Genove, G.; DeMarco, U.; Xu, H.; Goins, W. F.; Ahrens, E. T. A new transgene reporter for in vivo magnetic resonance imaging. *Nature Medicine* **2005**, *11* (4), 450-454. DOI: 10.1038/nm1208.
5. Campan, M.; Lionetti, V.; Aquaro, G. D.; Forini, F.; Matteucci, M.; Vannucci, L.; Chiuppesi, F.; Di Cristofano, C.; Faggioni, M.; Maioli, M.; et al. Ferritin as a reporter gene for in vivo tracking of stem cells by 1.5-T cardiac MRI in a rat model of myocardial infarction. *American Journal of Physiology-Heart and Circulatory Physiology* **2011**, *300* (6), H2238-H2250. DOI: 10.1152/ajpheart.00935.2010 (acccessed 2021/10/18).
6. Cohen, B.; Ziv, K.; Plaks, V.; Israely, T.; Kalchenko, V.; Harmelin, A.; Benjamin, L. E.; Neeman, M. MRI detection of transcriptional regulation of gene expression in transgenic mice. *Nature Medicine* **2007**, *13* (4), 498-503. DOI: 10.1038/nm1497.

7. Iordanova, B.; Ahrens, E. T. In vivo magnetic resonance imaging of ferritin-based reporter visualizes native neuroblast migration. *NeuroImage* **2012**, *59* (2), 1004-1012. DOI: https://doi.org/10.1016/j.neuroimage.2011.08.068.
8. Lilley, L. M.; Kamper, S.; Caldwell, M.; Chia, Z. K.; Ballweg, D.; Vistain, L.; Krimmel, J.; Mills, T. A.; MacRenaris, K.; Lee, P.; et al. Self-Immolative Activation of β-Galactosidase-Responsive Probes for In Vivo MR Imaging in Mouse Models. *Angewandte Chemie International Edition* **2020**, *59* (1), 388-394, https://doi.org/10.1002/anie.201909933. DOI: https://doi.org/10.1002/anie.201909933 (acccessed 2021/10/18).
9. Szulc, D. A.; Lee, X. A.; Cheng, H.-Y. M.; Cheng, H.-L. M. Bright Ferritin—a Reporter Gene Platform for On-Demand, Longitudinal Cell Tracking on MRI. *iScience* **2020**, *23* (8), 101350. DOI: https://doi.org/10.1016/j.isci.2020.101350.
10. Kelly John, J.; Saee-Marand, M.; Nyström Nivin, N.; Evans Melissa, M.; Chen, Y.; Martinez Francisco, M.; Hamilton Amanda, M.; Ronald John, A. Safe harbor-targeted CRISPR-Cas9 homology-independent targeted integration for multimodality reporter gene-based cell tracking. *Science Advances* *7* (4), eabc3791. DOI: 10.1126/sciadv.abc3791 (acccessed 2021/10/25).
11. Eid, M.; Abougabal, A. Subtraction images: A really helpful tool in non-vascular MRI. *The Egyptian Journal of Radiology and Nuclear Medicine* **2014**, *45* (3), 909-919. DOI: https://doi.org/10.1016/j.ejrnm.2014.04.013.
12. Perlman, O.; Ito, H.; Gilad, A. A.; McMahon, M. T.; Chiocca, E. A.; Nakashima, H.; Farrar, C. T. Redesigned reporter gene for improved proton exchange-based molecular MRI contrast. *Scientific Reports* **2020**, *10* (1), 20664. DOI: 10.1038/s41598-020-77576-z.

13. Mukherjee, A.; Wu, D.; Davis, H. C.; Shapiro, M. G. Non-invasive imaging using reporter genes altering cellular water permeability. *Nature Communications* **2016**, *7* (1), 13891. DOI: 10.1038/ncomms13891.
14. Natsume, T.; Kanemaki, M. T. Conditional Degrons for Controlling Protein Expression at the Protein Level. *Annual Review of Genetics* **2017**, *51* (1), 83-102. DOI: 10.1146/annurev-genet-120116-024656 (acccessed 2021/10/24).
15. Clackson, T.; Yang, W.; Rozamus, L. W.; Hatada, M.; Amara, J. F.; Rollins, C. T.; Stevenson, L. F.; Magari, S. R.; Wood, S. A.; Courage, N. L.; et al. Redesigning an FKBP–ligand interface to generate chemical dimerizers with novel specificity. *Proceedings of the National Academy of Sciences* **1998**, *95* (18), 10437.
16. Banaszynski, L. A.; Chen, L.-c.; Maynard-Smith, L. A.; Ooi, A. G. L.; Wandless, T. J. A Rapid, Reversible, and Tunable Method to Regulate Protein Function in Living Cells Using Synthetic Small Molecules. *Cell* **2006**, *126* (5), 995-1004. DOI: https://doi.org/10.1016/j.cell.2006.07.025.
17. Nishimura, K.; Fukagawa, T.; Takisawa, H.; Kakimoto, T.; Kanemaki, M. An auxin-based degron system for the rapid depletion of proteins in nonplant cells. *Nature Methods* **2009**, *6* (12), 917-922. DOI: 10.1038/nmeth.1401.
18. Bonger, K. M.; Chen, L.-c.; Liu, C. W.; Wandless, T. J. Small-molecule displacement of a cryptic degron causes conditional protein degradation. *Nature Chemical Biology* **2011**, *7* (8), 531-537. DOI: 10.1038/nchembio.598.
19. Chung, H. K.; Jacobs, C. L.; Huo, Y.; Yang, J.; Krumm, S. A.; Plemper, R. K.; Tsien, R. Y.; Lin, M. Z. Tunable and reversible drug control of protein production via a self-excising degron. *Nature Chemical Biology* **2015**, *11* (9), 713-720. DOI: 10.1038/nchembio.1869.

20. Iwamoto, M.; Björklund, T.; Lundberg, C.; Kirik, D.; Wandless, T. J. A General Chemical Method to Regulate Protein Stability in the Mammalian Central Nervous System. *Chemistry & Biology* **2010**, *17* (9), 981-988. DOI: https://doi.org/10.1016/j.chembiol.2010.07.009.
21. Li, S.; Prasanna, X.; Salo, V. T.; Vattulainen, I.; Ikonen, E. An efficient auxin-inducible degron system with low basal degradation in human cells. *Nature Methods* **2019**, *16* (9), 866-869. DOI: 10.1038/s41592-019-0512-x.
22. Miyazaki, Y.; Imoto, H.; Chen, L.-c.; Wandless, T. J. Destabilizing Domains Derived from the Human Estrogen Receptor. *Journal of the American Chemical Society* **2012**, *134* (9), 3942-3945. DOI: 10.1021/ja209933r.
23. Nabet, B.; Roberts, J. M.; Buckley, D. L.; Paulk, J.; Dastjerdi, S.; Yang, A.; Leggett, A. L.; Erb, M. A.; Lawlor, M. A.; Souza, A.; et al. The dTAG system for immediate and target-specific protein degradation. *Nature Chemical Biology* **2018**, *14* (5), 431-441. DOI: 10.1038/s41589-018-0021-8.
24. Auffenberg, E.; Jurik, A.; Mattusch, C.; Stoffel, R.; Genewsky, A.; Namendorf, C.; Schmid, R. M.; Rammes, G.; Biel, M.; Uhr, M.; et al. Remote and reversible inhibition of neurons and circuits by small molecule induced potassium channel stabilization. *Scientific Reports* **2016**, *6* (1), 19293. DOI: 10.1038/srep19293.
25. Doan, N. B.; Nguyen, H. S.; Alhajala, H. S.; Jaber, B.; Al-Gizawiy, M. M.; Ahn, E.-Y. E.; Mueller, W. M.; Chitambar, C. R.; Mirza, S. P.; Schmainda, K. M. Identification of radiation responsive genes and transcriptome profiling via complete RNA sequencing in a stable radioresistant U87 glioblastoma model. *Oncotarget* **2018**, *9* (34), 23532-23542. DOI: 10.18632/oncotarget.25247 PubMed.

26. Varshavsky, A. N-degron and C-degron pathways of protein degradation. *Proceedings of the National Academy of Sciences* **2019**, *116* (2), 358. DOI: 10.1073/pnas.1816596116.
27. Wachsberger, P. R.; Burd, R.; Cardi, C.; Thakur, M.; Daskalakis, C.; Holash, J.; Yancopoulos, G. D.; Dicker, A. P. VEGF Trap in Combination With Radiotherapy Improves Tumor Control in U87 Glioblastoma. *International Journal of Radiation Oncology*Biology*Physics* **2007**, *67* (5), 1526-1537. DOI: https://doi.org/10.1016/j.ijrobp.2006.11.011.
28. Wachsberger, P. R.; Burd, R.; Marero, N.; Daskalakis, C.; Ryan, A.; McCue, P.; Dicker, A. P. Effect of the Tumor Vascular-Damaging Agent, ZD6126, on the Radioresponse of U87 Glioblastoma. *Clinical Cancer Research* **2005**, *11* (2), 835.
29. Endo, M.; Jain, R. K.; Witwer, B.; Brown, D. Water Channel (Aquaporin 1) Expression and Distribution in Mammary Carcinomas and Glioblastomas. *Microvascular Research* **1999**, *58* (2), 89-98. DOI: https://doi.org/10.1006/mvre.1999.2158.
30. Bartelle, B. B.; Szulc, K. U.; Suero-Abreu, G. A.; Rodriguez, J. J.; Turnbull, D. H. Divalent metal transporter, DMT1: A novel MRI reporter protein. *Magnetic Resonance in Medicine* **2013**, *70* (3), 842-850, https://doi.org/10.1002/mrm.24509. DOI: https://doi.org/10.1002/mrm.24509 (acccessed 2021/11/21).
31. Törnroth-Horsefield, S.; Wang, Y.; Hedfalk, K.; Johanson, U.; Karlsson, M.; Tajkhorshid, E.; Neutze, R.; Kjellbom, P. Structural mechanism of plant aquaporin gating. *Nature* **2006**, *439* (7077), 688-694. DOI: 10.1038/nature04316.
32. Yesbolatova, A.; Saito, Y.; Kanemaki, M. T. Constructing Auxin-Inducible Degron Mutants Using an All-in-One Vector. *Pharmaceuticals* **2020**, *13* (5). DOI: 10.3390/ph13050103.

33. Ningaraj, N. S. Drug delivery to brain tumours: challenges and progress. *Expert Opinion on Drug Delivery* **2006**, *3* (4), 499-509. DOI: 10.1517/17425247.3.4.499.
34. Lee, M.; Baek, S.-E.; Moon, J.; Roh, Y. H.; Lim, J. S.; Park, M.-S.; Kim, M.-J.; Kim, H. Dynamic contrast-enhanced MRI coupled with a subtraction technique is useful for treatment response evaluation of malignant melanoma hepatic metastasis. *Oncotarget; Vol 7, No 25* **2016**. (acccessed 2016).
35. Vickstrom, C. R.; Snarrenberg, S. T.; Friedman, V.; Liu, Q.-s. Application of optogenetics and in vivo imaging approaches for elucidating the neurobiology of addiction. *Molecular Psychiatry* **2021**. DOI: 10.1038/s41380-021-01181-3.
36. Reijmers, L.; Mayford, M. Genetic control of active neural circuits. *Frontiers in Molecular Neuroscience* **2009**, *2*, 27, 10.3389/neuro.02.027.2009.

## G. Supplementary Figures

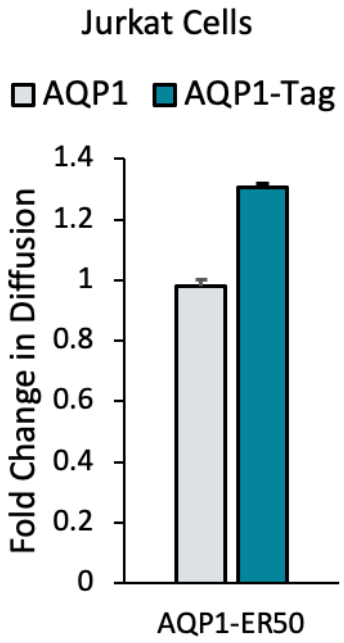


**Figure II.G.S1.** Fold change in diffusion of AQP1-ER50 Jurkat cells with either 0.1% DMSO vehicle or 10 µM 4-OHT stabilizing ligand for 24 h. $P < 0.05$, n = 4 biological replicates, t-test. Error bars are represented as standard error mean (s.e.m.).

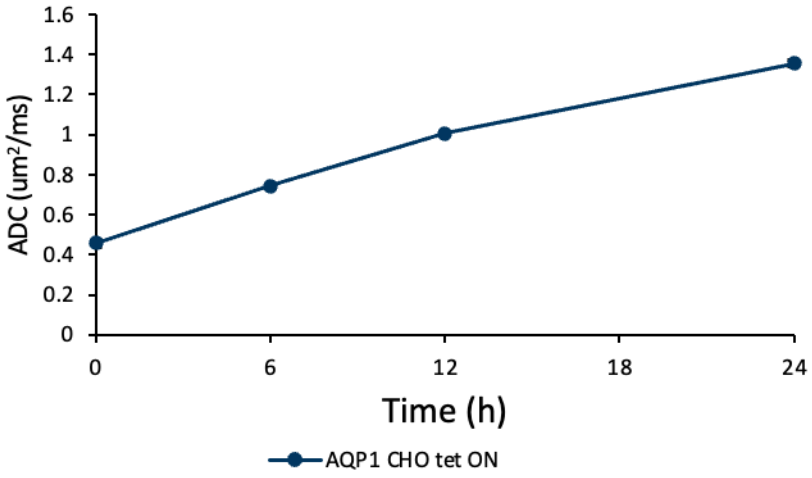

**Figure II.G.S2.** Kinetic profile of AQP1 expression in CHO tet ON cells after the addition of 1 µg/mL of doxycycline. Error bars are represented as standard error mean (s.e.m.) for n = 3 biological replicates.

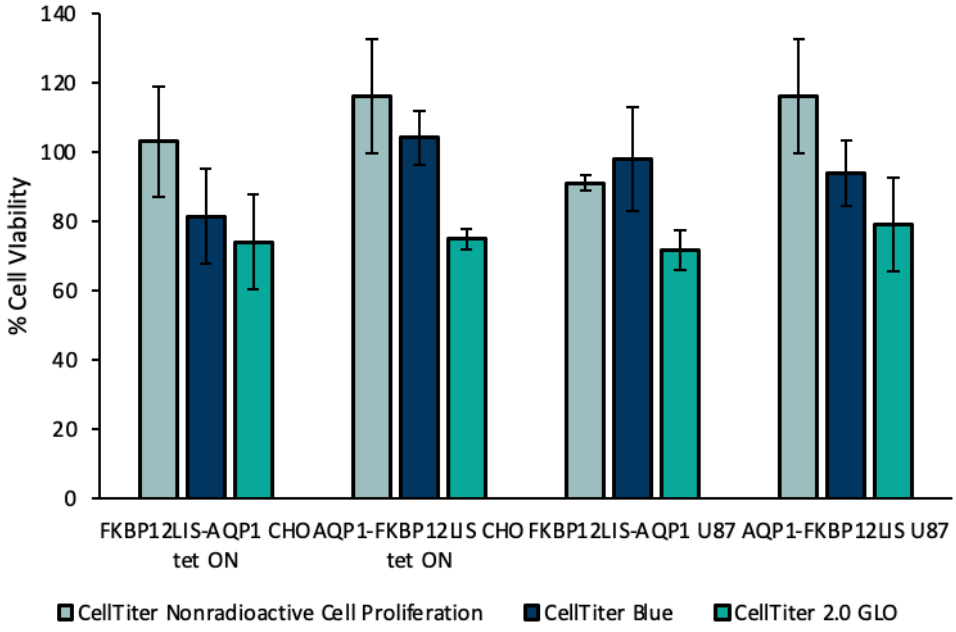


**Figure II.G.S3.** Cell toxicity based off three cell toxicity tests of 0.1% DMSO vehicle control to FKBP12LIS tagged-AQP1 in both CHO tet ON and U87 cells. Error bars are represented as standard error mean (s.e.m.) for n = 3 biological replicates.

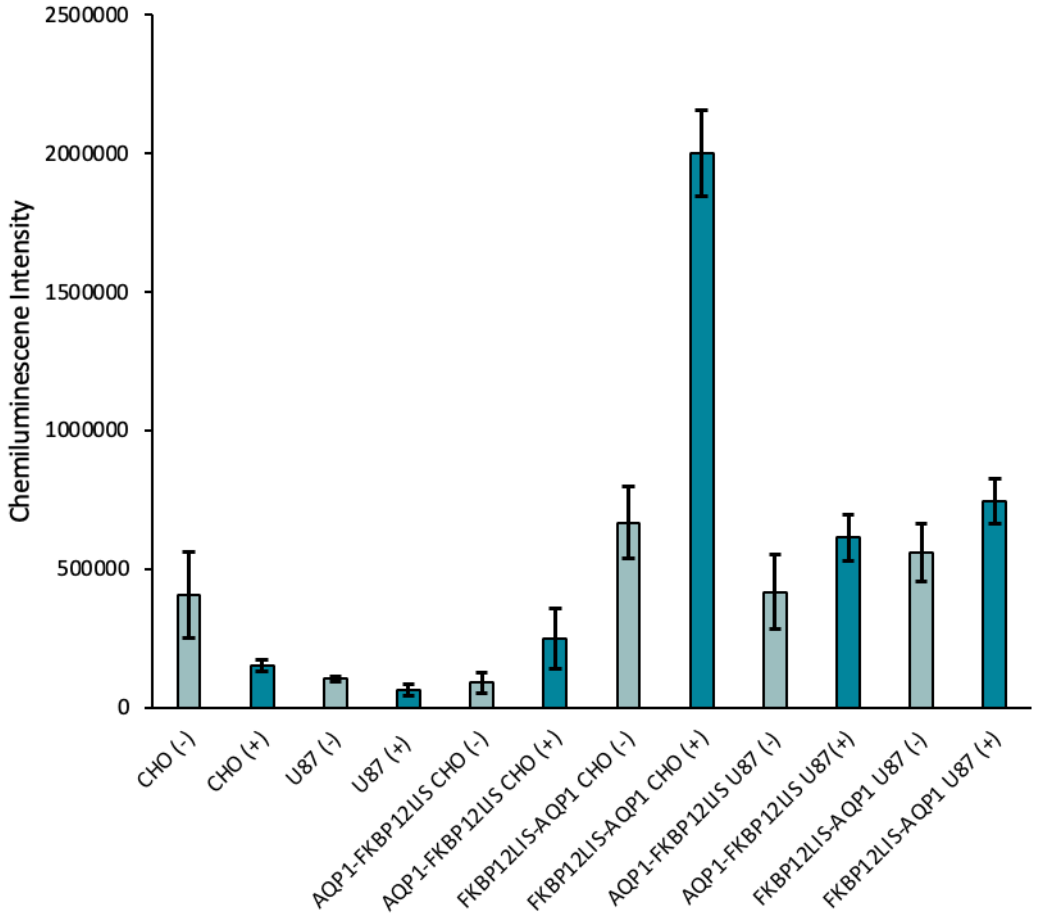


**Figure II.G.S4.** Biotinylation-NeutrAvidin ELISA assay where relative levels of membrane localized FKBP12LIS tagged-AQP1 were measured based off chemiluminescence. There is a general increase in signal intensity after the addition of Shield-1 stabilizing FKBP12LIS tagged-AQP1 on the membrane. Error bars are represented as standard error mean (s.e.m.) for n = 3 biological replicates.

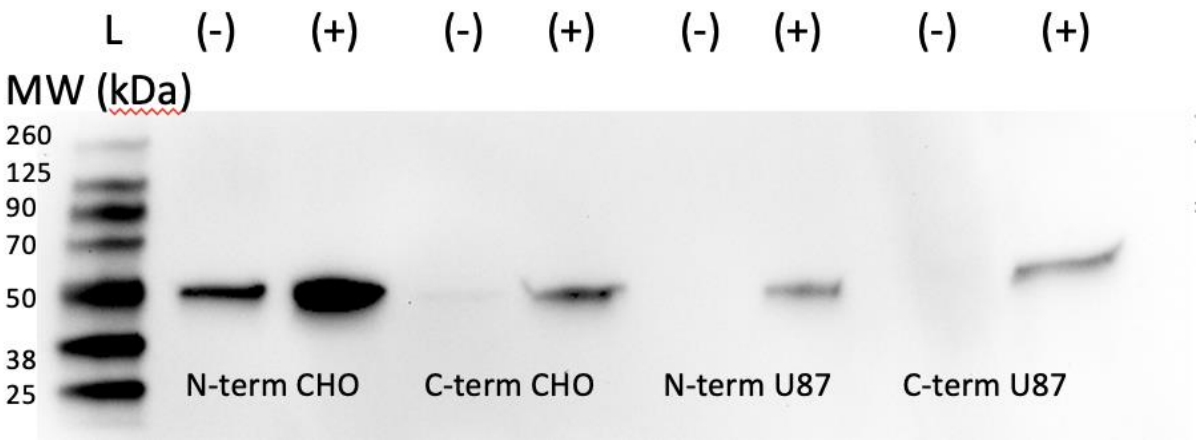


**Figure II.G.S5.** Full picture of membrane fractioned western blot samples of FKBP12LIS tagged-AQP1 CHO tet ON and U87 cell lines. Each pair of cells were loaded with the same amount of total protein concentration based off BSA assay.

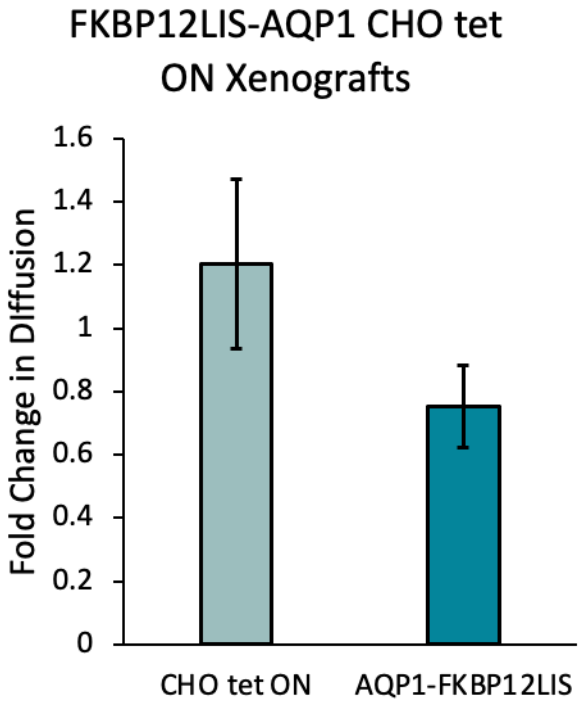


**Figure II.G.S6.** In vivo FKBP12LIS-AQP1 CHO tet ON and wild-type CHO tet on flank xenografts fold change in diffusion measurements. $P > 0.05$, n = 4 biological replicates, t-test. Error bars are represented as standard error mean (s.e.m.).

## H. DNA Sequences of Constructs

| Construct | 5' to 3' DNA Sequence |
|---|---|
| FLAG-AQP1 | ATGGACTACAAGGACGACGACGACAAGGCCAGCGAGTTCAAGA<br>AGAAGCTCTTCTGGAGGGCAGTGGTGGCCGAGTTCCTGGCCACG<br>ACCCTCTTTGTCTTCATCAGCATCGGTTCTGCCCTGGGCTTCAAA<br>TACCCGGTGGGGAACAACCAGACGGCGGTCCAGGACAACGTGA<br>AGGTGTCGCTGGCCTTCGGGCTGAGCATCGCCACGCTGGCGCAG<br>AGTGTGGGCCACATCAGCGGCGCCCACCTCAACCCGGCTGTCAC<br>ACTGGGGCTGCTGCTCAGCTGCCAGATCAGCATCTTCCGTGCCCT<br>CATGTACATCATCGCCCAGTGCGTGGGGGCCATCGTCGCCACCG<br>CCATCCTCTCAGGCATCACCTCCTCCCTGACTGGGAACTCGCTTG<br>GCCGCAATGACCTGGCTGATGGTGTGAACTCGGGCCAGGGCCTG<br>GGCATCGAGATCATCGGGACCCTCCAGCTGGTGCTATGCGTGCT<br>GGCTACTACCGACCGGAGGCGCCGTGACCTTGGTGGCTCAGCCC<br>CCCTTGCCATCGGCCTCTCTGTAGCCCTTGGACACCTCCTGGCTA<br>TTGACTACACTGGCTGTGGGATTAACCCTGCTCGGTCCTTTGGCT<br>CCGCGGTGATCACACACAACTTCAGCAACCACTGGATTTTCTGG<br>GTGGGGCCATTCATCGGGGGAGCCCTGGCTGTACTCATCTACGA<br>CTTCATCCTGGCCCCACGCAGCAGTGACCTCACAGACCGCGTGA<br>AGGTGTGGACCAGCGGCCAGGTGGAGGAGTATGACCTGGATGC<br>CGACGACATCAACTCCAGGGTGGAGATGAAGCCCAAATAG |
| FLAG-AQP1-DHFR | ATGGACTACAAGGACGACGACGACAAGGCCAGCGAGTTCAAGA<br>AGAAGCTCTTCTGGAGGGCAGTGGTGGCCGAGTTCCTGGCCACG<br>ACCCTCTTTGTCTTCATCAGCATCGGTTCTGCCCTGGGCTTCAAA<br>TACCCGGTGGGGAACAACCAGACGGCGGTCCAGGACAACGTGA<br>AGGTGTCGCTGGCCTTCGGGCTGAGCATCGCCACGCTGGCGCAG<br>AGTGTGGGCCACATCAGCGGCGCCCACCTCAACCCGGCTGTCAC<br>ACTGGGGCTGCTGCTCAGCTGCCAGATCAGCATCTTCCGTGCCCT<br>CATGTACATCATCGCCCAGTGCGTGGGGGCCATCGTCGCCACCG<br>CCATCCTCTCAGGCATCACCTCCTCCCTGACTGGGAACTCGCTTG<br>GCCGCAATGACCTGGCTGATGGTGTGAACTCGGGCCAGGGCCTG<br>GGCATCGAGATCATCGGGACCCTCCAGCTGGTGCTATGCGTGCT<br>GGCTACTACCGACCGGAGGCGCCGTGACCTTGGTGGCTCAGCCC<br>CCCTTGCCATCGGCCTCTCTGTAGCCCTTGGACACCTCCTGGCTA<br>TTGACTACACTGGCTGTGGGATTAACCCTGCTCGGTCCTTTGGCT<br>CCGCGGTGATCACACACAACTTCAGCAACCACTGGATTTTCTGG<br>GTGGGGCCATTCATCGGGGGAGCCCTGGCTGTACTCATCTACGA<br>CTTCATCCTGGCCCCACGCAGCAGTGACCTCACAGACCGCGTGA<br>AGGTGTGGACCAGCGGCCAGGTGGAGGAGTATGACCTGGATGC<br>CGACGACATCAACTCCAGGGTGGAGATGAAGCCCAAAATCAGT<br>CTGATTGCGGCGTTAGCGGTAGATCACGTTATCGGCATGGAAAC<br>CGTCATGCCGTGGAACCTGCCTGCCGATCTCGCCTGGTTTAAAC<br>GCAACACCTTAAATAAACCCGTGATTATGGGCCGCCATACCTGG<br>GAATCAATCGGTCGTCCGTTGCCAGGACGCAAAAATATTATCCT<br>CAGCAGTCAACCGAGTACGGACGATCGCGTAACGTGGGTGAAG<br>TCGGTGGATGAAGCCATCGCGGCGTGTGGTGACGTACCAGAAAT<br>CATGGTTATTGGCGGCGGTCGCGTTTATGAACAGTTCTTGCCAA<br>AAGCGCAAAAACTGTATCTGACGCATATCGACGCAGAAGTGGA<br>AGGCGACACCCATTTCCCGGATTACGAGCCGGATGACTGGGAAT<br>CGGTATTCAGCGAATTCCACGATGCTGATGCGCAGAACTCTCAC<br>AGCTATTGCTTTGAGATTCTGGAGCGGCGATGA |

| | |
|---|---|
| FLAG-AQP1-ER50 | ATGGACTACAAGGACGACGACGACAAGGCCAGCGAGTTCAAGA<br>AGAAGCTCTTCTGGAGGGCAGTGGTGGCCGAGTTCCTGGCCACG<br>ACCCTCTTTGTCTTCATCAGCATCGGTTCTGCCCTGGGCTTCAAA<br>TACCCGGTGGGGAACAACCAGACGGCGGTCCAGGACAACGTGA<br>AGGTGTCGCTGGCCTTCGGGCTGAGCATCGCCACGCTGGCGCAG<br>AGTGTGGGCCACATCAGCGGCGCCCACCTCAACCCGGCTGTCAC<br>ACTGGGGCTGCTGCTCAGCTGCCAGATCAGCATCTTCCGTGCCCT<br>CATGTACATCATCGCCCAGTGCGTGGGGGCCATCGTCGCCACCG<br>CCATCCTCTCAGGCATCACCTCCTCCCTGACTGGGAACTCGCTTG<br>GCCGCAATGACCTGGCTGATGGTGTGAACTCGGGCCAGGGCCTG<br>GGCATCGAGATCATCGGGACCCTCCAGCTGGTGCTATGCGTGCT<br>GGCTACTACCGACCGGAGGCGCCGTGACCTTGGTGGCTCAGCCC<br>CCCTTGCCATCGGCCTCTCTGTAGCCCTTGGACACCTCCTGGCTA<br>TTGACTACACTGGCTGTGGGATTAACCCTGCTCGGTCCTTTGGCT<br>CCGCGGTGATCACACACAACTTCAGCAACCACTGGATTTTCTGG<br>GTGGGGCCATTCATCGGGGGAGCCCTGGCTGTACTCATCTACGA<br>CTTCATCCTGGCCCCACGCAGCAGTGACCTCACAGACCGCGTGA<br>AGGTGTGGACCAGCGGCCAGGTGGAGGAGTATGACCTGGATGC<br>CGACGACATCAACTCCAGGGTGGAGATGAAGCCCAAAGAATTC<br>AGCCTTGCCCTGTCACTTACAGCCGACCAGATGGTTTCCGCGCTT<br>CTCGACGCTGAACCTCCAATTCTCTATTCCGAATACGACCCAACC<br>AGGCCGTTCTCCGAGGCATCTATGATGGGTCTGCTGACAAATCT<br>GGCAGACAGGGAACTGGTGCACATGATCAATTGGGCGAAGCGC<br>GTACCCGGATTCGTCGATCTTGCACTCCATGATCAGGTGCACTTG<br>CTGGAGTGCGCTTGGATGGAGATCCTCATGATCGGGCTGGTGTG<br>GCGGAGTATGGAACACCCCGGCAAGTTGCTGTTTGCGCCTAACC<br>TCCTGTTGGACAGGAACCAGGGGAAATGTGTGGAGGGCGGTGT<br>GGAAATCTTTGACATGCTCCTCGCTACCTCAAGCCGGTTTAGGAT<br>GATGAATCTGCAGGGCGAAGAGTTCGTGTGTCTCAAATCTATCA<br>TACTGTTGAACAGCGGAGTCTACACCTTCCTCTCCAGTACTCTGA<br>AATCTCTGGAGGAGAAAGATCATATCCATCGCGTGCTGGACAAG<br>ATAACCGACACGTTGATTCACTTGATGGCCAAAGCTGGGCTCAC<br>TCTGCAACAACAACATCAGCGACTGGCACAGCTGTTGCTGATTT<br>TGAGCCACATTCGGCACATGTCCAGCAAGAGAATGGAGCACCTC<br>TATAGTATGAAGTGCAAGAACGTCGTACCCCTGTCAGATCTGCT<br>TCTTGAAATGCTTGATGCCCACCGGCTGTGA |
| FLAG-AQP1-FKBP12LIS | ATGGACTACAAGGACGACGACGACAAGGCCAGCGAGTTCAAGA<br>AGAAGCTCTTCTGGAGGGCAGTGGTGGCCGAGTTCCTGGCCACG<br>ACCCTCTTTGTCTTCATCAGCATCGGTTCTGCCCTGGGCTTCAAA<br>TACCCGGTGGGGAACAACCAGACGGCGGTCCAGGACAACGTGA<br>AGGTGTCGCTGGCCTTCGGGCTGAGCATCGCCACGCTGGCGCAG<br>AGTGTGGGCCACATCAGCGGCGCCCACCTCAACCCGGCTGTCAC<br>ACTGGGGCTGCTGCTCAGCTGCCAGATCAGCATCTTCCGTGCCCT<br>CATGTACATCATCGCCCAGTGCGTGGGGGCCATCGTCGCCACCG<br>CCATCCTCTCAGGCATCACCTCCTCCCTGACTGGGAACTCGCTTG<br>GCCGCAATGACCTGGCTGATGGTGTGAACTCGGGCCAGGGCCTG<br>GGCATCGAGATCATCGGGACCCTCCAGCTGGTGCTATGCGTGCT<br>GGCTACTACCGACCGGAGGCGCCGTGACCTTGGTGGCTCAGCCC<br>CCCTTGCCATCGGCCTCTCTGTAGCCCTTGGACACCTCCTGGCTA<br>TTGACTACACTGGCTGTGGGATTAACCCTGCTCGGTCCTTTGGCT<br>CCGCGGTGATCACACACAACTTCAGCAACCACTGGATTTTCTGG<br>GTGGGGCCATTCATCGGGGGAGCCCTGGCTGTACTCATCTACGA<br>CTTCATCCTGGCCCCACGCAGCAGTGACCTCACAGACCGCGTGA |

| | |
|---|---|
| | AGGTGTGGACCAGCGGCCAGGTGGAGGAGTATGACCTGGATGC<br>CGACGACATCAACTCCAGGGTGGAGATGAAGCCCAAAGGAGTG<br>CAGGTGGAAACCATCTCCCCAGGAGACGGGCGCACCTTCCCCAA<br>GCGCGGCCAGACCTGTGTGGTGCACTACACCGGGATGCTTGAAG<br>ATGGAAAGAAAGTCGATTCCTCCCGGGACAGAAACAAGCCCTTT<br>AAGTTTATGCTAGGCAAGCAGGAGGTGATCCGAGGCTGGGAAG<br>AAGGGGTTGCCCAGATGAGTGTGGGTCAGAGAGCCAAACTGAC<br>TATATCTCCAGATTATGCCTATGGTGCCACTGGGCACCCAGGCA<br>TCATCCCACCACATGCCACTCTCGTCTTCGATGTGGAGCTTCTAA<br>AACCGGAATAG |
| FKBP12LIS-<br>AQP1- FLAG | ATGGGAGTGCAGGTGGAAACCATCTCCCCAGGAGACGGGCGCA<br>CCTTCCCCAAGCGCGGCCAGACCTGTGTGGTGCACTACACCGGG<br>ATGCTTGAAGATGGAAAGAAAGTCGATTCCTCCCGGGACAGAA<br>ACAAGCCCTTTAAGTTTATGCTAGGCAAGCAGGAGGTGATCCGA<br>GGCTGGGAAGAAGGGGTTGCCCAGATGAGTGTGGGTCAGAGAG<br>CCAAACTGACTATATCTCCAGATTATGCCTATGGTGCCACTGGG<br>CACCCAGGCATCATCCCACCACATGCCACTCTCGTCTTCGATGTG<br>GAGCTTCTAAAACCGGAAGCCAGCGAGTTCAAGAAGAAGCTCTT<br>CTGGAGGGCAGTGGTGGCCGAGTTCCTGGCCACGACCCTCTTTG<br>TCTTCATCAGCATCGGTTCTGCCCTGGGCTTCAAATACCCGGTGG<br>GGAACAACCAGACGGCGGTCCAGGACAACGTGAAGGTGTCGCT<br>GGCCTTCGGGCTGAGCATCGCCACGCTGGCGCAGAGTGTGGGCC<br>ACATCAGCGGCGCCCACCTCAACCCGGCTGTCACACTGGGGCTG<br>CTGCTCAGCTGCCAGATCAGCATCTTCCGTGCCCTCATGTACATC<br>ATCGCCCAGTGCGTGGGGGCCATCGTCGCCACCGCCATCCTCTC<br>AGGCATCACCTCCTCCCTGACTGGGAACTCGCTTGGCCGCAATG<br>ACCTGGCTGATGGTGTGAACTCGGGCCAGGGCCTGGGCATCGAG<br>ATCATCGGGACCCTCCAGCTGGTGCTATGCGTGCTGGCTACTAC<br>CGACCGGAGGCGCCGTGACCTTGGTGGCTCAGCCCCCCTTGCCA<br>TCGGCCTCTCTGTAGCCCTTGGACACCTCCTGGCTATTGACTACA<br>CTGGCTGTGGGATTAACCCTGCTCGGTCCTTTGGCTCCGCGGTGA<br>TCACACACAACTTCAGCAACCACTGGATTTTCTGGGTGGGGCCA<br>TTCATCGGGGGAGCCCTGGCTGTACTCATCTACGACTTCATCCTG<br>GCCCCACGCAGCAGTGACCTCACAGACCGCGTGAAGGTGTGGAC<br>CAGCGGCCAGGTGGAGGAGTATGACCTGGATGCCGACGACATC<br>AACTCCAGGGTGGAGATGAAGCCCAAAGACTACAAGGACGACG<br>ACGACAAGTAG |
| FLAG-AQP1-<br>FKBP12LID | ATGGACTACAAGGACGACGACGACAAGGCCAGCGAGTTCAAGA<br>AGAAGCTCTTCTGGAGGGCAGTGGTGGCCGAGTTCCTGGCCACG<br>ACCCTCTTTGTCTTCATCAGCATCGGTTCTGCCCTGGGCTTCAAA<br>TACCCGGTGGGGAACAACCAGACGGCGGTCCAGGACAACGTGA<br>AGGTGTCGCTGGCCTTCGGGCTGAGCATCGCCACGCTGGCGCAG<br>AGTGTGGGCCACATCAGCGGCGCCCACCTCAACCCGGCTGTCAC<br>ACTGGGGCTGCTGCTCAGCTGCCAGATCAGCATCTTCCGTGCCCT<br>CATGTACATCATCGCCCAGTGCGTGGGGGCCATCGTCGCCACCG<br>CCATCCTCTCAGGCATCACCTCCTCCCTGACTGGGAACTCGCTTG<br>GCCGCAATGACCTGGCTGATGGTGTGAACTCGGGCCAGGGCCTG<br>GGCATCGAGATCATCGGGACCCTCCAGCTGGTGCTATGCGTGCT<br>GGCTACTACCGACCGGAGGCGCCGTGACCTTGGTGGCTCAGCCC<br>CCCTTGCCATCGGCCTCTCTGTAGCCCTTGGACACCTCCTGGCTA<br>TTGACTACACTGGCTGTGGGATTAACCCTGCTCGGTCCTTTGGCT<br>CCGCGGTGATCACACACAACTTCAGCAACCACTGGATTTTCTGG<br>GTGGGGCCATTCATCGGGGGAGCCCTGGCTGTACTCATCTACGA |

| | |
|---|---|
| | CTTCATCCTGGCCCCACGCAGCAGTGACCTCACAGACCGCGTGA<br>AGGTGTGGACCAGCGGCCAGGTGGAGGAGTATGACCTGGATGC<br>CGACGACATCAACTCCAGGGTGGAGATGAAGCCCAAAGGAGTG<br>CAGGTGGAAACCATCTCCCCAGGAGACGGGCGCACCTTCCCCAA<br>GCGCGGCCAGACCTGCGTGGTGCACTACACCGGGATGCTTGAAG<br>ATGGAAAGAAAGTTGATTCCTCCCGGGACAGAAACAAGCCCTTT<br>AAGTTTATGCTAGGCAAGCAGGAGGTGATCCGAGGCTGGGAAG<br>AAGGGGTTGCCCAGATGAGTGTGGGTCAGAGAGCCAAACTGAC<br>TATATCTCCAGATTATGCCTATGGTGCCACTGGGCACCCAGGCA<br>TCATCCCACCACATGCCACTCTCGTCTTCGATGTGGAGCTTCTAA<br>AACTGGAATAG |
| FLAG-AQP1-SMASh | ATGGACTACAAGGACGACGACGACAAGGCCAGCGAGTTCAAGA<br>AGAAGCTCTTCTGGAGGGCAGTGGTGGCCGAGTTCCTGGCCACG<br>ACCCTCTTTGTCTTCATCAGCATCGGTTCTGCCCTGGGCTTCAAA<br>TACCCGGTGGGGAACAACCAGACGGCGGTCCAGGACAACGTGA<br>AGGTGTCGCTGGCCTTCGGGCTGAGCATCGCCACGCTGGCGCAG<br>AGTGTGGGCCACATCAGCGGCGCCCACCTCAACCCGGCTGTCAC<br>ACTGGGGCTGCTGCTCAGCTGCCAGATCAGCATCTTCCGTGCCCT<br>CATGTACATCATCGCCCAGTGCGTGGGGGCCATCGTCGCCACCG<br>CCATCCTCTCAGGCATCACCTCCTCCCTGACTGGGAACTCGCTTG<br>GCCGCAATGACCTGGCTGATGGTGTGAACTCGGGCCAGGGCCTG<br>GGCATCGAGATCATCGGGACCCTCCAGCTGGTGCTATGCGTGCT<br>GGCTACTACCGACCGGAGGCGCCGTGACCTTGGTGGCTCAGCCC<br>CCCTTGCCATCGGCCTCTCTGTAGCCCTTGGACACCTCCTGGCTA<br>TTGACTACACTGGCTGTGGGATTAACCCTGCTCGGTCCTTTGGCT<br>CCGCGGTGATCACACACAACTTCAGCAACCACTGGATTTTCTGG<br>GTGGGGCCATTCATCGGGGGAGCCCTGGCTGTACTCATCTACGA<br>CTTCATCCTGGCCCCACGCAGCAGTGACCTCACAGACCGCGTGA<br>AGGTGTGGACCAGCGGCCAGGTGGAGGAGTATGACCTGGATGC<br>CGACGACATCAACTCCAGGGTGGAGATGAAGCCCAAAGGCTCTT<br>CCGGGACAGGCTCCGGATCCGGCACTAGTGCGCCCATCACGGCG<br>TACGCCCAGCAGACGAGAGGCCTCCTAGGGTGTATAATCACCAG<br>CCTGACTGGCCGGGACAAAAACCAAGTGGAGGGTGAGGTCCAG<br>ATCGTGTCAACTGCTACCCAAACCTTCCTGGCAACGTGCATCAA<br>TGGGGTATGCTGGGCAGTCTACCACGGGGCCGGAACGAGGACC<br>ATCGCATCACCCAAGGGTCCTGTCATCCAGATGTATACCAATGT<br>GGACCAAGACCTTGTGGGCTGGCCCGCTCCTCAAGGTTCCCGCT<br>CATTGACACCCTGTACCTGCGGCTCCTCGGACCTTTACCTGGTCA<br>CGAGGCACGCCGATGTCATTCCCGTGCGCCGGCGAGGTGATAGC<br>AGGGGTAGCCTGCTTTCGCCCCGGCCCATTTCCTACTTGAAAGG<br>CTCCTCTGGGGGTCCGCTGTTGTGCCCCGCGGGACACGCCGTGG<br>GCCTATTCAGGGCCGCGGTGTGCACCCGTGGAGTGGCTAAAGCG<br>GTGGACTTTATCCCTGTGGAGAACCTAGAGACAACCATGAGATC<br>CCCGGTGTTCACGGACAACTCCTCTCCACCAGCAGTCACCCTGA<br>CGCACCCAATCACCAAAATCGATACCAAATACATCATGACATGC<br>ATGTCGGCCGACCTGGAGGTCGTCACGAGCACCTGGGTGCTCGT<br>TGGCGGCGTCCTGGCTGCTCTGGCCGCGTATTGCCTGTCAACAG<br>GCTGCGTGGTCATAGTGGGCAGGATCGTCTTGTCCGGGAAGCCG<br>GCAATTATACCTGACAGGGAGGTTCTCTACTGA |
| FLAG-AQP1-miniIAA7 | ATGGACTACAAGGACGACGACGACAAGGCCAGCGAGTTCAAGA<br>AGAAGCTCTTCTGGAGGGCAGTGGTGGCCGAGTTCCTGGCCACG<br>ACCCTCTTTGTCTTCATCAGCATCGGTTCTGCCCTGGGCTTCAAA<br>TACCCGGTGGGGAACAACCAGACGGCGGTCCAGGACAACGTGA |

| | |
|---|---|
| | AGGTGTCGCTGGCCTTCGGGCTGAGCATCGCCACGCTGGCGCAG<br>AGTGTGGGCCACATCAGCGGCGCCCACCTCAACCCGGCTGTCAC<br>ACTGGGGCTGCTGCTCAGCTGCCAGATCAGCATCTTCCGTGCCCT<br>CATGTACATCATCGCCCAGTGCGTGGGGGCCATCGTCGCCACCG<br>CCATCCTCTCAGGCATCACCTCCTCCCTGACTGGGAACTCGCTTG<br>GCCGCAATGACCTGGCTGATGGTGTGAACTCGGGCCAGGGCCTG<br>GGCATCGAGATCATCGGGACCCTCCAGCTGGTGCTATGCGTGCT<br>GGCTACTACCGACCGGAGGCGCCGTGACCTTGGTGGCTCAGCCC<br>CCCTTGCCATCGGCCTCTCTGTAGCCCTTGGACACCTCCTGGCTA<br>TTGACTACACTGGCTGTGGGATTAACCCTGCTCGGTCCTTTGGCT<br>CCGCGGTGATCACACACAACTTCAGCAACCACTGGATTTTCTGG<br>GTGGGGCCATTCATCGGGGGAGCCCTGGCTGTACTCATCTACGA<br>CTTCATCCTGGCCCCACGCAGCAGTGACCTCACAGACCGCGTGA<br>AGGTGTGGACCAGCGGCCAGGTGGAGGAGTATGACCTGGATGC<br>CGACGACATCAACTCCAGGGTGGAGATGAAGCCCAAAGGCTTCT<br>CTGAGACCGTGGACCTGATGCTGAACCTGCAGTCCAATAAGGAG<br>GGCTCTGTGGATCTGAAGAACGTGAGCGCCGTGCCTAAGGAGAA<br>GACCACACTGAAGGACCCATCCAAGCCCCCTGCCAAGGCACAG<br>GTGGTGGGATGGCCACCCGTGCGGAACTACAGAAAGAATATGA<br>TGACCCAGCAGAAGACAAGCTCCTAG |
| AtAFB2 | ATGAACTACTTTCCCGATGAGGTCATTGAGCACGTCTTTGATTTC<br>GTCACAAGCCACAAGGATAGGAACGCCATTAGCCTGGTCTGTAA<br>GAGCTGGTACAAGATCGAGCGGTATTCCAGACAGAAGGTGTTCA<br>TCGGCAACTGCTACGCCATCAATCCAGAGAGGCTGCTGCGGAGA<br>TTTCCCTGTCTGAAGAGCCTGACCCTGAAGGGCAAGCCCCACTT<br>CGCCGACTTTAACCTGGTGCCTCACGAGTGGGGAGGATTCGTGC<br>TGCCATGGATCGAGGCCCTGGCACGGTCCAGAGTGGGCCTGGAG<br>GAGCTGAGGCTGAAGCGCATGGTGGTGACAGACGAGTCTCTGG<br>AGCTGCTGTCTCGGAGCTTCGTGAACTTCAAGAGCCTGGTGCTG<br>GTGTCCTGCGAGGGCTTTACCACAGATGGCCTGGCAAGCATCGC<br>AGCAAACTGTAGGCACCTGCGGGACCTGGACCTGCAGGAGAAT<br>GAGATCGACGATCACAGAGGCCAGTGGCTGTCCTGCTTCCCCGA<br>TACCTGTACCACACTGGTGACACTGAACTTTGCCTGCCTGGAGG<br>GCGAGACAAATCTGGTGGCCCTGGAGAGGCTGGTGGCACGCTCT<br>CCCAACCTGAAGAGCCTGAAGCTGAATAGGGCAGTGCCTCTGGA<br>CGCACTGGCAAGACTGATGGCATGCGCACCACAGATCGTGGATC<br>TGGGCGTGGGCTCCTACGAGAACGACCCTGATTCCGAGTCTTAT<br>CTGAAGCTGATGGCCGTGATCAAGAAGTGTACCAGCCTGCGCAG<br>CCTGTCCGGCTTCCTGGAGGCAGCACCTCACTGCCTGTCCGCCTT<br>TCACCCAATCTGTCACAACCTGACATCCCTGAATCTGTCTTACGC<br>CGCCGAGATCCACGGCTCCCACCTGATCAAGCTGATCCAGCACT<br>GCAAGAAGCTGCAGAGGCTGTGGATCCTGGACTCCATCGGCGAT<br>AAGGGCCTGGAGGTGGTGGCCTCTACCTGTAAGGAGCTGCAGGA<br>GCTGCGCGTGTTCCCATCTGACCTGCTGGGAGGAGGAAACACCG<br>CAGTGACAGAGGAGGGCCTGGTGGCAATCTCTGCCGGATGCCCC<br>AAGCTGCACAGCATCCTGTATTTTTGTCAGCAGATGACCAACGC<br>CGCCCTGGTGACAGTGGCCAAGAACTGCCCCAATTTCATCAGGT<br>TTCGCCTGTGCATCCTGGAGCCCAATAAGCCTGACCACGTGACA<br>TCTCAGCCTCTGGATGAGGGCTTCGGCGCCATCGTGAAGGCCTG<br>CAAGAGCCTGAGGCGCCTGTCTCTGAGCGGCCTGCTGACCGACC<br>AGGTGTTCCTGTACATCGGCATGTATGCCAACCAGCTGGAGATG<br>CTGTCTATCGCCTTTGCCGGCGACACAGATAAGGGCATGCTGTA<br>CGTGCTGAATGGCTGTAAGAAGATGAAGAAGCTGGAGATCAGA |

| | |
|---|---|
| | GACAGCCCTTTTGGCGATACCGCCCTGCTGGCAGACGTGAGCAA<br>GTATGAGACAATGCGGAGCCTGTGGATGAGCTCCTGCGAGGTGA<br>CCCTGAGCGGCTGTAAGAGACTGGCCGAGAAGGCCCCATGGCTG<br>AACGTGGAGATCATCAACGAGAATGACAACAATAGGATGGAGG<br>AGAATGGCCACGAGGGCCGCCAGAAGGTGGATAAGCTGTATCT<br>GTATAGGACCGTCGTCGGGACTCGGATGGATGCCCCCCCCTTTG<br>TCTGGATTCTGTAG |
| OsTIR1 | ATGACATACTTTCCTGAAGAGGTCGTCGAACACATTTTTAGCTTC<br>CTGCCTGCACAGAGAGATAGAAACACAGTGAGCCTGGTCTGCAA<br>AGTGTGGTACGAGATCGAACGCCTGAGCCGGAGAGGAGTGTTC<br>GTCGGCAACTGCTATGCTGTGAGAGCAGGCAGGGTCGCCGCTAG<br>GTTTCCAAATGTGCGCGCACTGACCGTCAAGGGGAAACCCCACT<br>TCGCCGACTTTAACCTGGTGCCCCCTGATTGGGGAGGATACGCC<br>GGCCCTTGGATCGAGGCAGCCGCTCGCGGCTGTCATGGACTGGA<br>GGAACTGCGCATGAAGCGAATGGTGGTCTCTGACGAAAGTCTGG<br>AGCTGCTGGCTCGGAGCTTCCCTAGGTTTCGCGCACTGGTGCTG<br>ATTTCTTGCGAAGGCTTCAGCACCGATGGACTGGCAGCCGTGGC<br>CTCCCACTGTAAGCTGCTGCGGGAGCTGGACCTCCAGGAGAATG<br>AAGTGGAGGATAGAGGCCCCAGATGGCTGTCTTGCTTCCCAGAC<br>TCATGTACCAGCCTGGTGTCCCTGAACTTTGCCTGCATCAAAGGC<br>GAAGTGAATGCTGGGTCCCTGGAGCGGCTGGTCTCAAGAAGCCC<br>CAACCTGAGGTCTCTGCGGCTGAACCGGAGCGTGAGCGTGGACA<br>CTCTGGCTAAGATTCTGCTGAGAACCCCTAACCTGGAGGATCTG<br>GGAACCGGCAATCTGACAGACGATTTCCAGACAGAATCCTACTT<br>TAAACTGACTTCTGCCCTGGAGAAGTGTAAAATGCTGAGGAGTC<br>TGTCAGGATTCTGGGATGCTTCACCCGTGTGCCTGAGCTTTATCT<br>ACCCTCTGTGTGCACAGCTGACAGGCCTGAACCTGAGCTATGCA<br>CCAACCCTGGACGCCAGTGATCTGACAAAGATGATCTCACGCTG<br>CGTGAAACTCCAGCGACTGTGGGTGCTGGACTGTATTTCCGATA<br>AGGGGCTCCAGGTGGTCGCCAGCTCCTGCAAGGACCTCCAGGAG<br>CTGAGAGTGTTCCCATCTGATTTTTACGTGGCCGGATATAGTGCT<br>GTCACTGAGGAAGGCCTGGTGGCAGTCTCACTGGGATGCCCAAA<br>GCTGAACAGCCTGCTGTATTTCTGTCATCAGATGACTAATGCTGC<br>ACTGGTGACCGTCGCCAAGAACTGCCCTAATTTCACCCGATTTC<br>GGCTGTGTATTCTGGAACCAGGCAAACCCGACGTGGTCACATCC<br>CAGCCACTGGATGAAGGGTTTGGAGCTATCGTGAGAGAGTGCAA<br>GGGACTCCAGAGGCTGAGCATTTCCGGCCTGCTGACAGACAAAG<br>TGTTCATGTACATCGGCAAGTATGCTAAGCAGCTGGAGATGCTG<br>AGCATTGCATTTGCCGGAGACTCCGATAAGGGCATGATGCACGT<br>GATGAACGGGTGTAAGAATCTGCGAAAACTGGAAATCCGGGAC<br>AGCCCTTTCGGGGATGCCGCTCTGCTGGGAAACTTTGCCAGATA<br>CGAGACAATGAGGAGCCTGTGGATGTCTAGTTGCAATGTGACTC<br>TGAAGGGCTGTCAGGTCCTGGCTAGTAAAATGCCTATGCTGAAC<br>GTGGAAGTCATTAATGAGCGGGACGGGTCTAACGAAATGGAGG<br>AAAATCATGGCGACCTGCCAAAGGTGGAGAAACTGTATGTGTAT<br>CGGACCACCGCAGGGGCAAGAGATGATGCTCCCAACTTTGTGAA<br>GATTCTGTGA |

# III. A Simple-in-Design Mouse Cradle for Magnetic Resonance Imaging

## A. Abstract

Acquiring consistent and reliable in vivo data for magnetic resonance imaging (MRI) based studies are contingent on the quality of the scanner and sample in addition to the livelihood of the animal subject. Emphasis has been placed more so on the former, yet obtaining reproducible in vivo work is dependent on animal welfare during imaging procurement. We have engineered an inexpensive and simple-in-design animal cradle to achieve maximal animal comfort without reducing image quality. Here, we have implemented a convenient and elaborate anesthetic gas flow system with switchable ease to control gas flow from the induction chamber to the animal cradle. In tandem, we have utilized a respiration, heartbeat, and temperature monitoring system to display animal vitals throughout each imaging session. Proper safety precautions have been integrated using charcoal canisters and in-house vacuum lines to protect the user from anesthetic gas during each experiment. Our setup can be implemented easily with other Bruker MRI probes and potentially with other MRI manufacturers with similar hardware.

## B. Introduction

MRI is widely used in both preclinical and clinical settings and serves many purposes in the field of biomedicine spanning from basic to clinical research.[1,2,3] The ability to noninvasively generate high spatial resolution images with relatively high temporal resolution has opened many avenues for its use in the biomedical space. This imaging modality plays a critical role in developing imaging methodologies, diagnostic techniques, drug development and patient treatment.

The highly variable nature of live animal experiments[4,5] combined with the complex MR imaging instrumentation presents several challenges for obtaining suitable preclinical results. To optimize experimental success with preclinical imaging, there are many factors to consider: proper anesthetic dosing, subject body temperature monitoring, various contrast agent administration, proper animal handling and quality control. These parameters play an influential role in minimizing variability in small animal imaging.[6] A satisfactory animal cradle is necessary in maintaining the baseline of all the aforementioned parameters. Having a small animal cradle that provides life support, anesthesia, and monitoring of vitals is critical in preclinical research. A well-built cradle will minimize discomfort to the animals and save valuable laboratory resources.

There is a lack of readily available and simple-in-design universal animal cradles that comprehensively cover the needs of preclinical imaging. Understanding the components and modularity of animal life support cradles will be necessary to provide consistent results across instruments supplied by different manufacturers.[7] To keep animal subjects comfortably and achieve the optimal imaging capabilities, we built a custom mouse life support cradle.

Making a life support cradle for mice that fits animal welfare standards for our unique imaging setup requires custom cradle design and engineering. To address these needs, we have designed a cost-effective and simple animal cradle for the purpose of imaging mice while maintaining physiological temperatures around 35 °C and monitoring temperature, respiration rate, and heartbeat rate throughout the entire imaging session. The simplicity and ease-of-use of our animal cradle monitoring system can be easily adapted to other MRI probes with minimal complexity and provides a basis for enhancing animal survival and data consistency.

## C. Methodology

### 1. Ethics Statement

All animal studies and protocols were approved by the University of California, Santa Barbara Institutional Animal Care and Use Committee.

### 2. MRI and Animal Life Support System

We carry out all MRI animal experiments with a vertical Bruker 300 MHz Super-Wide Bore (SWB) magnet. The MRI system is composed of SWB magnets, probes, temperature control units and driver hardware. The MRI hardware is run by ParaVision software on a PC. The animal life support system contains all of the equipment to keep the animals alive and anesthetized while in the SWB probe. This includes medical grade oxygen, isoflurane, isoflurane nebulizer, and BIOPAC vital monitoring hardware and software which is monitored on a laptop. Figure III.C.2.1 is an overview schematic of the two systems that facilitate humane MR imaging of mice in our research lab.

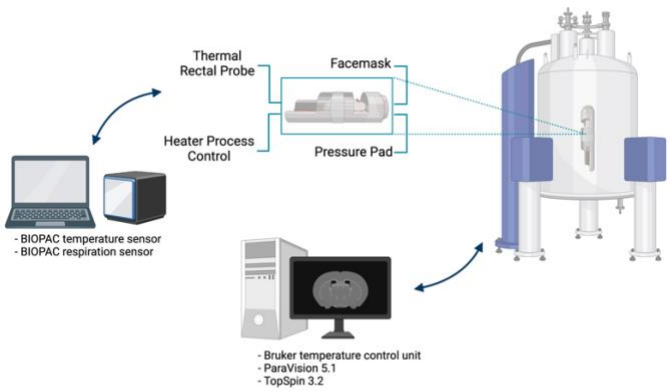


**Figure III.C.2.1.** An overview schematic of the hardware that comprise the MRI system and the animal life support system.

### 3. Animal Cradle Design and Loading Into MRI

All the components are fixed to the animal cradle (Figure III.3.1). The gas lines and vital monitoring wires are attached to the cradle prior to setting the mouse inside. Once the mouse is loaded and confirmed to be in a stabilized anesthetized state using the toe-pinch strategy, the cradle is taken upright and secured within the bore of the MRI. After the animal cradle is loaded, the air conduit tubing and wiring is connected to the cradle. The respiration and temperature of the mouse is monitored via BIOPAC AcqKnowledge software, and the temperature of the air is controlled with TopSpin v3.2.

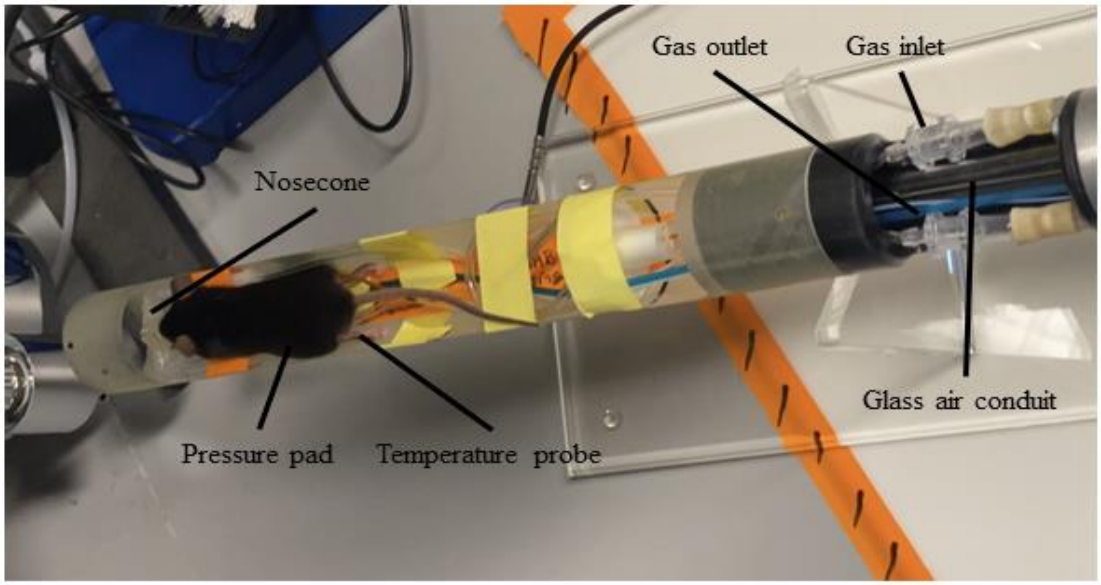


**Figure III.C.3.1.** Photograph of the loading tube and animal cradle.

**4. Gas System and Procedure for Mouse Anesthesia**

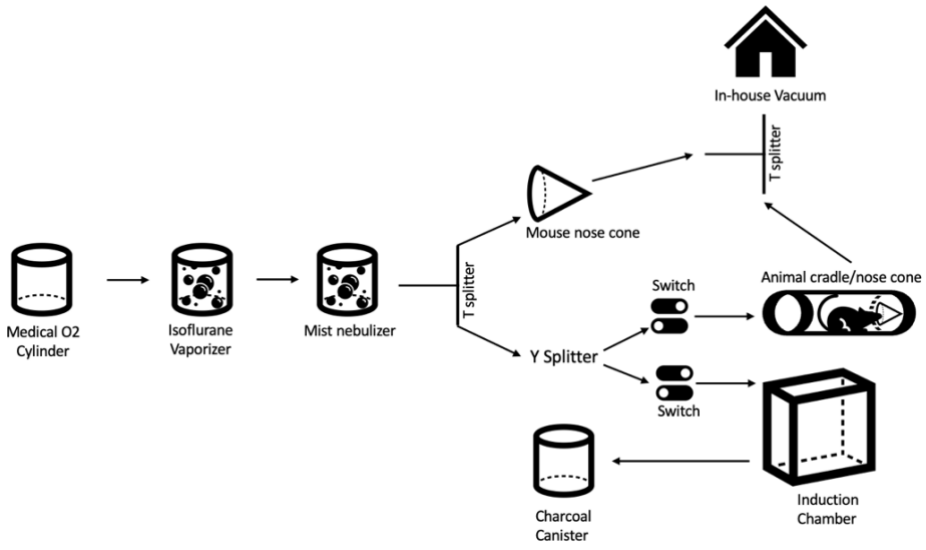


**Figure III.C.4.1.** Flowchart of oxygen and isoflurane to the nose cone, animal cradle/nose cone system, and induction chamber.

USP 300 medical grade oxygen is connected to the isoflurane vaporizer with an oxygen regulator. From there, the vaporizer flows isoflurane through the mist nebulizer to humidify the isoflurane through T splitter (Diverting valves with barbed fittings ¼" tube inner diameter). Anesthetic gas can flow either to the external mouse nose cone or further to either the induction chamber connected to a charcoal trap or the internal mouse nose cone located in the animal cradle necessary for MRI sessions. Tubing lies within the MRI probe (Mini BW57, Bruker) for isoflurane inlet and vacuum outlet. The switches located after the Y-splitter can be switched on and off to regulate where the isoflurane gas flows. For isoflurane outlet, both the external mouse nose cone and the animal cradle nose cone system are connected to a T-splitter that regulates where vacuum pulls the isoflurane from.

First, the switches and T-splitters are correctly oriented such that isoflurane flows only to the induction chamber. After anesthetizing the mouse, the isoflurane vaporizer is turned off and medical oxygen is bypassed to the induction chamber to purge the chamber before transferring the mouse to the animal cradle. Upon transferring the mouse, both switches are reversed to allow isoflurane flow only towards the animal cradle and at the same time, the in-house vacuum is turned on. Post imaging session, the medical oxygen, isoflurane vaporizer, and vacuum are switched off, and the mouse is placed on the heating pad (K&H Pet Products Electric Small Animal Heated Pad) with supplemental heat from the heating lamp (BN-LINK Digital Heat Mat Thermostat Controller for Seed Germination) for recovery.

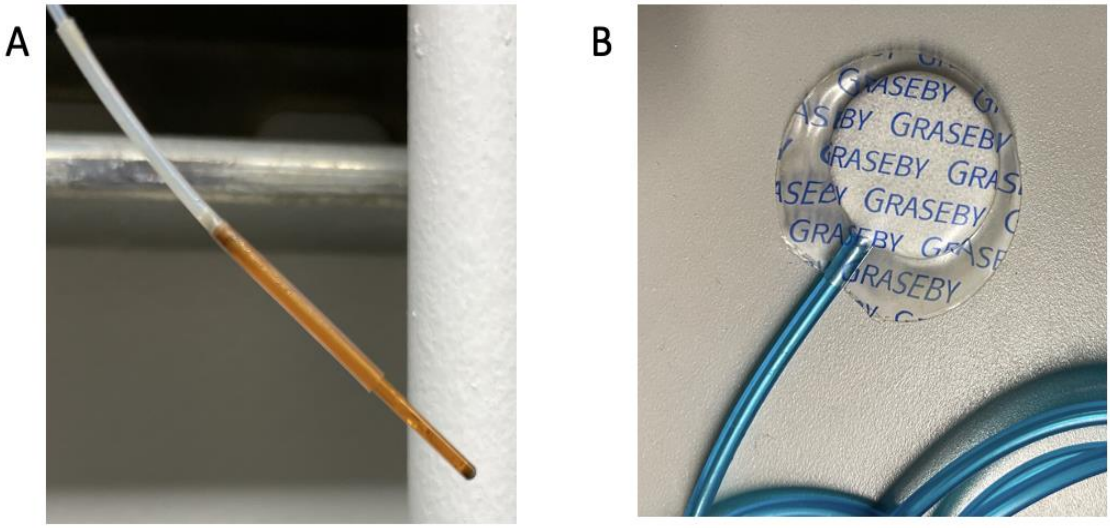


**Figure III.C.4.2** (A) Fiber optic probe inserted in the rectum of the mouse for accurate temperature monitoring. (B) Pressure pad placed under the mouse within the animal cradle for respiration monitoring.

Respiration rate and temperature is monitored using standard commercial MP160 base unit with DA100C/TSD160B respiration unit. The AMD100D interfacing unit

connected to an OpSens AccusSens unit hooked up with a fiber optic sensor is used for temperature monitoring.

**5. Heating and Imaging System Design and Procedure**

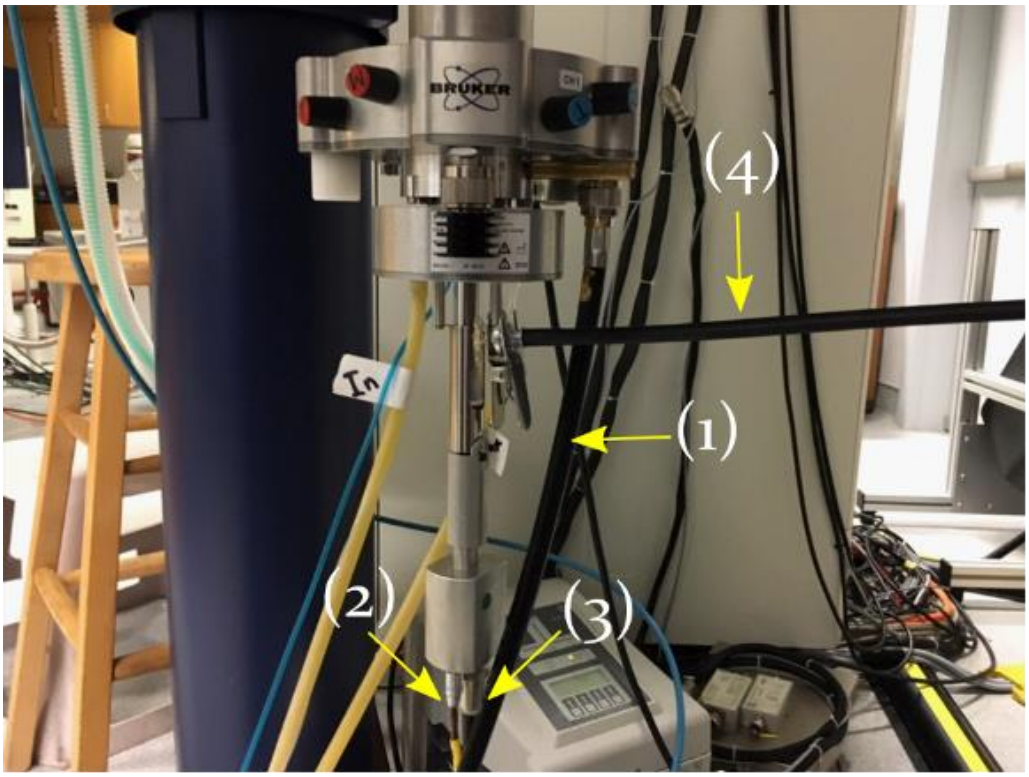


**Figure III.C.5.1 Photograph of the animal cradle heating system set up.** (1) Black RF cable, (2) brown cable temperature sensor, (3) gray power cable for heating filament, (4) black tubing for air flow towards the mouse inside the scanner.

Once the mouse is secured onto the animal cradle, the animal cradle is placed inside the outer casing to fit inside the MRI scanner. The air flow black tubing (Figure III.C.5.1 Tube 4) is fitted onto the glass conduit secured with a clamp, and the gray power cable (Figure III.C.5.1 Cable 3) and brown cable (Figure III.C.5.1 Cable 2) are connected at the bottom of the probe for powering the heating coil and sensing temperature fluctuations, respectively. Once those 3 cables are connected, the on button is clicked through

ParaVision v2.1 software, initiating temperature increase to 316K with 800 lph flow rate. These settings achieved 35°C mouse internal temperature within 30 minutes. After the internal mouse temperature is stabilized through the Acknowledge BIOPAC software, the black RF cable (Figure III.C.5.1 Cable 1) is connected for imaging.

**D. Conclusions**

We have described here the simplicity and inexpensive design of our animal cradle capable of providing quality MR images while maintaining consistent heat and vital monitoring of mice. This design and system can be easily translated across other Bruker MRI scanners and coils and potentially with other manufacturers.

**E. Materials**

Hardware

- Glass conduit fabricated by Richard Cobb of the UCSB Chemistry Glass Shop.
- Glass conduit rack fabricated by Roger Green of the UCSB Chemistry Machine Shop.
- 40 mm coil with animal cradle (MiniWB57, Bruker)
- Heating filament rack designed and fabricated by Lincoln Satterthwaite in the Chemistry and Biochemistry Department.
- Diverting valves with barbed fittings ¼” tube inner diameter (4757K57, McMaster-Carr)
- Switches used after Y-splitter
- Rodent isoflurane facemask kit (OC-MFM-KIT, World Precision Instruments)
    - 2 x flexible medical grade PVC tubing 1/4" outer and 1/8" inner diameter x 6' length

    - 2 x 1/4" Tubing Adapters and 2 x 3/8" Tubing Adapters
- Low profile anesthesia mask, small (SOMNO-0801, Ken Scientific Corporation)
    - 2 x 1/4” and 2 x 3/8” tube adapters with traditional kits
    - 2 x male luer fittings with SomnoSuite kits
- MICRO Mist Nebulizer (Hudson RCI)
- K&H Pet Products Electric Small Animal Heated Pad Tan 9 X 12 Inches
- Heating Lamp (BN-LINK Digital Heat Mat Thermostat Controller for Seed Germination, Reptiles and Brewing Breeding Incubation Greenhouse, 40-108°F, 8.3A 1000W ETL Listed)
- Induction chamber (VetEquip)
- Isoflurane vaporizer with oxygen regulator stand (VetEquip)
- Isoflurane
- Air blower (Bruker)
- Medical grade O2 (USP300)
- Charcoal Canister (Omnicon f/air)
- BioPac respiration (MP160, AM100D, DA100C, TSD160B)
- Biopac fiber optic temperature probe (OpSens fiber optic sensor)
- Computer (Samsung core i5)

Software

- TopSpin 3.2
- ParaVision 5.1
- AcqKnowledge (BIOPAC Systems, Inc.)

## F. References


1. Colosimo, C.; Knopp, M. V.; Barreau, X.; Gérardin, E.; Kirchin, M. A.; Guézénoc, F.; Lodemann, K. P. A comparison of Gd-BOPTA and Gd-DOTA for contrast-enhanced MRI of intracranial tumours. *Neuroradiology* **2004**, *46* (8), 655-665. DOI: 10.1007/s00234-003-1128-4.
2. Dhingra, K.; Fousková, P.; Angelovski, G.; Maier, M. E.; Logothetis, N. K.; Tóth, É. Towards extracellular Ca2+ sensing by MRI: synthesis and calcium-dependent 1H and 17O relaxation studies of two novel bismacrocyclic Gd3+ complexes. *JBIC Journal of Biological Inorganic Chemistry* **2008**, *13* (1), 35-46. DOI: 10.1007/s00775-007-0296-9.
3. Oudkerk, M.; Sijens, P. E.; Van Beek, E. J.; Kuijpers, T. J. Safety and efficacy of dotarem (Gd-DOTA) versus magnevist (Gd-DTPA) in magnetic resonance imaging of the central nervous system. *Investigative radiology* **1995**, *30* (2), 75-78. DOI: 10.1097/00004424-199502000-00002 PubMed.
4. Alegre, M.-L. Mouse microbiomes: overlooked culprits of experimental variability. *Genome Biology* **2019**, *20* (1), 108. DOI: 10.1186/s13059-019-1723-2.
5. David, J. M.; Knowles, S.; Lamkin, D. M.; Stout, D. B. Individually Ventilated Cages Impose Cold Stress on Laboratory Mice: A Source of Systemic Experimental Variability. *Journal of the American Association for Laboratory Animal Science* **2013**, *52* (6), 738-744.
6. Vanhove, C.; Bankstahl, J. P.; Krämer, S. D.; Visser, E.; Belcari, N.; Vandenberghe, S. Accurate molecular imaging of small animals taking into account animal models, handling, anaesthesia, quality control and imaging system performance. *EJNMMI Physics* **2015**, *2* (1), 31. DOI: 10.1186/s40658-015-0135-y.

7. Kersemans, V.; Gilchrist, S.; Allen, P. D.; Wallington, S.; Kinchesh, P.; Prentice, J.; Tweedie, M.; Warner, J. H.; Smart, S. C. A System-Agnostic, Adaptable and Extensible Animal Support Cradle System for Cardio-Respiratory-Synchronised, and Other, Multi-Modal Imaging of Small Animals. *Tomography* **2021**, *7* (1). DOI: 10.3390/tomography7010004.

# IV. Conclusions and Future Directions

## A. Development of genetically encodable reporters for background-free MRI

Genetically encodable optical-based reporters have been deemed the impetus for our current understanding of biomolecular events. Their high-resolution imaging capabilities intrinsic to optical instrumentation and high temporal resolution to monitor neuronal stimulation on the order of milliseconds are milestones that other imaging modalities pale in comparison.[1] However, the one major drawback to optical reporters is their inability to provide biomolecular information in deep-tissue due to photon absorption and scattering.[2,3] Use of invasive optical fibers and two-photon microscopy have pushed the imaging depth boundaries, but these tools are still limited in their abilities to noninvasively image deeper-seated tissue with a wider field-of-view.[4]

An area of research that has gained increasing interests in the field of molecular imaging is engineering genetically encodable MRI reporters to circumvent the limitations of their optical counterparts. This special class of protein-based reporters can utilize the advantages of MRI where molecular images can be obtained noninvasively with unlimited tissue depth. Given the variety of physical mechanisms of MRI modalities such as T1, T2, diffusion-weighted, and CEST, researchers have developed MRI reporters based off these various modalities previously mentioned in Chapter 1. Although MRI reporters produce contrast in deeper tissue regions, these reporters currently lack the sensitivity to reliably provide localized signal contrast beyond endogenous background noise even with millimolar concentrations of paramagnetic metal ion addition, which can lead to the generation of reactive oxygen species.[5] To address this need, we have engineered a novel metal-free MRI

reporter AQP1 with tunable contrast abilities to enable sensitive background-free gene expression in deeper-seated tissue.

In Chapter 2, we demonstrated the utility of using ligand responsive degradations tags termed as degrons to tune AQP1-dependent contrast with the administration of the degron's cognate ligand. This has allowed consistent control of contrast at the protein-level rather than the transcriptional level providing faster signal output and potentially in a reversible fashion shown with GFP.[6] Additionally, we measured the efficiency of this technology in more biologically interesting cell types such as human T cells for potentially tracking T cell therapy against solid tumors, human glioblastoma cancer cells to provide further clarity in the biology behind heterogenous aggressive cancer models in the brain, and murine macrophages for potentially imaging immune response.[7-9] From our initial screen of 7 different degradation tags, FKBP12LIS has shown to be the most promising degron outperforming other constructs significantly. Moving with this construct *in vivo*, we required an animal cradle that could allow for live small animal imaging experiments maintaining physiological temperatures and respiration monitoring within the scanner during acquisition.

To meet this demand, we designed and built an animal cradle for viable mice imaging described in further detail in Chapter 3. This required 6 months of designing and machining various parts on the animal cradle. We incorporated a heating coil that ran through the MRI probe to ensure steady heating supply between 35-37˚C during scan time using Bruker software's process control. In addition, we set up a respiration monitoring system though BIOPAC hardware and software that accurately detects subtle amounts of pressure applied to a pressure pad placed right under the underside of the mouse during the imaging session. The BIOPAC software also calculates the respiration rate and converts it into heart beats per minute providing an additional vital measurement. Using this in-house manufactured set up,

we displayed the efficiency of this degron *in vivo* xenograft tumor models in immunocompromised NSG mice and obtained a background-free image enhancing our reporter sensitivity. Given the reversible property of ligand responsive degrons, we can apply this work for dynamic imaging maximizing the advantage of longitudinal and repetitive MRI studies, which can be useful for bolstering our understanding of biomolecular phenomena in the field of molecular imaging and biomedicine.

## B. Future Directions

### B.1. Intracranial injections of AQP1-FKBP12LIS CHO tet ON and human glioblastoma U87 cells

Expanding the AQP1-degron system for *in vivo* applications, we plan to intracranially inject stably expressing C-terminally placed FKBP12LIS degron on AQP1 in human glioblastoma U87 xenografts to demonstrate imaging in the brain, which is a useful organ model for testing treatments against glioblastoma patient derived xenografts.[8,10,11] To this end, we acquired the necessary surgical room, equipment, and accessories to pursue this endeavor (Figure. IV.B.1.1). From here, I will be explaining the surgical setup in depth.

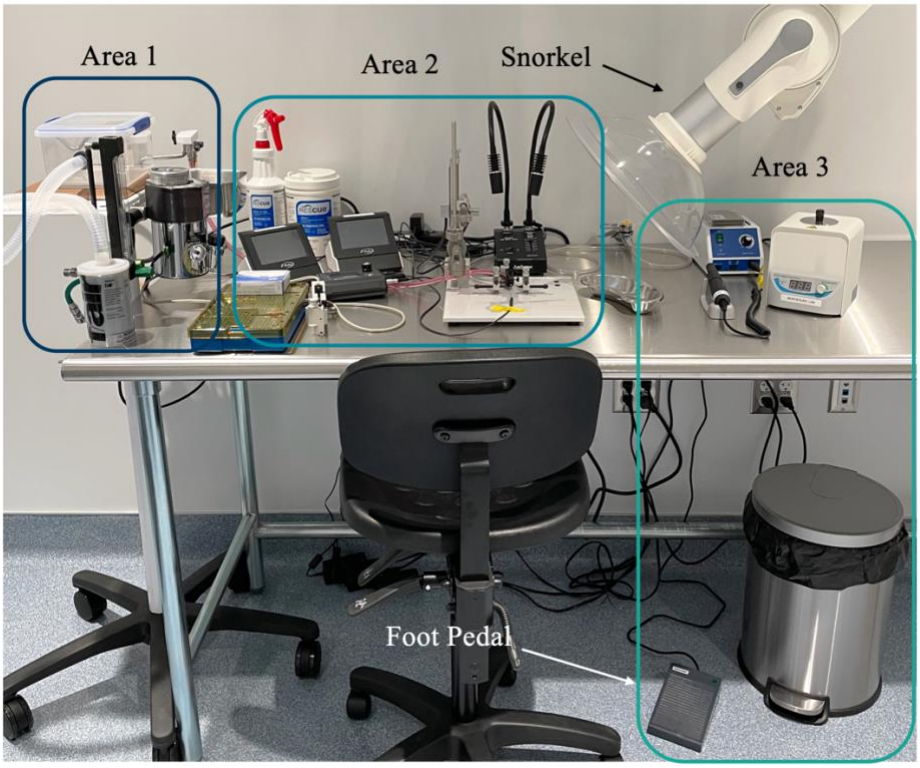


**Figure IV.B.1.1 Intracranial injection setup.** Area 1 is the "dirty zone" where mice anesthetized to easily shave hair from the head region. Area 2 is the "sterile zone" where the intracranial injections are performed is where surgical tools can be kept sterile using the microbead sterilizer and a foot pedal to power the drill for exposing brain tissue for injections.

Our surgical set up can be segmented into 3 areas. Area 1 can be thought of as the "dirty zone" where mice are anesthetized to allow quick hair shaving from the head region for easier access with the scalpel later on. Area 2 is the "sterile zone" where the intracranial injections are done on the stereotaxic platform first by exposing the skull after the initial incision of the skin and drilling holes through the skull to expose brain tissue for easier access of the needle to penetrate brain tissue. An in-house snorkel protruding from the roof captures any lingering isoflurane escaping from the gas mask

mounted on the stereotax for the surgeon's protection. Vacuum lines are attached to the anesthetic gas mask to ensure most of the isoflurane minimizes exposure to the surgeon.


**Figure IV.B.1.2. Area 1: anesthetic supply.** (1) Airflow meter (2) Isoflurane vaporizer (3A) Pink tubing flowing isoflurane from dual manifold to the stereotax (3B) Yellow tubing flowing isoflurane from dual manifold to (4) induction chamber (5) activated charcoal trap for isoflurane waste.

In area 1, medical grade oxygen is regulated using an airflow meter (Figure IV.B.1.2.1) at 2 L/min, which then flows through the isoflurane vaporizer (Figure IV.B.1.2.2) set anywhere from 0-3% isoflurane per our IACUC protocol. From there, vaporized isoflurane flows the dual manifold system that directs equalized anesthetic gas to either the stereotaxic setup connected by the pink tubing (Figure IV.B.1.2.3A) or the induction chamber (Figure IV.B.1.2.4) through the yellow tubing (Figure IV.B.1.2.3B). For safety measures, an activated charcoal trap (Figure IV.B.1.2.5) is used to capture any isoflurane escaping from the induction chamber after setting the isoflurane dial to off and

performing and oxygen flush using the bypass button located near the airflow meter. At this point the mouse head hair has been shaved and can be quickly transferred to area 2 to prep intracranial injections.

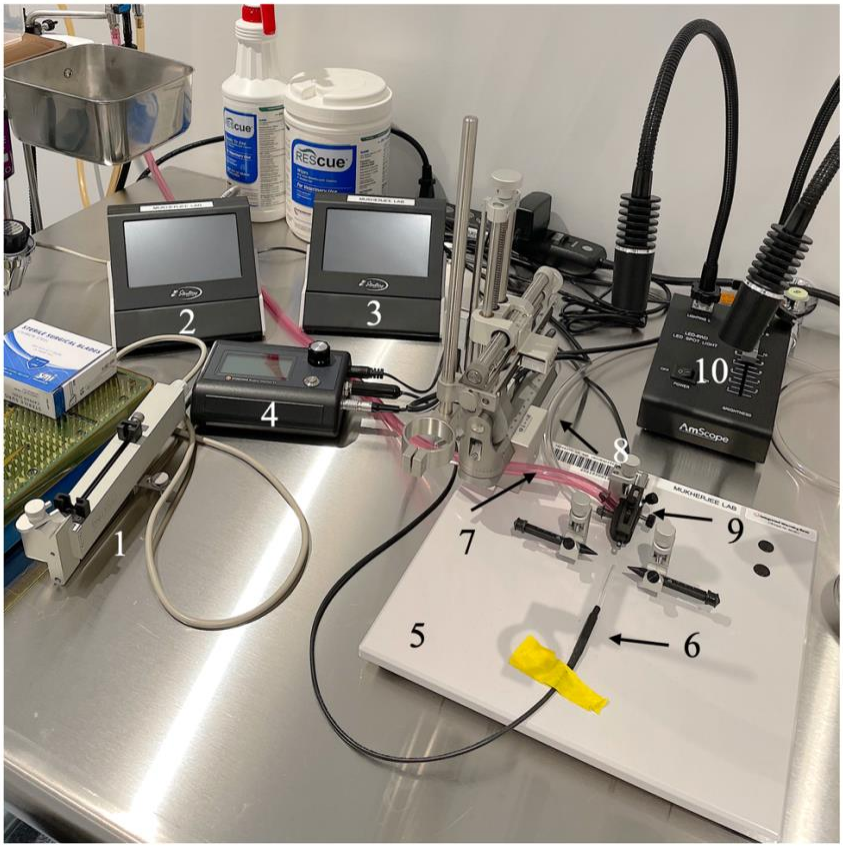


**Figure IV.B.1.3 Area 2: Stereotaxic setup for intracranial injections.** (1) Automated injector (2) Display interface for flow rate input (3) Display interface for anterior/posterior, dorsal/ventral, and medial/later movements on the stereotax for accurate injection coordinates (4) Process control device for heating of the (5) stereotaxic platform (6) thermal rectal probe (7) isoflurane inlet tubing (8) vacuum outlet tubing (9) anesthetic gas mask (10) Dual gooseneck light illuminator.

Before transferring the head-shave mouse to area 2, ensuring the stereotaxic platform (Figure IV.B.1.3.5) has been disinfected with Rescue™ will minimize pathogenic

exposure. Additionally, setting the flow rate of injections using the display interface (Figure IV.B.1.3.2) beforehand will minimize intracerebral damage further along the procedure. After the necessary preparatory steps have been accounted for, the mouse can be fixed onto the anesthetic gas mask (Figure IV.B.1.3.9) and the surgical site can be illuminated using the dual gooseneck LED lights (Figure IV.B.1.3.10). The thermal rectal probe (Figure IV.B.1.3.6) must also be inserted into the mouse immediately to reliably set the platform temperature to 37˚C using the process-controlled device (Figure IV.B.1.3.4). At this point, the surgical incision and subsequent injections can be performed accordingly. All equipment and accessories have been carefully investigated for optimal surgical procedures minimizing pain and discomfort for the mouse subject and ease-of-use for the surgeon.

**B.2. Multiplexed imaging using orthogonal degradation tags**

Multiplex imaging allows one to resolve cellular compartments, cellular processes, and expression of multiple genes in different regions of an organ or within single cell by using orthogonal reporters.[12] It would reasonably follow suit that MRI genetic reporters can be engineered to provide multiplexing capabilities by actuating other orthogonal signatures inherent to the specific MRI modality and not by tuning emission wavelengths like in the case of fluorescent proteins.

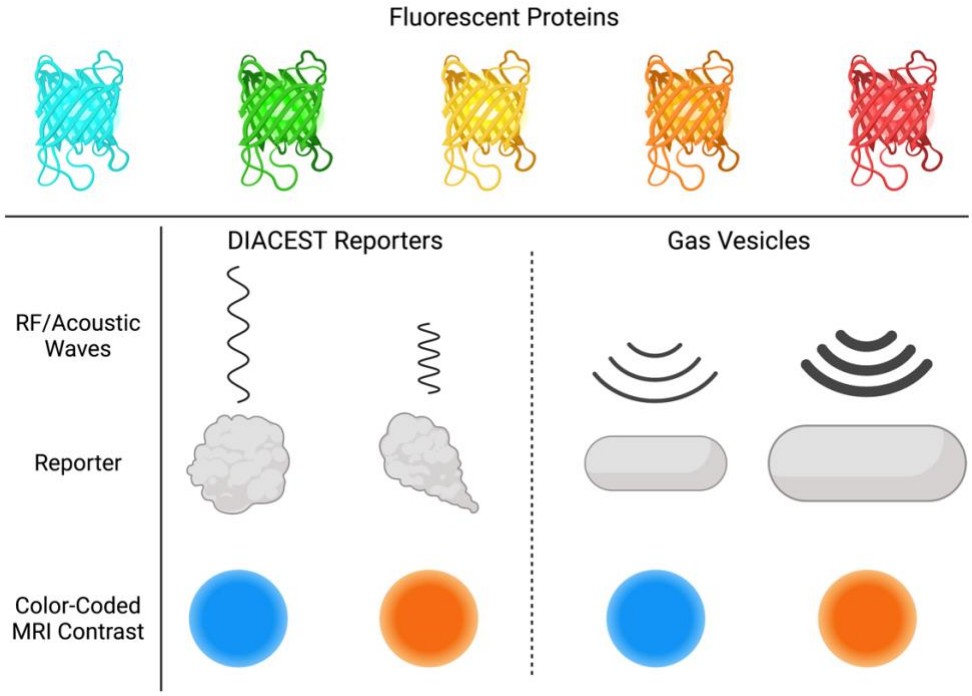


**Figure IV.B.2.1 Multiplexed imaging using colorful fluorescent proteins and orthogonal MRI reporters.**

For example, in Chapter 1 I presented CEST reporters that can produce contrast through the repetitive process of applying saturating radiofrequency (RF) pulses to exchangeable protons on the reporter and subsequently exchanging onto the bulk water leading to the attenuation of background noise. Scientists that have previously engineered CEST reporters, have also designed diamagnetic CEST (DIACEST) reporters that have distinct saturation RF motifs that essentially allow the user to color-code each unique reporter to enable multiplex imaging.[13] Multiplexing has also been showcased in Mikhail Shapiro's lab, by selectively applying varying acoustic pressures to collapse gas vesicles (GVs). This was achieved in two different ways by removing the outer scaffolding protein GvpC and by expressing GVs with varying morphologies.[14] Both methods have demonstrated that multiplexing is possible with genetically encoded MRI reporters.

Our ligand responsive degron tagged-AQP1 system could also enable for multiplexing capabilities since each degron has a unique cognate ligand that modulates AQP1-dependent contrast in an orthogonal manner.

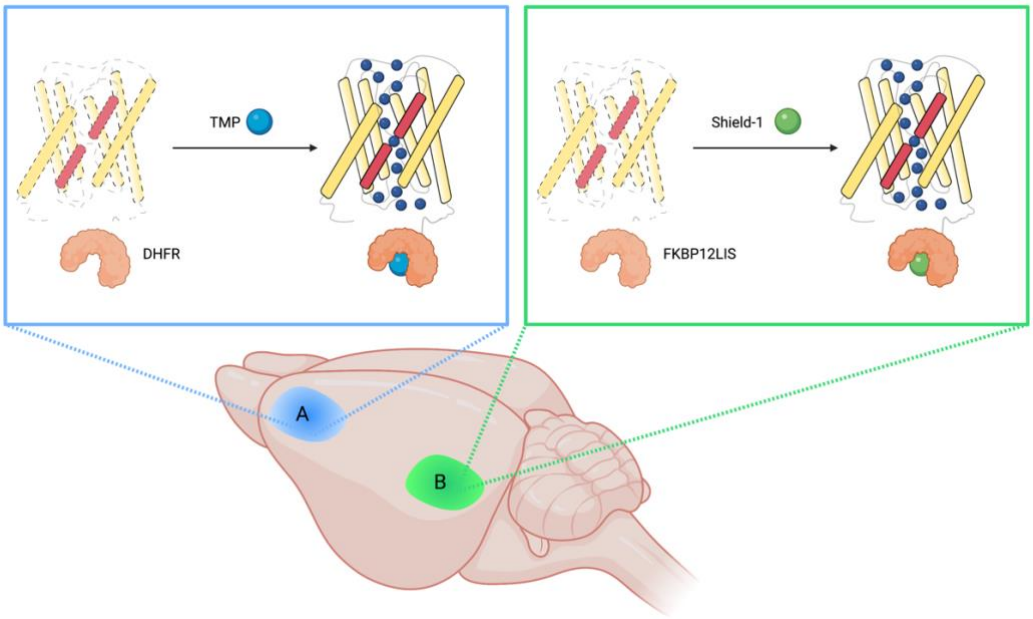


**Figure IV.B.2.2 Multiplexed imaging separate regions of the brain with orthogonal stabilizing degrons.**

This has been demonstrated with fluorescent reporters by exposing doubly transduced NIH3T3 cells expressing DHFR-YFP and FKBP12LIS-mCherry to trimethoprim and/or shield-1 at varying concentrations. YFP fluorescence was only observed in the presence of trimethoprim stabilizing DHFR and mCherry fluorescence was only observed in the presence of shield-1 stabilizing FKBP12LIS.[15] Given that we have shown AQP1-dependent contrast to these separate degrons, it is conceivable that our system can also multiplex image. To leverage the advantages of MRI for longitudinal imaging studies, we could transduce several regions of the mouse brain with different AQP1-degron constructs and map behavioral patterns triggered though neural stimulation upon ligand stabilization (Figure IV.B.2.2). Fortunately, the cognate ligands used to stabilize DHFR

and FKBP12LIS have been able to cross the blood-brain barrier, thus we are not limited to only multiplexing regions outside of the brain.[15,16] Since optical imaging has a limited field-of-view, MRI is really the best way to map whole-organ neuronal stimulation. Functional MRI (fMRI) has provided insight to understanding brain patterns, however, the signal to noise ratio is often difficult to deconvolve.[17] In addition, fMRI doesn't measure direct expression of neuronal genes, only fluctuations in blood flow in a certain region of the brain. It is unclear then whether fMRI signals are contributed by a strong neuronal stimulation from a small subset of neurons or a weak neuronal stimulation from a large subset of neurons. There is a need for more specific brain pattern mapping, and if proven feasible with high enough sensitivity, using AQP1-degron technology to multiplex brain patterns would immensely impact the neuroscience community.

### B.3. Incorporating directed evolution and establishing an optimal screening platform for enhanced membrane trafficked and degradation of ligand responsive aquaporins

Our AQP1-degron system robustly confers AQP1-dependent contrast within a reasonable timescale of several hours useful to image cellular proliferation and gene expression.[18,19] However, the off-state diffusion values measured for AQP1 fused to the majority of the ligand inducible degradation and stabilization tags did not efficiently actuate AQP1 degradation in a shorter time frame than GFP degradation kinetics ultimately, minimizing dynamic range and rapid degradation response. A nobel prize winning technology given to Caltech professor Francis Arnold in 2018 for her work in using directed evolution to introduce enhanced and novel functionalities in proteins can be used to engineer more efficiently degradable degrons in the context of AQP1 fusions.[20] Here, I present two feasible options currently available to our lab's resources

for screening degron variants possessing low basal stability, large dynamic range, predictable dose-response output, and rapid degradation kinetics.

### B.3.1 Using diffusion-weighted imaging to screen for enhanced degradable AQPs

Choice of screening is ideally done in the context of the protein's function, especially when performing low-throughput screens.[21] Provided we are directly interested in diffusion values from membrane trafficked AQP1, we will use diffusion-weighted MRI to screen the influence from introduced mutations on AQP1 diffusion. Given the limited temporal resolution in DWI compared to fluorescence imaging.[22] using this method will severely limit screening throughput. Thus, to minimize slower turnover rate of our directed evolution workflow, variants will be screened in yeast. Reasons for using this eukaryotic system are due to its relatively quicker DNA incorporations into host cells similar to bacteria, which can be done overnight. This is a stark contrast to stable cell line generation in mammalian cells, which can take greater than a week depending on the mode of transgene insertion: stable transfection, lentiviral transduction, adeno-associated viral transduction, or CRISPR insertion. Additionally, colony selection is easily identified and accounted for during DWI screening with yeast. To our benefit, DHFR, FKBP12, and AID, degrons we screened in Chapter 2, have all been tested in yeast for protein stabilization and degradation applications.[23,24]

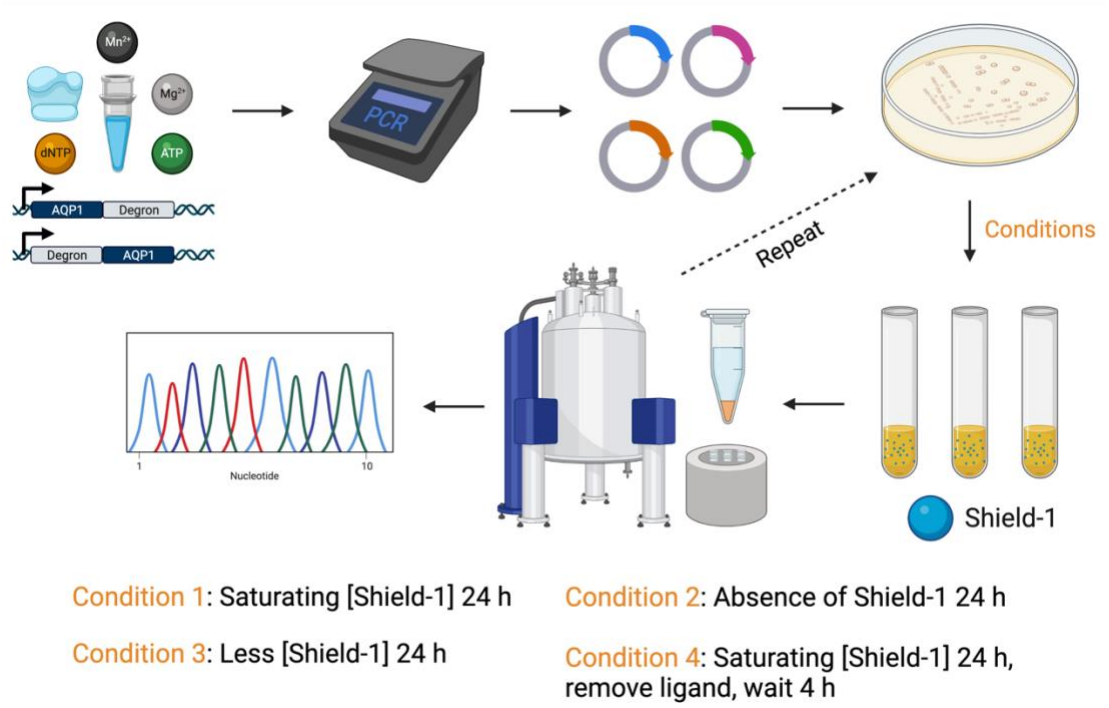


**Figure IV.B.3.1.1 Directed evolution workflow in yeast for higher membrane trafficked AQP1-degron.**

The workflow for engineering LIS degrons involves 4 screening rounds based off the Wandless group.[15,25]: (1) Construct library by error-prone PCR on degron genes cloned in frame on either 5' or 3' ends of AQP1. (2) Shotgun clone using Gibson assembly to insert mutated genes into yeast plasmid backbone. (3) Transform library plasmids into yeast. (4) Randomly pick colonies, culture them in saturating concentrations of stabilizing ligand based off literature for 24 h, and pellet cells into PCR tubes for each colony. (5) Screen by DWI and choose colonies that exhibit AQP1-dependent contrast. (6) Colonies selected from the first screen are cultured without stabilizing ligand for 24 h and pelleted. (7) Screen by DWI and choose colonies that exhibit cells lacking AQP1-dependent contrast. This will select for ligand responsive tags that exhibit low basal AQP1 stabilization. (8) Colonies

selected from the second screen are cultured with stabilizing ligand concentrations an order of magnitude apart from saturating levels for 24 h and pelleted. (9) Screen by DWI and choose colonies that respond to lower concentrations of ligand. This will select for degrons that can detect lower concentrations of stabilizing ligand. (10) To improve rapid degradation off-state kinetics, colonies selected from the third screen are cultured with saturating concentrations of stabilizing ligand for 24 h, washed to remove ligand, wait a few hours (4 ± 1 hr) to allow protein degradation, and pellet. (11) Screen by DWI and choose colonies that lack AQP1 contrast signifying rapid degradation kinetics. This entire process can be adopted for engineering LID tags by screening without destabilizing ligand first and then conducting the opposite conditions for subsequent screenings. Additional screening of a narrow subset of winning candidates must be done before translating them to mammalian cells for functional screening.[26]

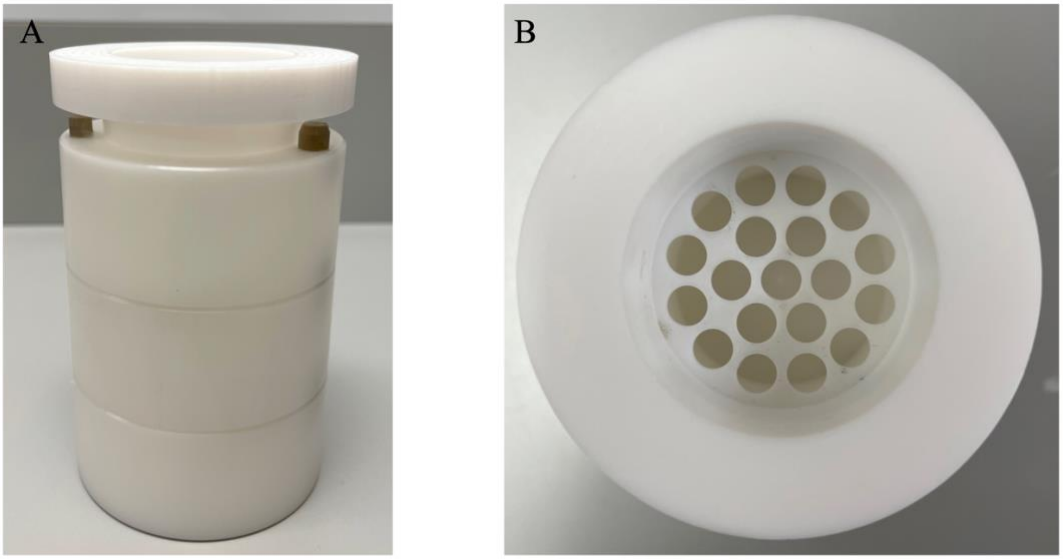


**Figure IV.B.3.1.2. Stackable 3D-printed phantom molds for screening yeast cell pellets in the MRI.**

Further improvements to increase screening throughput would be to 3D print several stackable phantom molds that can maximally fit a set number of individual yeast pellets in PCR tubes (Figure IV.B.3.1.2). In addition, another device that can mechanically move the height of the stack would need to be designed and built. To fully automate the entire process, a feedback controller that can mediate between the completion of a diffusion-weighted scan and the operation of the mechanical device to adjust the height of stackable phantoms would greatly enhance screening throughput time and prevent researcher fatigue.

Although having the instrumentation to automate and increase screening throughput would simplify the whole workflow, the major limitation still depends on the number of yeast colonies that can be reasonably collected. Using multislice-DWI to image 2 phantom's worth of yeast colonies would double work-output within the same timeframe. Even with this, we could at best screen anywhere from 100-1000 colonies per week depending on the number of researchers graciously tasked with this effort. This range pales in comparison to screening a library of cells on the order of millions in a single fluorescence-activated cell sorting (FACS) session. To this end in the next section, I describe using FACS to screen for highly responsive degrons possessing desirable aforementioned traits in the context of mammalian cells.

### B.3.2 Using a mammalian cell based FACS screening for enhanced degradable AQPs

In order to use fluorescence as a readout for engineering more efficiently dynamic AQP1-degron variants, we would first need to find amenable insertion sites on the extracellular loops of AQP1 to incorporate artificial antigens (e.g. FLAG tag DYKDDDDK) without perturbing water flux. This would enable fluorescently-

labeled antibodies (Ab) to bind to these exposed antigen-binding sites reporting successful expression and membrane trafficked AQP1-degron constructs. To our knowledge, the only anti-AQP1 Abs offered by commercial vendors target intracellular regions of AQP1, which cannot penetrate the cellular membrane without first permeabilizing the cell membrane and fixing cells. This is not ideal for capturing live cells expressing the reporter system and is practically impossible to use fixed, dead cells for downstream screening processes.

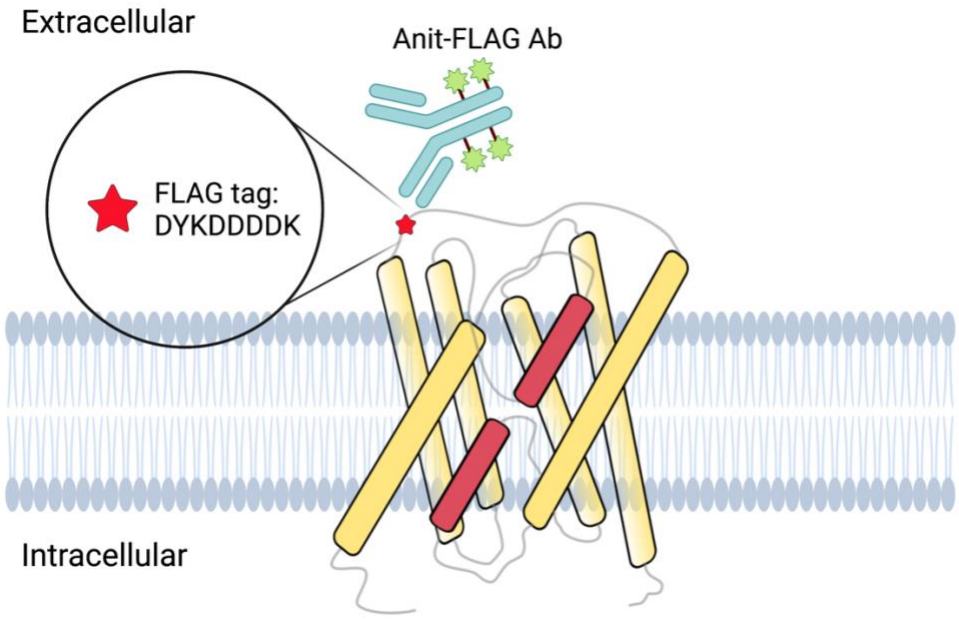


**Figure IV.B.3.2.1 Inserting FLAG tag sequence to amenable sites on the extracellular loops of AQP1 for probing membrane bound AQP1.**

Here, we lose out on direct AQP1 functional screening. However, being able to feasibly screen and select from larger libraries of variants that introduce advantageous mutations in mammalian cells far outweigh the necessity for contextual screening in nonideal yeast cells. Fortunately, membrane trafficked AQP1 is associated with the ability to facilitate water diffusion, so we are not too indirect in

this screening approach. The workflow for applying iterative directed evolution using the mammalian cell based FACS system follows similarly to the procedure mentioned in the above section Chapter IV.3.2. with slight modifications adapted more closely to the references from the Wandless group. They have shown to use this FACS screening process with degradation of other membrane proteins using dye-labeled antibodies. With this optimized platform, we have no doubt this will effectively select for mutants with increased diffusion fold changes and rapid degradation kinetics.

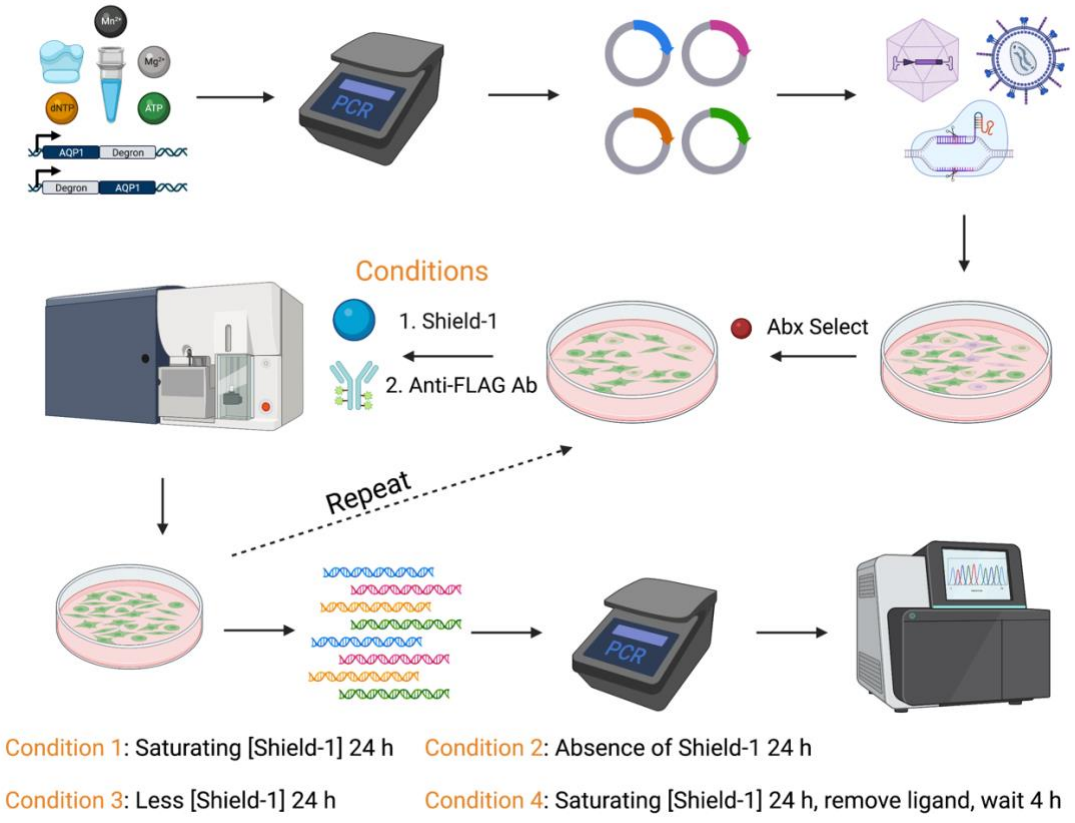


**Figure IV.B.3.2.2 Directed evolution workflow in mammalian cells for higher membrane trafficked AQP1-degron.**

The FACS-based workflow is as follows: (1) Construct library by error-prone PCR on degron genes cloned in frame on either 5’ or 3’ ends of FLAG tag inserted AQP1. (2) Shotgun clone using Gibson assembly to insert mutated genes into

lentiviral (LV), adeno-associated viral (AAV), or CRISPR plasmid backbone. (3) Produce viruses to transduce target mammalian cell lines with ideally single library transgene infection or use CRISPR single integration to minimize multiple insertions. It is good to have a complement fluorescent reporter under a constitutive promoter to normalize Ab staining to transgene incorporation efficiency. (4) Use antibiotic selection to select out noninfected cells. For screening round 1 to identify responsive degradation mutants (5), culture stable cells in saturating concentrations of stabilizing ligand based off literature for 24 h. (6) Add fluorescently-labeled anti-FLAG Ab to label cells. (7) Sort for highly fluorescently-labeled cells that successfully expressed and membrane trafficked FLAG tagged-AQP1 degron variants. (8) Grow cells out and ensure all ligands have washed out from cells through repetitive centrifugation, aspiration, and resuspension in ligand-free media. For screening round 2 to select for mutants that exhibit higher degradation of AQP1, (9) culture cells in the absence of stabilizing ligand for 24 h and repeat step (6). (10) Sort for low levels of fluorescence and repeat step (8). For screening round 3 to improve mutant responsiveness to lower concentration of stabilizing ligand (11), culture cells with stabilizing ligand concentrations an order of magnitude apart from saturating levels for 24 h and repeat step (6-8). For screening round 4 to improve rapid degradation off-state kinetics, (12) culture cells with saturating concentrations of stabilizing ligand for 24 h, wash to remove ligand (8), wait a few hours (4 ± 1 hr) to allow protein degradation, and repeat step (10). After 4 rounds of sorting conditions, (13) propagate cells, extract their genomic DNA, and PCR amplify selected library. (14) Repeat steps (2-4) but culture the cells in the absence or presence of saturating levels of stabilizing ligand. (15) Sort for mutants that exhibit low basal fluorescence and high dynamic range.

(16) Genome extract using barcoded primers for next-generation sequencing using an Illumina NextSeq machine. (17) Generate stable cell lines of these identified variants for further validation studies. The entire process can be adopted for engineering LID tags by screening without destabilizing ligand first and then conducting the opposite conditions for subsequent screenings.

**C. Concluding remarks**

Developing sensitive genetically encodable MRI reporters is still in its infancy and has much more room to make advances toward translatable science. It is only a matter of time that these MRI reporters will be routinely used in the clinic thanks to the contributions in gene therapy and impact the field of biomedicine in novel ways that complement preexisting imaging modalities. With the combination of directed evolution and advancements toward MRI hardware, genetically encodable MRI reporters will illuminate areas of biology that have yet to be discovered.

## D. References


1. Dana, H.; Sun, Y.; Mohar, B.; Hulse, B. K.; Kerlin, A. M.; Hasseman, J. P.; Tsegaye, G.; Tsang, A.; Wong, A.; Patel, R.; et al. High-performance calcium sensors for imaging activity in neuronal populations and microcompartments. *Nature Methods* **2019**, *16* (7), 649-657. DOI: 10.1038/s41592-019-0435-6.

2. Ji, N. The Practical and Fundamental Limits of Optical Imaging in Mammalian Brains. *Neuron* **2014**, *83* (6), 1242-1245. DOI: https://doi.org/10.1016/j.neuron.2014.08.009.

3. Ntziachristos, V. Going deeper than microscopy: the optical imaging frontier in biology. *Nature Methods* **2010**, *7* (8), 603-614. DOI: 10.1038/nmeth.1483.

4. Guan, H.; Liang, W.; Li, A.; Gau, Y.-T. A.; Chen, D.; Li, M.-J.; Bergles, D. E.; Li, X. Multicolor fiber-optic two-photon endomicroscopy for brain imaging. *Optics Letters* **2021**, *46* (5), 1093-1096. DOI: 10.1364/OL.412760.

5. Lelyveld, V. S.; Atanasijevic, T.; Jasanoff, A. Challenges for molecular neuroimaging with MRI. *International Journal of Imaging Systems and Technology* **2010**, *20* (1), 71-79, https://doi.org/10.1002/ima.20221. DOI: https://doi.org/10.1002/ima.20221 (acccessed 2021/11/23).

6. Banaszynski, L. A.; Chen, L.-c.; Maynard-Smith, L. A.; Ooi, A. G. L.; Wandless, T. J. A Rapid, Reversible, and Tunable Method to Regulate Protein Function in Living Cells Using Synthetic Small Molecules. *Cell* **2006**, *126* (5), 995-1004. DOI: https://doi.org/10.1016/j.cell.2006.07.025.

7. Murty, S.; Labanieh, L.; Murty, T.; Gowrishankar, G.; Haywood, T.; Alam, I. S.; Beinat, C.; Robinson, E.; Aalipour, A.; Klysz, D. D.; et al. PET Reporter Gene Imaging and

Ganciclovir-Mediated Ablation of Chimeric Antigen Receptor T Cells in Solid Tumors. *Cancer Research* **2020**, *80* (21), 4731. DOI: 10.1158/0008-5472.CAN-19-3579.

8. Jacob, F.; Salinas, R. D.; Zhang, D. Y.; Nguyen, P. T. T.; Schnoll, J. G.; Wong, S. Z. H.; Thokala, R.; Sheikh, S.; Saxena, D.; Prokop, S.; et al. A Patient-Derived Glioblastoma Organoid Model and Biobank Recapitulates Inter- and Intra-tumoral Heterogeneity. *Cell* **2020**, *180* (1), 188-204.e122. DOI: https://doi.org/10.1016/j.cell.2019.11.036.

9. Aghighi, M.; Theruvath, A. J.; Pareek, A.; Pisani, L. L.; Alford, R.; Muehe, A. M.; Sethi, T. K.; Holdsworth, S. J.; Hazard, F. K.; Gratzinger, D.; et al. Magnetic Resonance Imaging of Tumor-Associated Macrophages: Clinical Translation. *Clinical Cancer Research* **2018**, *24* (17), 4110. DOI: 10.1158/1078-0432.CCR-18-0673.

10. Hoffmann, N.; Fernández, V.; Pereira, R. C.; Rancati, S.; Pelizzoli, R.; De Pietri Tonelli, D. A Xenotransplant Model of Human Brain Tumors in Wild-Type Mice. *iScience* **2020**, *23* (1), 100813. DOI: https://doi.org/10.1016/j.isci.2019.100813.

11. Haddad, A. F.; Young, J. S.; Amara, D.; Berger, M. S.; Raleigh, D. R.; Aghi, M. K.; Butowski, N. A. Mouse models of glioblastoma for the evaluation of novel therapeutic strategies. *Neuro-Oncology Advances* **2021**, *3* (1). DOI: 10.1093/noajnl/vdab100 (acccessed 11/23/2021).

12. Patriarchi, T.; Mohebi, A.; Sun, J.; Marley, A.; Liang, R.; Dong, C.; Puhger, K.; Mizuno, G. O.; Davis, C. M.; Wiltgen, B.; et al. An expanded palette of dopamine sensors for multiplex imaging in vivo. *Nature Methods* **2020**, *17* (11), 1147-1155. DOI: 10.1038/s41592-020-0936-3.

13. McMahon, M. T.; Gilad, A. A.; DeLiso, M. A.; Cromer Berman, S. M.; Bulte, J. W. M.; van Zijl, P. C. M. New “multicolor” polypeptide diamagnetic chemical exchange saturation transfer (DIACEST) contrast agents for MRI. *Magnetic Resonance in Medicine* **2008**, *60* (4), 803-812, https://doi.org/10.1002/mrm.21683. DOI: https://doi.org/10.1002/mrm.21683 (acccessed 2021/11/27).

14. Lu, G. J.; Farhadi, A.; Szablowski, J. O.; Lee-Gosselin, A.; Barnes, S. R.; Lakshmanan, A.; Bourdeau, R. W.; Shapiro, M. G. Acoustically modulated magnetic resonance imaging of gas-filled protein nanostructures. *Nature Materials* **2018**, *17* (5), 456-463. DOI: 10.1038/s41563-018-0023-7.

15. Iwamoto, M.; Björklund, T.; Lundberg, C.; Kirik, D.; Wandless, T. J. A General Chemical Method to Regulate Protein Stability in the Mammalian Central Nervous System. *Chemistry & Biology* **2010**, *17* (9), 981-988. DOI: https://doi.org/10.1016/j.chembiol.2010.07.009.

16. Auffenberg, E.; Jurik, A.; Mattusch, C.; Stoffel, R.; Genewsky, A.; Namendorf, C.; Schmid, R. M.; Rammes, G.; Biel, M.; Uhr, M.; et al. Remote and reversible inhibition of neurons and circuits by small molecule induced potassium channel stabilization. *Scientific Reports* **2016**, *6* (1), 19293. DOI: 10.1038/srep19293.

17. Li, N.; Jasanoff, A. Local and global consequences of reward-evoked striatal dopamine release. *Nature* **2020**, *580* (7802), 239-244. DOI: 10.1038/s41586-020-2158-3.

18. Hesse, M.; Raulf, A.; Pilz, G.-A.; Haberlandt, C.; Klein, A. M.; Jabs, R.; Zaehres, H.; Fügemann, C. J.; Zimmermann, K.; Trebicka, J.; et al. Direct visualization of cell division using high-resolution imaging of M-phase of the cell cycle. *Nature Communications* **2012**, *3* (1), 1076. DOI: 10.1038/ncomms2089.

19. Longo, D.; Hasty, J. Dynamics of single-cell gene expression. *Molecular Systems Biology* **2006**, *2* (1), 64, https://doi.org/10.1038/msb4100110. DOI: https://doi.org/10.1038/msb4100110 (acccessed 2021/11/28).

20. Arnold, F. H. Design by Directed Evolution. *Accounts of Chemical Research* **1998**, *31* (3), 125-131. DOI: 10.1021/ar960017f.

21. Packer, M. S.; Liu, D. R. Methods for the directed evolution of proteins. *Nature Reviews Genetics* **2015**, *16* (7), 379-394. DOI: 10.1038/nrg3927.

22. Farhadi, A.; Sigmund, F.; Westmeyer, G. G.; Shapiro, M. G. Genetically encodable materials for non-invasive biological imaging. *Nature Materials* **2021**, *20* (5), 585-592. DOI: 10.1038/s41563-020-00883-3.

23. Tucker, C. L.; Fields, S. A yeast sensor of ligand binding. *Nature Biotechnology* **2001**, *19* (11), 1042-1046. DOI: 10.1038/nbt1101-1042.

24. Yesbolatova, A.; Saito, Y.; Kitamoto, N.; Makino-Itou, H.; Ajima, R.; Nakano, R.; Nakaoka, H.; Fukui, K.; Gamo, K.; Tominari, Y.; et al. The auxin-inducible degron 2 technology provides sharp degradation control in yeast, mammalian cells, and mice. *Nature Communications* **2020**, *11* (1), 5701. DOI: 10.1038/s41467-020-19532-z.

25. Miyazaki, Y.; Imoto, H.; Chen, L.-c.; Wandless, T. J. Destabilizing Domains Derived from the Human Estrogen Receptor. *Journal of the American Chemical Society* **2012**, *134* (9), 3942-3945. DOI: 10.1021/ja209933r.

26. Armbruster, B. N.; Li, X.; Pausch, M. H.; Herlitze, S.; Roth, B. L. Evolving the lock to fit the key to create a family of G protein-coupled receptors potently activated by an inert

ligand. *Proceedings of the National Academy of Sciences* **2007**, *104* (12), 5163. DOI: 10.1073/pnas.0700293104.